CUKUROVA UNIVERSITY

INSTITUTE OF NATURAL AND APPLIED SCIENCES

PhD THESIS

Heat Transfer and Fluid Flow Enhancement of Tube Bank Heat Exchangers with Various Cross-Sections Using Computational Fluid Dynamics Integrated with Multi-Objective Genetic Algorithm Optimization Method

Arif Emre AKTAŞ

Automotive Engineering Department

October, 2023

CUKUROVA UNIVERSITY

INSTITUTE OF NATURAL AND APPLIED SCIENCES

PhD THESIS APPROVAL

Heat Transfer and Fluid Flow Enhancement of Tube Bank Heat Exchangers with Various Cross-Sections Using Computational Fluid Dynamics Integrated with Multi-Objective Genetic Algorithm Optimization Method

---

Arif Emre AKTAŞ

Automotive Engineering Department

This Doctorate Thesis was evaluated by the following Jury Members on 20/10/2023 and was approved by unanimity of votes.

Jury : Prof. Dr. Mehmet BİLGİLİ (Advisor) ……

: Assoc. Prof. Dr. Mustafa Atakan AKAR ……

: Assoc. Prof. Dr. Gökhan TÜCCAR ……

: Assoc. Prof. Dr. Arif ÖZBEK ……

: Assoc. Prof. Dr. Erinç ULUDAMAR ……

This Thesis was written in the Department of Automotive Engineering, Institute of Natural and Applied Sciences.

Thesis Number:

Prof. Dr. Sadık DİNÇER
Director
Institute of Natural and Applied Sciences

This work was supported by the Scientific Research Office of Çukurova University.
Project ID: FDK-2020-13186

Note: The usage of the presented specific declarations, tables, figures, and photographs either in this thesis or in any other reference without citation is subject to "The law of Arts and Intellectual Products" number of 5846 of Turkish Republic

CONTENTS

ABSTRACT I
ÖZ II
EXTENDED ABSTRACT III
GENİŞLETİLMİŞ ÖZET VII
ACKNOWLEDGEMENTS XI
LIST OF TABLES XII
LIST OF FIGURES XIV
SYMBOLS AND ABBREVIATIONS XVIII
1. INTRODUCTION 1
2. PRELIMINARY WORK 3
2.1. Circular Tube Banks 3
2.2. Different Shaped Tube Banks 7
2.3. Tube Bank Optimization Studies 11
3. MATERIAL AND METHOD 13
3.1. Description of Methodology 13
3.2. Data Analysis 14
3.3. Definition of the Tube Bank Geometries 14
3.4. Boundary Condition 18
3.5. Optimization Problem 19
3.6. Computational Details 21
3.7. Grid Independence Study 24
4. RESULTS AND DISCUSSIONS 25
4.1. Validation Studies 25
4.1.1. Validation of Circular Shaped Tube Bank with In-line and Staggered Arrangement 25
4.1.2. Validation of Diamond Shaped Tube Bank with Staggered Arrangement 28
4.2. Optimization of Tube Bank with Inline Arrangement 29
4.2.1. Comparison of Optimum Circular and Diamond Shaped Tube Bank with Inline Arrangement 30
4.2.2. Comparison of Optimum Diamond and Enhanced Shaped Tube Bank with Inline Arrangement 37
4.3. Optimization of Tube Bank with Staggered Arrangement 52
4.3.1. Comparison of Optimum Circular and Diamond Shaped Tube Bank with Staggered Arrangement 52

4.3.2. Comparison of Optimum Diamond and Enhanced Shaped Tube Bank with Staggered Arrangement 59
5. CONCLUSIONS 75
REFERENCES 79
CURRICULUM VITAE 87
APPENDICES 89

CUKUROVA UNIVERSITY
INSTITUTE OF NATURAL AND APPLIED SCIENCES

PhD THESIS

Heat Transfer and Fluid Flow Enhancement of Tube Bank Heat Exchangers with Various Cross-Sections Using Computational Fluid Dynamics Integrated with Multi-Objective Genetic Algorithm Optimization Method

Arif Emre AKTAŞ

Advisor: Prof. Dr. Mehmet BİLGİLİ
2nd Advisor: Assoc. Prof. Dr. Mehmet Tahir ERDİNÇ

Department of Automotive Engineering

ABSTRACT

Tube bank heat exchangers are commonly preferred in many applications, including automotive industry. In this thesis, comparative optimization studies are performed for circular, diamond, and enhanced shaped tube banks. Multi-objective Genetic Algorithm II (MOGA-II) is used to determine optimum tube bank geometries.

Firstly, validation studies are made comparing the experimental results of the circular and diamond shaped geometries from the literature. Then a new tube bank geometry, called the enhanced is introduced with its geometric description. The flow around the tube banks is assumed to be steady, incompressible, and turbulent. The inlet temperature of the fluid and the wall temperature of the tubes are assumed to be constant. The finite volume method is utilized to solve governing equations.

Objective functions for all analyzes are maximization heat transfer and minimization pump power at constant tube periphery. Optimization studies are carried out for two different tube bank arrangements which are inline and staggered. In each case, it is divided into two steps. In the first step circular and diamond shaped tube banks are compared. However, in the second step diamond and enhanced shaped tube banks are compared with defined constraints. All Pareto designs and selected optimum designs are tabulated and compared using the given parameters. The Study has shown that determined optimum tube bank design with enhanced geometry has better heat transfer and fluid flow performance than circular and diamond shaped tube banks in both inline and staggered arrangements.

Keywords: Tube Bank, Heat Exchanger, Computational Fluid Dynamics, Heat Transfer, Fluid Flow, Optimization.

ÇUKUROVA ÜNİVERSİTESİ
FEN BİLİMLERİ ENSTİTÜSÜ

DOKTORA TEZİ

Çok Amaçlı Genetik Algoritma Optimizasyon Yöntemi ile Bütünleştirilmiş Hesaplamalı Akışkanlar Dinamiği Kullanılarak Çeşitli Kesitlere Sahip Boru Demeti Isı Değiştiricilerinde Isı Transferi ve Akışın İyileştirilmesi

Arif Emre AKTAŞ

Danışman: Prof. Dr. Mehmet BİLGİLİ
2. Danışman Doç. Dr. Mehmet Tahir ERDİNÇ

Otomotiv Mühendisliği Anabilim Dalı

ÖZ

Boru demeti ısı değiştiricileri otomotiv sektörü de dahil olmak üzere birçok uygulamada yaygın olarak tercih edilmektedir. Bu tezde dairesel, elmas ve gelişmiş şekilli boru demetlerinin karşılaştırmalı eniyileme çalışmaları yapılmıştır. En iyi boru demeti geometrilerini belirlemek için Çok Amaçlı Genetik Algoritma II (MOGA-II) kullanılmıştır.

İlk olarak literatürdeki dairesel ve elmas şekilli geometrilerin deneysel sonuçları karşılaştırılarak doğrulama çalışmaları yapılmıştır. Daha sonra gelişmiş adı verilen yeni bir boru demeti geometrisi, geometrik tanımıyla birlikte sunulmuştur. Boru demetleri etrafındaki akışın daimi, sıkıştırılamaz ve türbülanslı olduğu varsayılmaktadır. Ayrıca akışkanın giriş sıcaklığı ve boruların duvar sıcaklığının sabit olduğu varsayılmaktadır. Korunum denklemlerini çözmek için sonlu hacim yöntemi kullanılmıştır.

Tüm analizlerin amaç fonksiyonları, sabit dış çevreye sahip borularda ısı transferini maksimuma çıkarmak ve pompa gücünü minimuma indirmektir. Optimizasyon çalışmaları sıralı ve saptırmalı olmak üzere iki farklı boru demeti için yapılmıştır. Her durumda çalışmalar iki adıma ayrılmıştır. İlk adımda dairesel ve elmas şeklindeki boru demetleri karşılaştırılmıştır. Ancak ikinci adımda elmas ve gelişmiş şekilli boru demetleri kısıt verilerek karşılaştırmıştır. Tüm Pareto tasarımları ve seçilen optimum tasarımlar, verilen parametreler kullanılarak tablolaştırılmış ve karşılaştırılmıştır. Çalışma, her iki sıralı ve saptırmalı dizilim için, gelişmiş geometriye sahip en iyi boru demeti tasarımının, dairesel ve elmas şeklindeki boru demetlerinden daha iyi ısı transferi ve akış performansı verdiğini göstermiştir.

Anahtar Kelimeler: Boru Demeti, Isı Değiştirici, Hesaplamalı Akışkanlar Dinamiği, Isı Transferi, Akış, Eniyileme.

EXTENDED ABSTRACT

In this thesis, a comparative optimization study is conducted for circular, diamond and enhanced shaped tube banks, geometry of which is presented for the first time in this study. First of all, the determination of horizontal and vertical edges for diamond and enhanced shaped tube bank geometry is given as equations. In addition, equations for calculating the perimeter as a function of diameter the diameter of curvature (D_{en}), front (θ_1) and rear (θ_2) attack angles, which are used as variables in the solutions for enhanced shaped geometry. The finite volume method was used to determine heat transfer and flow behavior. To verify the reliability of the solution method and mesh structure, a comparative validation study was carried out comparing with experimental results on circular and diamond shaped tube banks in the literature. In this validation study, it was decided to use RNG (Renormalization Group) k-ε, one of the most realistic turbulence models, and COUPLED, one of the most common algorithms, for all solutions.

The flow around the tube banks is assumed to be steady, incompressible and turbulent. Heat transfer by conduction and radiation is neglected. The inlet temperature of the fluid and the wall temperature of the tubes are assumed to be constant. In addition, it is assumed that the fluid properties are not changed throughout the flow. Air is used as the fluid in all analyzes. In addition to the mass, momentum and energy conservation equations used in the background of the computational fluid dynamics software, the general equations of the preferred RNG k-ε turbulence model are given.

The geometries used in the calculations are 3-dimensional and 4 tubes with diameter D are drawn for each tube bank. In order to minimize the solution time, symmetry boundary conditions are given to the considered flow field from the bottom, top and sides. To obtain better convergence, the length of the entrance section of the flow was taken as 6xD, and to prevent backflow, the length of the exit section was taken as 12xD. The inlet velocity is assigned as constant over the entire surface at the inlet cross section. In addition, constant atmospheric pressure is given to the outlet. A no-slip boundary condition at constant temperature was given to the tube surfaces.

3D solution domains and mesh structures are created using ANSYS Workbench. The outlet temperature, inlet pressure, heat flux, skewness and y+ value were determined as the output variables of the ANSYS Fluent. Python programming language was used to edit the fluid data outputs compatible with the modeFRONTIER software. The Design of Experiments (DOE) method was used to obtain initial designs in the modeFRONTIER environment that controls the ANSYS program. The Sobol method was used for the distribution of optimization variables. 20 DOEs were created to obtain the best designs in all studies. The 'Calculator' module of the modeFRONTIER software was used to calculate values such as logarithmic mean temperature, heat transfer area, cross-sectional area, tube perimeter and total heat transfer. MOGA-II is used as the algorithm in the optimization study. Maximization of heat transfer and minimization of required pumping power are chosen as objective functions in the optimization studies. Two groups of optimization studies are carried out independently for inline and staggered tube bank arrangements.

In the first step, circular cross-section tube bank with inline arrangement and diamond cross-section tube banks are compared at fixed volume and constant periphery. In circular geometry, the variables are inlet velocity (V_{in}), longitudinal pitch ratio (S_L^*) and transversal pitch ratio (S_T^*), while in diamond geometry, attack angle (θ) is taken in addition to these variables. Definition ranges for inlet velocity, longitudinal pitch ratio and transversal pitch ratio, which are variables used in circular, diamond and advanced geometry with both inline and staggered arrangements, are $1<V_{in}<6$, $1< S_L^*<6$ is limited to $1<S_T^*<6$, and the steps are determined as 1 m/s for V_{in} and 0.5 for S_L^* & S_L^*. The definition range for all attack angles used only in diamond and geometries is $10° < \theta <170°$ and the steps are determined as 5°. At the end of the optimization study in step 1 of the first group, 483 designs are obtained for circular geometry with inline arrangement, and 87 of them are determined as Pareto designs. A total of 647 designs are obtained for the diamond shaped inline arrangement tube bank, and 84 of them are defined as Pareto. The obtained Pareto designs are compared in graphs where total heat transfer, required pumping power, inlet velocity, longitudinal/ transversal pitch ratio and attack angle are used as variables. It has been observed that the pumping power requirement increases with heat transfer. For equal pumping power, all diamond shaped inline Pareto designs show much higher heat transfer performance than circular ones. According to the results, 969.87 W heat transfer and 54.55 W pumping power requirement are obtained in the optimum circular cross geometry, while 2046.6 W heat transfer and 26.53 W pumping power requirement are obtained in the diamond shaped geometry. For both geometries, the highest heat transfer are obtained under the conditions V_{in}=6 m/s, S_L^*=1.2, S_T^*=1.2 and θ=10° (for diamond shaped inline tube bank). The designs obtained for diamond shaped geometries are collected in the range of 10-25°, and the most of them are obtained at 10°.

In the second step optimization study of inline tube banks, a comparison of diamond shaped and enhanced shaped tube bank geometries are made. In addition to the objective functions in the first step, length constraint $L_D \leq 1$ is applied. At the end of the optimization study, 422 designs are obtained for diamond shaped geometry with inline arrangement, and 55 of them are determined as Pareto designs. A total of 1757 designs are obtained for the pipe bundle with enhanced shaped inline arrangement tube bank, and 117 of them are defined as Pareto. Similarly, the Pareto designs obtained are compared in graphs where total heat transfer, required pumping power, inlet velocity, longitudinal/ transversal pitch ratio and attack angles are used as variables. In general, it has been observed that total heat transfer value increase with pomp power. In the region where $\dot{W}_{pump} < 0.7$ W, higher heat transfer is obtained in diamond shaped tube bank. On the contrary, higher heat transfer is obtained in tube banks with enhanced shaped geometry in the region where $\dot{W}_{pump} > 0.7$ W. According to the results, 442.87 W heat transfer and 10.05 W pumping power requirement are obtained in the optimum diamond shaped geometry, while 503.74 W heat transfer and 9.28 W pumping power requirement are obtained in the enhanced shaped geometry. For diamond shaped tube bank, optimum design is obtained in the case of V_{in}=5 m/s, S_L^*=2.7, S_T^*=1.2 and θ=30°, while in enhanced shaped tube bank the optimum design is obtained in the case of V_{in}=4.5 m/s, S_L^*=2, S_T^*=1.2, θ_1=50° ve θ_2=30°. All Pareto designs are tabulated for diamond and enhanced shaped tube banks.

Additionally, streamlines, temperature and pressure contours of the optimum designs selected among Pareto designs are depicted.

In the second part of the thesis, similarly, geometries with staggered arranged are compared in a similar way in two steps. In the first step, circular and diamond shaped tube banks are compared. Likewise, objective functions are maximization of heat transfer and minimization of required pumping power. At the end of the optimization study, 477 designs are obtained for circular geometry with staggered arrangement, and 108 of them are determined as Pareto designs. A total of 736 designs are obtained for the diamond shaped staggered arrangement tube bank, and 99 of them are defined as Pareto. The obtained Pareto designs are compared in graphs where heat transfer, required pumping power, inlet velocity, longitudinal/transversal pitch ratio and attack angle are used as variables. Likewise in inline arrangement, all diamond shaped staggered Pareto designs show much higher heat transfer performance than circular ones for equal pumping power. Optimization results indicated that, 1089.88 W heat transfer and 61.36 W pumping power requirement are obtained in the circular shaped geometry, which provides the highest heat transfer, while 6161.32 W heat transfer and 1472.3 W pumping power requirement are obtained in the diamond shaped geometry. For circular shaped geometry, the highest heat transfer occurred under the conditions V_{in}=6 m/s, S_L^*=1.2, S_T^*=1.2 and for diamond shaped geometry, these values are V_{in}=4 m/s, S_L^*=1.4, S_T^*=1.3 and θ=170°. The designs obtained for diamond cross-section geometries were located in the range of 10-40° and 170°.

In the second step of the optimization study of staggered tube banks, a comparison of diamond and enhanced shaped tube banks is made. In addition to the objective functions in the first stage, length constraint $L_D \leq 1$ is applied for diamond staggered tube bank. In enhanced tube bank, the tube length is taken as L_D=1 m. Thus, it is possible to obtain smaller volume pipe bundles. At the end of the optimization study, 229 designs are obtained for diamond shaped geometry with staggered arrangement, and 28 of them are determined as Pareto designs. A total of 1642 designs are obtained for the tube bank with enhanced shaped staggered arrangement, and 146 of them are defined as Pareto. Pareto designs obtained in the same way are compared in graphs where total heat transfer, required pumping power, inlet velocity, longitudinal/transversal pitch ratio and attack angle are used as variables. For diamond geometry, the optimum design is obtained in the case of V_{in}=3 m/s, S_L^*=1.3, S_T^*=1.2 and θ=120°, while in enhanced geometry optimum design is obtained in the case of V_{in}=6 m/s, S_L^*=1.3, S_T^*=1.2, θ_1=50° ve θ_2=85°. All obtained Pareto designs are tabulated for diamond and enhanced shaped tube banks. Results showed that 766.77 W heat transfer, 51.92 W pumping power requirement and 0.00075 m^3 tube bank volume are achieved in the optimum diamond shaped geometry, while 771.31 W heat transfer, 42.65 W pumping power requirement and 0.000684 m^3 tube bank volume are achieved in the enhanced shaped geometry. Additionally, streamlines, temperature and pressure contours of the optimum designs are shown.

GENİŞLETİLMİŞ ÖZET

Bu tezde sıralı ve şaşırtmalı dizilime sahip dairesel, elmas ve bu çalışmada geometrisi ilk kez tanıtılan gelişmiş geometrili boru demetlerinin karşılaştırmalı eniyileme çalışması yapılmıştır. Öncelikle elmas ve gelişmiş kesitli boru demeti geometrisi için yatay ve dikey ayrıtların hesaplanışı eşitlik olarak verilmiştir. Ayrıca, gelişmiş kesitli geometriye için çözümlerde değişken olarak kullanılan eğrilik çapına, ön ve arka atak açılarına bağlı çevreyi hesaplayabilmek için eşitlikler verilmiştir. Isı transferi ve akış davranışının belirlenmesinde sonlu hacimler yöntemi kullanılmıştır. Çözüm yönteminin ve ağ yapısının güvenirliği için öncelikle literatürdeki dairesel ve elmas kesitli boru demetleri ile ilgili yapılmış deneysel sonuçlar ile karşılaştırmalı doğrulama çalışması yapılmıştır. Bu doğrulama çalışmasıyla beraber tüm çözümler için en gerçekçi türbülans modellerinden birisi olan RNG (Renormalization Group) k-ε ve en yaygın algoritmalardan birisi olan COUPLED kullanılmasına karar verilmiştir.

Boru demetleri etrafındaki akış daimi, sıkıştırılamaz ve türbülanslı olarak kabul edilmiştir. İletim ve ışıma ile olan ısı transferi ihmal edilmiştir. Akışkanın giriş sıcaklığı ve boruların duvar sıcaklığı sabit olarak belirlenmiştir. Ayrıca akışkan özelliklerinin akış boyunca değişmez olduğu kabul edilmiştir. Tüm analizlerde akışkan olarak hava kullanılmıştır. Hesaplamalı akışkanlar dinamiği yazılımının arka planında kullanılan kütle, momentum ve enerji korunum denklemlerinin yanı sıra tercih edilen RNG k-ε türbülans modeline ait genel denklemler verilmiştir.

Hesaplamalarda kullanılan geometriler 3 boyutlu olup her bir boru demeti geometrisi için D çaplı 4 adet boru çizilmiştir. Çözüm süresini en aza indirmek için ele alınan akış alanına alt, üst ve yanlardan simetri sınır şartı verilmiştir. Daha iyi yakınsama elde etmek için akışın giriş bölümü uzunluğu 6xD ve ters akışı önlemek için çıkış uzunluğu 12xD olarak alınmıştır. Giriş hızı giriş kesitinde tüm yüzey boyunca sabit olarak atanmıştır. Ayrıca çıkış kısmına sabit atmosfer basıncı verilmiştir. Boru yüzeylerine sabit sıcaklıkta kaymama sınır şartı verilmiştir.

3 boyutlu çözüm bölgeleri ve ağ yapısı ANSYS Workbench programı kullanılarak oluşturulmuştur. Çıkış sıcaklığı, giriş basıncı, ısı akısı, ağ çarpıklığı ve y+ değeri ANSYS Fluent programının çıkış değişkeni olarak belirlenmiştir. Fluent data çıktılarını modeFRONTIER yazılımına uygun hale getirmek için Python programa dili kullanılmıştır. ANSYS programını kontrol eden modeFRONTIER ortamında ilk tasarımları elde etmek için Deneylerin Tasarımı (DOE) yöntemi kullanılmıştır. Eniyileme değişkenlerinin dağılımı için ise Sobol yöntemi kullanılmıştır. Tüm çalışmalarda en iyi tasarımları elde etmek için 20 adet DOE oluşturulmuştur. Logaritmik ortalama sıcaklık, ısı transfer alanı, kesit alanı, boru çevresi ve toplam ısı transferi gibi değerlerin hesaplanmasında modeFRONTIER yazılımının ‘Hesaplayıcı’ modülü kullanılmıştır. Eniyileme çalışmasında algoritma olarak MOGA-II kullanılmıştır. Amaç fonksiyonu olarak toplam ısı transferi en yüksek gerekli olan pompa gücü ise en düşük olarak belirlenmiştir. Sıralı ve şaşırtmalı boru demeti için bağımsız olarak iki grup eniyileme çalışması yapılmıştır.

İlk bölümde öncelikle sıralı dizilime sahip dairesel kesitli boru demeti ile elmas kesitli boru demeti sabit hacimde ve sabit boru çevresi alınarak karşılaştırılmıştır. Dairesel geometride değişkenler giriş hızı (V_{in}), boyuna boyutsuz adım (S_L^*) ve enine boyutsuz adım (S_T^*) elmas geometride ise bu değişkenlere ek olarak atak açısı (θ) alınmıştır. Her iki sıralı ve şaşırtmalı dizilime sahip dairesel, elmas ve gelişmiş geometride kullanılan değişkenler olan giriş hızı (V_{in}), boyuna boyutsuz adım (S_L^*) ve enine boyutsuz adım (S_T^*) için tanım aralıkları $1<V_{in}<6$, $1<S_L^*<6$, $1<S_T^*<6$ olarak sınırlandırılmış olup adımlar V_{in} için 1 m/s ve S_L^* & S_T^* için 0,5 olarak belirlenmiştir. Sadece elmas ve geometrilerde kullanılan tüm atak açıları için tanım aralığı 10° < θ <170° olup adımlar 5° olarak belirlenmiştir. İlk bölümün 1. Adımındaki eniyileme çalışmasının sonunda sıralı dizilime sahip dairesel geometri için 483 tasarım elde edilmiş olup bunların 87 tanesi Pareto tasarım olarak belirlenmiştir. Elmas kesitli sıralı dizilime sahip boru demeti için ise toplam 647 tasarım elde edilmiş olup bunların 84'ü Pareto olarak tanımlanmıştır. Elde edilen Pareto tasarımlar toplam ısı transferi, gerekli pompalama gücü, giriş hızı, enine/boyuna boyutsuz adım ve atak açısının değişken olarak kullanıldığı grafiklerde karşılaştırılmıştır. Pompalama gereksiniminin ısı transferi ile artış gösterdiği görülmüştür. Eşit pompalama gücü için tüm elmas kesitli sıralı Pareto tasarımlar dairesel kesitlilere göre çok daha yüksek ısı transferi performansı göstermektedir. Sonuçlara göre en iyi dairesel kesitli geometride 969,87 W ısı transferi ve 54,55 W pompalama gücü gereksinimi elde edilirken elmas kesitli geometride 2046,6 W ısı transferi ve 26,53 W pompalama gücü gereksinimi elde edilmiştir. Her iki geometri için en yüksek ısı transferi V_{in}=6 m/s, S_L^*=1,2, S_T^*=1,2 ve θ=10° (elmas kesit için) koşullarında gerçekleşmiştir. Elmas kesitli geometriler için elde edilen tasarımlar 10-25° aralığında toplanmış olup büyük çoğunluğu 10°'de elde edilmiştir.

Sıralı boru demetlerinin 2. aşamadaki eniyileme çalışmasında elmas kesitli ile gelişmiş kesitli boru demeti geometrilerinin karşılaştırılması yapılmıştır. Birinci aşamadaki amaç fonksiyonlarına ek olarak boru uzunluğu L_D en fazla 1m olacak şekilde kısıt verilmiştir. Yapılan eniyileme çalışmasının sonunda sıralı dizilime sahip elmas kesitli geometri için 422 tasarım elde edilmiş olup bunların 55 tanesi Pareto tasarım olarak belirlenmiştir. Gelişmiş kesitli sıralı dizilime sahip boru demeti için ise toplam 1757 tasarım elde edilmiş olup bunların 117'ü Pareto olarak tanımlanmıştır. Benzer şekilde elde edilen Pareto tasarımlar toplam ısı transferi, gerekli pompalama gücü, giriş hızı, enine/boyuna boyutsuz adım ve atak açılarının değişken olarak kullanıldığı grafiklerde karşılaştırılmıştır. Genel olarak $\dot{Q}_{total}$ değerlerinin $\dot{W}_{pump}$ ile artış gösterdiği görülmüştür. $\dot{W}_{pump}$< 0,7 W olduğu bölgede elmas kesitli boru demetlerinde daha yüksek ısı transferi elde edilmiştir. Bunun aksine, $\dot{W}_{pump}$> 0,7 W olduğu bölgede gelişmiş kesitli boru demetlerinde daha yüksek ısı transferi elde edilmiştir. Sonuçlara göre en iyi elmas kesitli geometride 442,87 W ısı transferi ve 10,05 W pompalama gücü gereksinimi elde edilirken gelişmiş kesitli geometride 503,74 W ısı transferi ve 9,28 W pompalama gücü gereksinimi elde edilmiştir. Elmas geometri için en iyi tasarım V_{in}=5 m/s, S_L^*=2,7, S_T^*=1,2 ve θ=30° durumunda elde edilirken gelişmiş geometride en iyi tasarım V_{in}=4,5 m/s, S_L^*=2, S_T^*=1,2, θ_1=50° ve θ_2=30° durumunda elde edilmiştir.

Tüm Pareto tasarımlar elmas ve gelişmiş sıralı dizilime sahip boru demetleri için tablo halinde verilmiştir. Ayrıca Pareto tasarımlar arasında seçilen en iyi tasarımlara ait akış çizgileri, sıcaklık ve basınç konturları gösterilmiştir.

Tezin ikinci bölümünde ise şaşırtmalı dizilime sahip geometriler benzer şekilde iki aşamada karşılaştırılmıştır. İlk aşamada dairesel ile elmas kesitli boru demetleri karşılaştırılmıştır. Aynı şekilde amaç fonksiyonu olarak toplam ısı transferi en yüksek gerekli olan pompa gücü ise en düşük olarak belirlenmiştir. Eniyileme çalışmasının sonunda şaşırtmalı dizilime sahip dairesel geometri için 477 tasarım elde edilmiş olup bunların 108 tanesi Pareto tasarım olarak belirlenmiştir. Elmas kesitli sıralı dizilime sahip boru demeti için ise toplam 736 tasarım elde edilmiş olup bunların 99'u Pareto olarak tanımlanmıştır. Elde edilen Pareto tasarımlar toplam ısı transferi, gerekli pompalama gücü, giriş hızı, enine/boyuna boyutsuz adım ve atak açısının değişken olarak kullanıldığı grafiklerde karşılaştırılmıştır. Sıralı dizilimde olduğu gibi, eşit pompalama gücü için tüm elmas kesitli sıralı Pareto tasarımlar dairesel kesitlilere göre çok daha yüksek ısı transferi performansı göstermektedir. Elde edilen eniyileme sonuçlara göre en yüksek ısı transferi gerçekleştiren dairesel kesitli geometride 1089,88 W ısı transferi ve 61,36 W pompalama gücü gereksinimi elde edilirken elmas kesitli geometride 6161,32 W ısı transferi ve 1472,3 W pompalama gücü gereksinimi elde edilmiştir. Dairesel kesitli geometri için en yüksek ısı transferi V_{in}=6 m/s, S_L^*=1,2, S_T^*=1,2 koşullarında gerçekleşmiş olup bu değer elmas kesitli geometri için ise V_{in}=4 m/s, S_L^*=1,4, S_T^*=1,3 ve θ=170° koşullarında elde edilmiştir. Elmas kesitli geometriler için elde edilen tasarımlar 10-40° aralığında ve 170°'de toplanmıştır.

Şaşırtmalı boru demetlerinin eniyileme çalışmasının 2. aşamasında elmas kesitli ile gelişmiş kesitli boru demeti geometrilerinin karşılaştırılması yapılmıştır. Birinci aşamadaki amaç fonksiyonlarına ek olarak elmas kesitli geometri için boru uzunluğu L_D en fazla 1m olacak şekilde kısıt verilmiştir. Gelişmiş geometride ise boru uzunluğu L_D=1m olarak alınmıştır. Böylece daha küçük hacimli boru demetlerinin elde edilmesi mümkün kılınmıştır. Yapılan eniyileme çalışmasının sonunda sıralı dizilime sahip elmas kesitli geometri için 229 tasarım elde edilmiş olup bunların 28 tanesi Pareto tasarım olarak belirlenmiştir. Gelişmiş kesitli sıralı dizilime sahip boru demeti için ise toplam 1642 tasarım elde edilmiş olup bunların 146'sı Pareto olarak tanımlanmıştır. Aynı şekilde elde edilen Pareto tasarımlar toplam ısı transferi, gerekli pompalama gücü, giriş hızı, enine/boyuna boyutsuz adım ve atak açısının değişken olarak kullanıldığı grafiklerde karşılaştırılmıştır. Elmas geometri için en iyi tasarım V_{in}=3 m/s, S_L^*=1,3, S_T^*=1,2 ve θ=120° durumunda elde edilirken gelişmiş geometride en iyi tasarım V_{in}=6 m/s, S_L^*=1,3, S_T^*=1,2, θ_1=50° ve θ_2=85° durumunda elde edilmiştir. Elde edilen tüm Pareto tasarımlar elmas ve gelişmiş kesitli boru demetleri için ayrı ayrı tablo halinde verilmiştir. Sonuçlara göre en iyi elmas kesitli geometride 766,77 W ısı transferi, 51,92 W pompalama gücü gereksinimi ve 0,00075 m^3 elde edilirken gelişmiş kesitli geometride 771,31 W ısı transferi, 42,65 W pompalama gücü gereksinimi ve 0,000684 m^3 toplam hacim elde edilmiştir. Ayrıca elde edilen en iyi tasarımlara ait akış çizgileri, sıcaklık ve basınç konturları gösterilmiştir.

ACKNOWLEDGEMENTS

I would like to express my deepest gratitude to Prof. Dr. Mehmet BİLGİLİ and Assoc. Prof. Dr. M. Tahir ERDİNÇ for their supervision, patience and guidance throughout my studies. It was an incredible experience to have them as my supervisor.

I would like to express my most sincere gratitude to Asst. Prof. Dr. M. Nasıf KURU for sharing his knowledge, continual encouragement, and valuable time for this work.

I extend my heartfelt appreciation to, Prof. Dr. -Ing. Tuncay YILMAZ, for generously sharing his extensive academic knowledge and playing a pivotal role in helping me establish the key idea of this thesis. I also would like to thank Prof. Dr. Alper YILMAZ for his guidance at the beginning of my academic life. I would also like to thank Res. Ass. Dr. Oğuz BAŞ for his useful advices.

I would like to thank to Prof. Dr. Orhan AYDIN, Turkish Academy of Sciences and Thermal-Hydraulic and CFD Research Group of Tarsus University for allowing me to construct all fluid domain geometries/meshes and perform Computational Fluid Dynamics simulations using their facilities.

Besides, I am grateful to the Çukurova University Scientific Research Project Office for their financial support under contract no: FDK-2020-13186.

Last but not least, I would like to thank my most valuable possessions; my parents and sister. They encouraged me, worried about me, and gave me the necessary support throughout my life. I certainly would not have succeeded in finishing my thesis without their support.

LIST OF TABLES

Table 3.1. Boundary conditions for computational domains 19
Table 4.1. Input values for the validation study of inline and staggered tube bank 25
Table 4.2. Validation data from Sparrow and Grannis 28
Table 4.3. Thermo-physical properties of air at T=300 K 29
Table 4.4. Problem data for optimization studies of circular, diamond and enhanced-shaped tube banks 30
Table 4.5. Multi-objective design optimization problem for circular shaped inline tube bank 31
Table 4.6. Multi-objective design optimization problem for diamond shaped inline tube ban 32
Table 4.7. Selected designs of circular and diamond shaped inline tube banks from the first step optimization study. 33
Table 4.8. Second step multi-objective design optimization problem for diamond shaped inline tube bank 37
Table 4.9. Second step multi-objective design optimization problem for enhanced shaped inline tube bank 38
Table 4.10. Pareto designs for inline arranged diamond shaped tube bank 39
Table 4.11. Pareto designs for inline arranged enhanced shaped tube bank 41
Table 4.12. Selected designs of diamond and enhanced shaped inline tube bank from the second step optimization study. 45
Table 4.13. Multi-objective design optimization problem for circular shaped staggered tube bank 53
Table 4.14. Multi-objective design optimization problem for diamond shaped staggered tube bank 54
Table 4.15. Selected designs of circular and diamond shaped staggered tube banks from the first step optimization study. 55
Table 4.16. Multi-objective design optimization problem for diamond shaped staggered tube bank 60
Table 4.17. Multi-objective design optimization problem for enhanced shaped staggered tube bank 61
Table 4.18. Pareto designs for staggered arranged diamond shaped tube bank 62
Table 4.19. Pareto designs for staggered arranged enhanced shaped tube bank 63
Table 4.20. Selected designs of diamond and enhanced shaped staggered tube bank from the second step optimization study. 71
Table A.1. Boundary conditions for computational domains 100
Table A.2. Validation data from Sparrow and Grannis 103
Table A.3. Comparison of numerical errors of present study vs. literature 104

Table A.4. Problem data for optimization studies of circular and diamond-shaped arrangements 106
Table A.5. Thermo-physical properties of air at T=300 K 106
Table A.6. Multi-objective design optimization problem for circular geometry 107
Table A.7. Selected designs of circular geometry optimization study 108
Table A.8. Multi-objective design optimization problem for diamond shaped geometry 114
Table A.9. Selected designs of diamond shaped geometry optimization study 114
Table A.10. Comparison of optimum designs of circular and diamond shaped geometries 115

LIST OF FIGURES

Figure 1.1. Energy consumption of European Union by Sector 1
Figure 1.2. Heat exchanger classification based on construction 2
Figure 2.1. Different circular tube bank arrangements studied 5
Figure 2.2. Streamlines around (a) circular and (b) elliptic shaped tubes at Re:2382 8
Figure 2.3. Defined solution domain for the periodic flow around diamond shaped element 10
Figure 3.1. Solution domain for inline (a) circular (b) diamond (c) enhanced shaped tube banks 15
Figure 3.2. Solution domain for staggered (a) circular (b) diamond (c) enhanced shaped tube banks 16
Figure 3.3. Computational domain and boundaries 19
Figure 3.4. Optimization algorithm flowchart 22
Figure 3.5. Computational mesh created for circular staggered tube bank 23
Figure 3.6. Computational mesh created for diamond shaped staggered tube bank 23
Figure 3.7. Computational mesh created for enhanced shaped staggered tube bank 23
Figure 3.8. Grid independence study (Number of grids) 24
Figure 4.1. Friction Factor Comparison of Current Numerical Results with Experimental of Zukauskas (1987) for Inline Arrangement 26
Figure 4.2. Nusselt Number Comparison of Current Numerical Results with Experimental of Zukauskas (1987) for Inline Arrangement 27
Figure 4.3. Friction Factor Comparison of Current Numerical Results with Experimental of Zukauskas (1987) for Staggered Arrangement 27
Figure 4.4. Nusselt Number Comparison of Current Numerical Results with Experimental of Zukauskas (1987) for Staggered Arrangement 28
Figure 4.5. Friction factor Comparison of Current Numerical Results with Experimental of Sparrow and Grannis (1990; 1991) for Staggered Arrangement 29
Figure 4.6. Optimization workflow for inline arranged circular geometry 30
Figure 4.7. Optimization workflow for diamond shaped inline tube bank 31
Figure 4.8. Scatter of $Qtotal$ vs $Wpump$ 33
Figure 4.9. Scatter of $Qtotal$ vs Vin 34
Figure 4.10. Scatter of $Wpump$ vs Vin 34
Figure 4.11. (a) Scatter of $Qtotal$ vs $SL*$ (b) Scatter of $Qtotal$ vs $ST*$ 35
Figure 4.12. Scatter of $Qtotal$ vs θ 36
Figure 4.13. Optimization workflow for diamond shaped inline tube bank of the second optimization step. 38

Figure 4.14. Optimization workflow for enhanced shaped inline tube bank of the second optimization step. 39
Figure 4.15. Scatter of $Qtotal$ vs $Wpump$ 44
Figure 4.16. Scatter of Vin vs $Qtotal$ 45
Figure 4.17. Scatter of Vin vs $Wpump$ 46
Figure 4.18. (a) Scatter of $Qtotal$ vs $SL*$ (b) Scatter of $Qtotal$ vs $ST*$ 47
Figure 4.19. (a) Scatter of $Qtotal$ vs $\theta 1$ (b) Scatter of $Qtotal$ vs $\theta 2$ 48
Figure 4.20. Streamlines of optimum a) diamond b) enhanced shaped inline tube banks 49
Figure 4.21. Enlarge view of optimum diamond a. b (1.2) and enhanced inline c (3) shaped geometry streamlines 50
Figure 4.22. Temperature contours of optimum a) diamond b) enhanced shaped inline tube banks 51
Figure 4.23. Pressure contours of optimum a) diamond b) enhanced shaped inline tube banks 52
Figure 4.24. Optimization workflow for circular geometry 53
Figure 4.25. Optimization workflow for diamond shaped staggered tube bank 54
Figure 4.26. Scatter of $Qtotal$ vs $Wpump$ 55
Figure 4.27. Scatter of $Qtotal$ vs Vin 56
Figure 4.28. Scatter of $Wpump$ vs Vin 57
Figure 4.29. (a) Scatter of $Qtotal$ vs $SL*$ (b) Scatter of $Qtotal$ vs $ST*$ 58
Figure 4.30. Scatter of $Wpump$ vs θ 59
Figure 4.31. Optimization workflow for diamond shaped staggered tube bank of the second optimization step. 60
Figure 4.32. Optimization workflow for enhanced staggered tube bank of the second optimization step. 61
Figure 4.33. Scatter of $Qtotal$ vs $Wpump$ 66
Figure 4.34. Scatter of $Wpump$ vs Vin 67
Figure 4.35. Scatter of $Qtotal$ vs Vin 68
Figure 4.36. (a) Scatter of $Qtotal$ vs $SL*$ (b) Scatter of $Qtotal$ vs $ST*$ 69
Figure 4.37. (a) Scatter of $Qtotal$ vs $\theta 1$ (b) Scatter of $Qtotal$ vs $\theta 2$ 70
Figure 4.38. Streamlines of optimum a) diamond b) enhanced shaped staggered tube banks 71
Figure 4.39. Enlarge view of optimum diamond a. b (1.2) and enhanced c (3) shaped geometry streamlines 72
Figure 4.40. Temperature contours of optimum a) diamond b) enhanced shaped staggered tube banks 73

Figure 4.41. Pressure contours of optimum a) diamond b) enhanced shaped staggered tube banks 73
Figure A.1. Computational domain for (a) circular (b) diamond shaped geometries with staggered arrangements 91
Figure A.2. Possible flow areas for minimum cross-section of (a) circular (b) diamond shaped geometries 95
Figure A.3. Boundaries for diamond shaped geometry 100
Figure A.4. Optimization algorithm flowchart 101
Figure A.5. Mesh independence study 103
Figure A.6. Comparison of present study's friction factor values 104
Figure A.7. Comparison of f and Re values for present study and Jeng [2006] 105
Figure A.8. Comparison of Nu and Re values for present study and Jeng [2006] 105
Figure A.9. Optimization workflow for circular geometry 107
Figure A.10. Scatter of $Qtotal$ vs ΔP 108
Figure A.11. Scatter of $Nuave$ vs $Remax$ 109
Figure A.12. Scatter of $Qtotal$ vs $Remax$ 110
Figure A.13. Scatter of ΔP vs. $Remax$ 110
Figure A.14. (a) Scatter of $sL*$ vs. $Qtotal$ (b) Scatter of $sT*$ vs. $Qtotal$ 111
Figure A.15. (a.)Scatter of $sL*$ vs. ΔP (b) Scatter of $sT*$ vs. ΔP 112
Figure A.16. Optimization workflow for diamond shaped geometry 113
Figure A.17. Scatter of $Qtotal$ vs ΔP 115
Figure A.18. Scatter of $Nuave$ vs $Remax$ 116
Figure A.19. (a) Scatter of $sL*$ vs. $Qtotal$ (b) Scatter of $sT*$ vs. $Qtotal$ (c) Scatter of θ vs. $Qtotal$ 118
Figure A.20. Streamlines of optimum a) circular b) diamond shaped geometries 119
Figure A.21. Enlarge view of optimum circular shaped geometry streamlines 120
Figure A.22. Temperature contours of optimum a) circular b) diamond shaped geometries 121
Figure A.23. Pressure contours of optimum a) circular b) diamond shaped geometries 122

SYMBOLS AND ABBREVIATIONS

A_{heat} : heat transfer area (m^2)

c_p : fluid specific heat ($\frac{kJ}{kg \cdot K}$)

CFD : Computational Fluid Dynamics

D : diameter (m)

D_{en} : diameter of curvature of enhanced geometry (m)

DOE : Design of Experiment

f : friction factor

G_k : generation of turbulence kinetic energy (Pa/s)

k : thermal conductivity ($W/(m \cdot K)$)

L_D : tube length (m)

L_{en} : longitudinal length of enhanced geometry(m)

$\dot{m}$: mass flow rate over tube bank (kg/s)

MOGA : Multi-objective Genetic Algorithm

N_L : number of tubes in the flow domain

P : pressure (Pa), periphery (m)

Pr : Prandtl number

$\dot{q}$: heat flux (W/m^2)

$\dot{Q}_{total}$: total heat transfer (W)

Re_{max} : Maximum Reynolds number

S_L : streamwise tube spacing (mm)

S_T : transverse tube spacing (mm)

S_L^* : longitudinal pitch ratio

S_T^* : transversal pitch ratio

T : temperature (°C)

u : velocity in x direction (m/s)

V_{in} : inlet velocity (m/s)

v : velocity in y direction (m/s)

x : x coordinate

y : y coordinate

y+ : dimensionless wall distance

β : pressure gradient (Pa/m)

Δp : pressure drop (Pa)

ΔT_{lm} : logarithmic temperature difference (K)

ε : energy dissipation rate (m^2/s^3)

υ : kinematic viscosity (m^2/s)

θ : dimensionless temperature, attack angle ($^\circ$)

ρ : density (kg/m^3)

μ : dynamic viscosity ($Pa.s$)

1. INTRODUCTION

One of the most significant problems influencing the boundaries of industry, technology, and the economy is energy. Owing to the limited quantity and rising cost of energy resources researchers are focused on minimizing energy consumption using these resources efficiently. In the countries of the European Union energy consumption in the period 2010-2019 is distributed among the following sectors: 29.9% transport, 27.3% households, 25.74% industry, 14.15% services and 2.91% other areas (Buzatu et al., 2021) (see Figure 1.1). Heat exchangers have a high portion in these areas, which have a global market size of $16.7 billion in 2020 (Heat Exchanger Market Size, 2020). . Thus, the development and optimum design of heat exchangers is an essential topic.

A heat exchanger is a device that transfers heat between two mediums without mixing. There can be two or more fluids, solid to fluid or solid to solid at different temperatures. Mostly, fluids are separated by a solid wall with high thermal conductivity. They are used in the industries such as power generation, fossil fuels, transportation, air conditioning, refrigeration, cryogenics, and heat recovery. A heat exchanger consists of heat transfer elements like matrix or containing the surface for heat transfer and fluid moving gaps called inlet and outlet. Generally, it doesn't contain any moving parts. Extended surfaces called fin can be preferred to increase the heat transfer surface area in the side where the fluid with lower thermal conductivity. Classification of heat exchangers based on construction is shown in Figure 1.2.

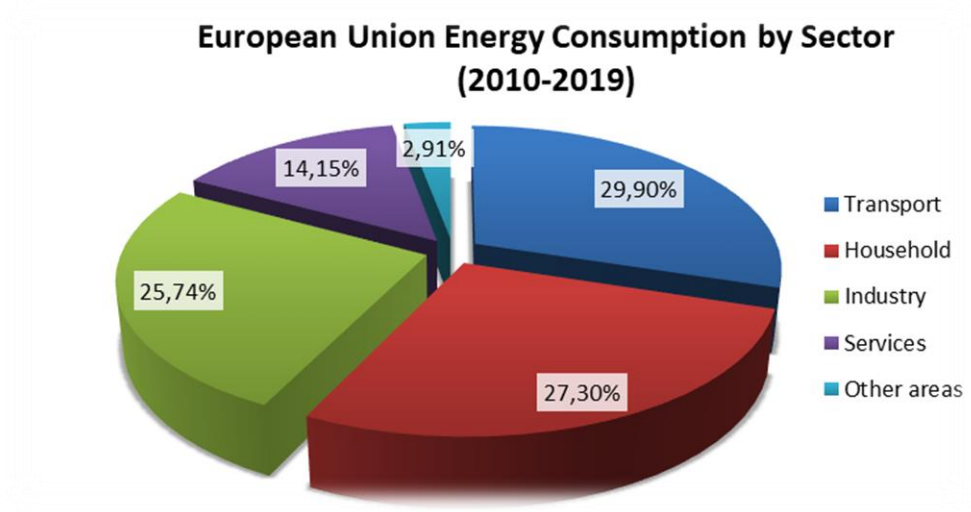


Figure 1.1. Energy consumption of European Union by Sector (average value between 2010 and 2019) (Buzatu et al., 2021)

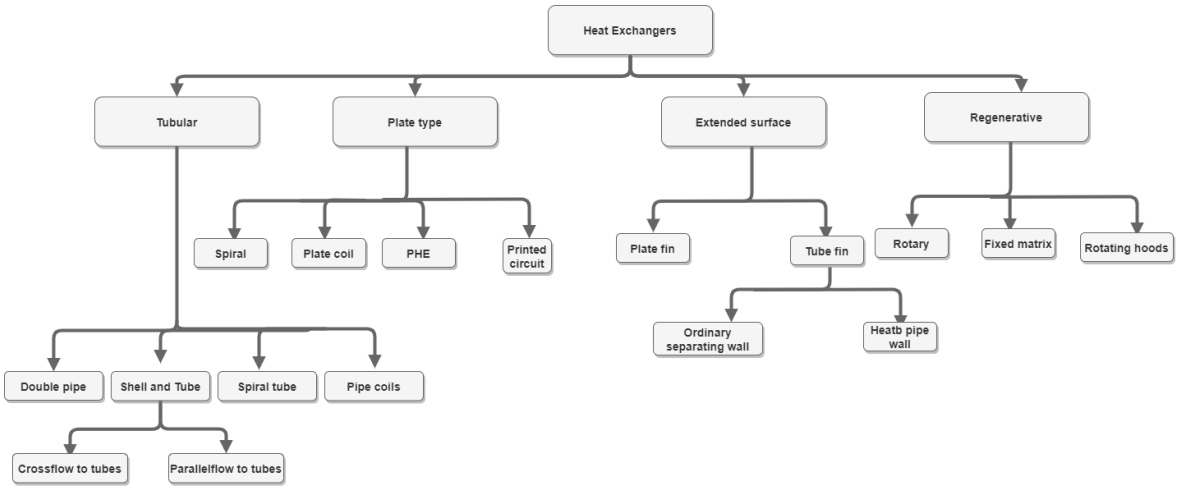


Figure 1.2. Heat exchanger classification based on construction (Shah and Sekuli, 2003)

Tube banks which are the sub component of shell and tube heat exchangers are broadly employed design components in heat exchangers. They are usually used in boilers, steam generators, Waste Heat Recovery Units, and Heat Recovery Steam Generators. The flow may be either single phase or multiphase such as boiler and condenser applications. Generally, one fluid flows over the tubes, while the other fluids at a different temperature flow through the tubes. Tube bank geometry is characterized by the transverse pitch and the longitudinal pitch between the tube centers. Reynolds number of the flow is usually defined based on the minimum possible cross section.

Most used tube bank configurations are inline and staggered arrangements. In general, inline arrangement is preferred for minimum pressure drop and staggered arrangement is preferred for maximum heat transfer (Baghban, 1987). Tube banks are frequently employed in shell and tube heat exchangers, which are used in practically all industries.

Heat transfer can be increased by the following ways:

- Making thinner the boundary layer: boundary layer can be reduced by placing grooves and ribs on the surface of heat transfer. These bumps disrupt the boundary layer to prevent thick boundary layer.
- Increasing the surface area: surface area can be increased by the usage of fins.
- Improving the fluid mixing:

Computer-aided analysis has helped improve engineering designs in many fields. Computational fluid dynamics (CFD) provides reliable solutions for industry with the help of improved computer technology. Compared to experimental studies, numerical method is much more popular due to the cost constraints of experimental test setups. In contrast, a single powerful computer can implement the numerical calculations and gives the results which have a high degree of agreement with the experimental studies (Erguvan, 2018).

2. PRELIMINARY WORK

2.1. Circular Tube Banks

The first studies of flow around a single tube with a circular cross-section were carried out in the the beginning of the 20th century. Pioneering researchers such as Reiher (1928), Griffiths and Awbery (1933), Hilpert (1933), and Zukauskas and Ziugzda (1985) investigated the cross flow around a single cylinder for different fluid velocities.

Fand (1965) investigated heat transfer around a single circular cylinder in crossflow for a Re range from 10^4 to 10^5. Experimental results were compared with the correlation of McAdams and a new correlation was derived.

Zukauskas (1972) made a comprehensive study on inline and staggered arranged tube banks. Comprehensive experimental data was analyzed in Reynolds number changed from 1 to $2x10^6$ and Prandtl number from 0.7 to 500. Values such as skin friction coefficient, drag coefficient, heat transfer and velocity distribution were monitored in detail.

Ishigai et al. (1972) made an experimental study on flow characteristics of two circular tubes with various configurations. It was seen that the vortex shedding frequency mainly depended on the size of vortex formation. Karman vortex was generated when longitudinal pitch was above 3.8. It was also observed that the size of vortex was highly affected by the distance between the tubes.

Ishigai and Nishikawa (1975) carried out a visualization study on cross flow around circular cylinders using Schlieren method. It was observed that basic characteristics of vortex formation highly rely on Coanda effect and tube spacing. For double row tubes, vortex is formed when transversal dimensionless pitch ratio is larger than 2 and longitudinal pitch ratio larger than 3. However, for single row tubes vortex formed when S_L^* is smaller than 1.5.

Churchill and Bernstein (1977) made a correlation study of heat and mass transfer on a circular cylinder in crossflow. Developed single equation embodies all range of Pr number and obtained data range of Re number. The composed equation was compared with the various experimental results from the literature.

Launder and Massey (1978) made a numerical study on laminar flow around staggered circular tube bank. Finite difference method was preferred to calculate flow behavior. Radial type meshes were used in the zone close to cylinder boundaries where the highest gradient occurs while the other zones were filled with Cartesian meshes. The obtained results were compared with the experimental results from the literature.

Aiba et al. (1980) made an experimental study on heat transfer and flow performance of inline arranged circular tube bank. Experiments were conducted for the Re numbers from 10000 to 50000 and pitch ratio from 1.15 to 3.4. The results showed that heat transfer value increases steeply for all cylinders till the pitch ratio of 1.3. For 1st and 2nd cylinders, maximum value is obtained at the pitch ratio of 1.5. However, there was no a distinct peak point for 3rd and 4th cylinders. In

addition, maximum pressure coefficient value was obtained between 3rd and 4th cylinders.

Aiba et al. (1982) carried out an experimental study on heat transfer and pressure drop behavior of inline tube bank. Experiments were implemented for seven rows under different longitudinal and transverse pitch ratios at Reynolds number ranging from 10^4 to $6x10^4$. Turbulence intensity at the upstream flow was measured as 2 to 6% for different cylinder arrangements. It was determined that local Nusselt number distribution trend is similar for third and further rows. Maximum local Nusselt number was obtained at about 50˚.

Zukauskas and Ulinskas (1985) made a correlation study on fluid flow and heat transfer characteristics flow over circular tube bank with inline and staggered arrangements based on previous experimental studies. Equations were obtained for the Re range from 1 to $2x10^6$ and Pr range from 0.7 to 10^4.

Fujii et al. (1984) carried out and numerical study of laminar flow over inline arranged tube bank. Finite difference equations were solved using explicit method to determine the pressure drop and heat transfer characteristics for the Re numbers of 60, 120 and 300. Periodic boundary condition was applied to save time and memory. Results showed that friction factor and average Nu number agree well with the experimental results of previously published papers.

Chen et al. (1988) made a numerical study on inline and staggered arranged circular shaped tube bank for laminar flow using finite element method. In addition to variation of surface shear stress Nusselt number and pressure drop characteristics were also evaluated. It was seen that maximum Nu number was obtained at the front and minimum Nu number was achieved at the rear stagnation point. It was also stated that heat transfer was influenced by both temperature difference and velocity.

Similarly, Beziel and Stephan (1992) implemented an experimental study on in line arranged circular tubes. Experiments were carried out for a Re number range from $4x10^3$ to $2x10^5$. Measurement shown that turbulence intensity which is varied between 0.8% and 38.8% increased with the increment in dimensionless longitudinal axis. It was also seen that drag coefficient increased till $2x10^4$ and started to decrease sharply after this point.

Zdravistch et al. (1995) carried out a numerical study on laminar and turbulent flow over circular shaped tube banks. Cell centered finite volume method was used to obtain discrete mass conservation and periodic boundary condition was applied using 3D geometry. 3D streamlines showed that turbulent flow has a higher resistant to adverse pressure gradient than laminar flow resulting weaker corner vortex. Nu number distribution was different for the first row due to no wake shading effect at the front of the first row. Consequently, thinner boundary causes a higher temperature gradient and hence higher heat transfer.

Mandhani et al. (2002) presented a numerical study on cross flow of staggered arranged circular tube bank using finite difference method for the Re number range of 1 to 500. Porosity, Prandtl number and Re number were used as parameters. Moreover, type of thermal boundary

conditions (constant heat flux and constant temperature) was compared. It was seen that minimum value of Nu number is obtained at the rear zone of the cylinder. It was also stated that increasing porosity results in decreasing Nu number for the range of studied Re number. Moreover, constant heat flux results in higher Nu number than a constant temperature condition.

Rahmani et al. (2005) presented a numerical study on laminar flow around staggered tube banks. Finite volume method is applied to solve the governing equations for the three different staggered tube bank configurations, which are equal spaced, equilateral triangle and rotated square (see Figure 2.1). Results verified that local friction coefficient and Nu distribution is lowest at first tube for all three configurations. It was also highlighted that, average skin friction coefficient decreases by increasing Re number.

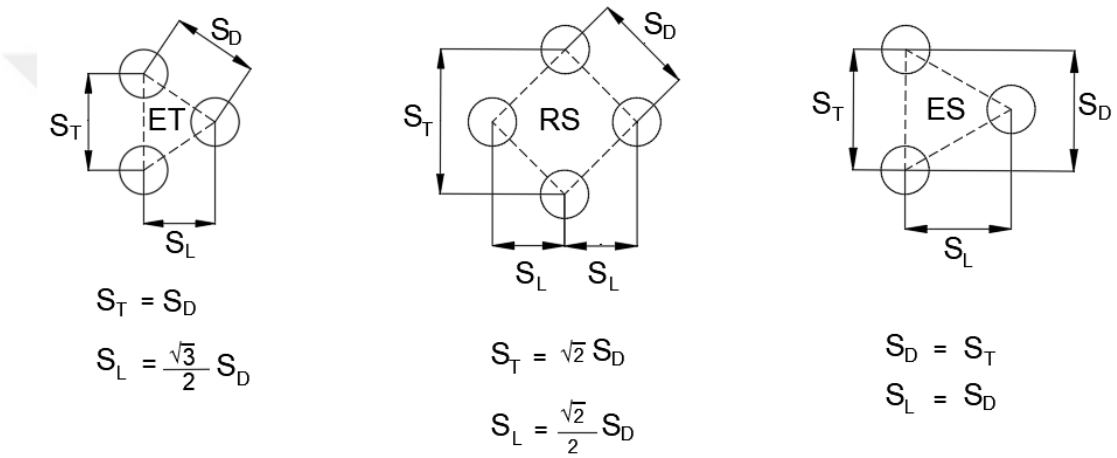


Figure 2.1. Different circular tube bank arrangements studied by Rahmani et al. (2005)

Khan et al. (2006a; 2006b) carried out an analytical study to evaluate heat transfer of circular tube bank in cross flow for both inline and circular arrangements. The obtained Nu value equation was dependent on the variables Re, Pr, longitudinal and transversal pitch ratio for both tube arrangements. Analytical results also compared with the empirical and experimental results from the literature.

Yoo et al. (2007) made an experimental study on heat transfer characteristics of staggered arranged circular tube bank. Naphthalene sublimation technique was used to monitor local mass transfer coefficient to make heat/mass transfer analogy. Results indicated that local heat transfer pattern varies from first to third tube after that they showed similar behavior. It was also seen that, minimum local heat transfer coefficient were obtained where transition to turbulence zone and turbulence boundary layer separation zone.

Erguvan and MacPhee (2019) carried out first and second law efficiencies of crossflow over inline arranged circular tube bank. Reynolds number, inlet temperature, pitch ratio, number of cylinder rows and heat transfer coefficient were used as parameters. For adiabatic condition, it was seen that increment in Re number of cylinder row results in lower energy and exergy efficiency.

Whereas, increment in energy and exergy efficiency was obtained from a Re number of 500 to 5000 for nonisolated condition. Primary reason of this is the high heat loss at low Re numbers which causes low efficiency values.

Sayed Ahmed et al. (2013) made an experimental and numerical study on heat transfer and effectiveness behavior of staggered arranged wing shaped tubes at various angle of attack. Their study covered the Re number range of 1800 and 9700 for different angle of attack from 0˚ to 330˚. Results showed that heat transfer was increased while angle of attack increased from 0˚ to 45˚ and decreased while angle of attack increased from 135˚ to 180˚. Maximum effectiveness value was obtained at 0˚ angle of attack. Furthermore, correlation study was made for Nu, St and heat transfer per unit pumping power.

Vessakosol and Charoensuk (2010) conducted a numerical study the effect of fouling on heat transfer around a circular cylinder using control volume finite element method (CVFEM). Analysis was performed using conjugate heat transfer approach for inline flow. It was seen that local heat transfer number decreases (mostly at the front side) with decreasing thermal conductivity ratio (ratio fouled layer thermal conductivity to fluid thermal conductivity). It was also determined that eccentricity reduces the side effect of fouling.

Beale and Spalding (1998) implemented a numerical study of the heat transfer and flow behavior of tube bank in cross flow. Computer program PHOENICS was used for square, rotated square and triangular arrangements assuming the periodic flow for the Re number from 10 to 1000 for different pitch ratio and Pr number. Results indicated that, there were significant differences in Nu curves for the three arrangements.

Lee et al. (2013) made a numerical study on unevenly longitudinally spaced even rows inline tube banks. Nu number of each row was measured independently to see the effect of different distributions. It was observed that there was a weak effect of dimensionless transverse pitch ratio on Nu number for various Re. Local Nu number significantly influenced by the uneven pitch ratio (S_{L1}/S_{L2}). It showed a trend of oscillation with rising pitch ratio.

Mehrabian (2006) made an experimental study on heat transfer and pressure drop behavior of circular shaped tube bank in cross flow. In addition to Nu number and velocity at different positions between successive tubes upstream and downstream velocities were measured at various throttle points. Moreover, an equation was derived to calculate drag coefficient by using upstream velocity and static pressure drop value.

Ikpotokin and Osueke (2014) made a research on heat transfer and flow characteristic for inline circular tube bank numerically and experimentally. FEMLAB 3.0 was utilized to simulate the study. It was seen that bypass stream occurs between the tubes. Additionally, vortex formation was observed in the recirculation zone.

Shah et al. (2013) carried out a numerical study on staggered arranged circular tube bank for Re number below 100. Pressure drop and friction factor values were compared with the correlation.

Molki and Bhamidipati (2004) made an experimental study on heat transfer behavior of circular tubes in the developing region induced by coronal wind. Experiment were conducted in the transition range of turbulent flow for the Re number range of 2500-13000. The study revealed that maximum increment of local and average heat transfer coefficients were 23% and 8%, respectively.

Erguvan and MacPhee (2018) examined the energy and exergy behavior of flows over circular cylinders. Numerical simulation for the unsteady flow was carried out for the Re range from 5000 to 30000. Their results showed that energy and exergy efficiency rangers were 72-98% and 40-64%, respectively. It was also highlighted that pitch ratio was a critical parameter to minimize the exergy destruction.

Ram et al. (2016) investigated the inline arranged circular tube bank for two dimensional laminar flow conditions. Flow was modeled considering periodic flow regime for the Reynolds range of 1-40 and Pr number range of 0.7-100. It was determined that drag coefficient decreases with increasing Re and volume fraction.

Wilson and Bassiouny (2000) presented a mathematical method for calculating heat transfer and pressure drop using the finite volume method for staggered tube bundles. The highest average values of Nusselt number are obtained when S_L is close to 3. Increasing S_L leads to an increase in pressure drop. It was also seen that there was no significant improvement in pressure drop and average Nusselt number for values of S_L above 1.5.

Alavi and Goshayeshi (2009) numerically investigated the non-isothermal fluid flow around inline arranged circular tube bank. Petrov-Galerkin scheme was applied to solve the governing equation. It was found that thin boundary layer on the first tube surface causes a higher temperature gradient.

2.2. Different Shaped Tube Banks

Castiglia et al. (2001) made study on subcritical crossflow over inline arranged elliptical tubes both numerically and experimentally. Experiments were performed in a closed-loop water tunnel and tubes were made of acrylic plastic. Numerical study of subcritical flow was made using large eddy simulation method. It was inferred that nearly same turbulence level was observed through the successive rows. In addition, a weak vortex shedding phenomena was observed with a Strouhal number of 0.11.

Tanda (2001) conducted an experimental study of the heat transfer and pressure drop characteristics of diamond shaped geometries in staggered and inline arrangements. The longitudinal and transverse distances were 4 to 8 and 4 to 8.5 for the inline and staggered arrangements, respectively. Liquid crystal thermography was attached to measure the heat transfer coefficients. It was found that heat transfer was improved by 65% for the same pumping power compared to rectangular geometries. In addition, correlations were also made to determine the average Nusselt number.

Ibrahim and Gomaa (2009) investigated heat transfer and pressure drop characteristics of elliptic tube bank in a cross flow experimentally and numerically. Reynolds number, pitch ratios and angle of attack were used as parameters. Results showed that maximum heat transfer was obtained at 90˚ of attack angle. However, maximum area goodness factor, which considered both heat transfer and pressure drop, obtained at 0˚ of attack angle. Moreover, correlation was given for Nu number and friction factor based on the studied three parameters.

Park et al. (2015) numerically and experimentally investigated the cross flow over elliptic tube bank for a Re range of 7190-50350. Outcomes revealed that elliptical cylinder has significantly lower friction loss with only a 9% lower Nu value. Experiments were implemented for inline two rows tube bank and water was used as working fluid. It was seen that flow separation starts in the range of 120 to 140˚ and 80 to 100˚ for elliptic and circular geometries, respectively (see Figure 2.2).

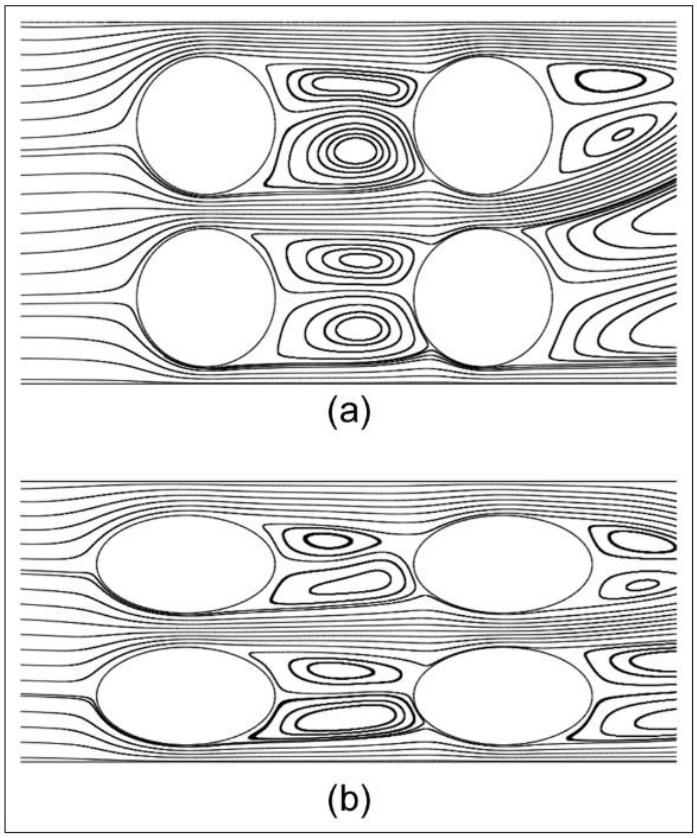


Figure 2.2. Streamlines around (a) circular and (b) elliptic shaped tubes at Re:2382 (Park et al., 2015)

Widodo and Hanifah (2016) presented a numerical investigation flow over staggered elliptic tube bank. Transversal and longitudinal pitch ratios were used as parameters at constant heat flux condition and RNG k-e model was used to model turbulence flow. Their study showed that highest heat transfer performance was obtained at the configuration with lowest transversal and longitudinal pitch ratio.

Bayat et al. (2014) made an experimental study on fluid flow and heat transfer performance of cam shaped tube bank. Experiments was performed for the Re number range of 27000-42500 using air as working fluid. It was revealed that drag coefficient of cam geometry was 64% lower than that of circular ones. Friction factor was approximately 92.5% lower than circular tube banks.

Saraireh et al. (2017) carried out a numerical study on heat transfer characteristics of inline and staggered arranged elliptic tube bank. Results shown that average Nu number increased by more than 35% when Re number increased from 400 to 600. It was also seen that inline arrangement showed better heat transfer performance than staggered arrangement.

Gharbi et al. (2015) carried out a numerical comparison study between circular, ellipsoid and drop shaped tube banks. Under the similar conditions pressure drop, exergy and enthalpy values were compared to determine the optimum geometry. In general, circular tube bank showed the highest pressure drop while elliptic one showed the lowest value. For entropy generation, there was no optimum geometry for all Re ranges.

Wahid et al. (2013) performed a numerical study of laminar flow around a circular flat and elliptic shaped tube bank using nanofluids. Alumina-water 4% was used as a nanofluid to compare with water. Results indicated that using nanofluid rather than a pure fluid resulted in higher pressure loss and higher Nu number value. Among studied geometries flat shaped tube bank resulted in the highest and elliptic shaped tube bank lowest Nu number value.

Fullerton and Anand (2010) made a numerical research on flow and heat transfer characteristics of flat and oval shaped tube bank for laminar flow. Control volume based finite element method is applied assuming a fully developed periodic flow and 2 dimensional geometry for the Re range of 50 to 350, and Pr numbers of 7 and 0.7. Although both of them had lower Nu number than circular shape, flat and oval tubes showed higher heat transfer performance ratio which compromise both Nu number and friction factor.

Sparrow and Grannis (1990; 1991) experimentally and numerically carried out flow characteristics on diamond shaped pin fin heat exchanger. Research was made for the Reynolds number range from 20 to 2200 and a periodic flow regime was applied for the simulation using finite element method (see Figure 2.3). Two different diamond shaped geometries which were studied, namely 45˚ and 90˚. The study showed that, geometry with 45˚ attack angle showed higher pressure loss at lower Re number where friction dominated, whereas, at larger Re number opposite was true due to the dominance of inertia.

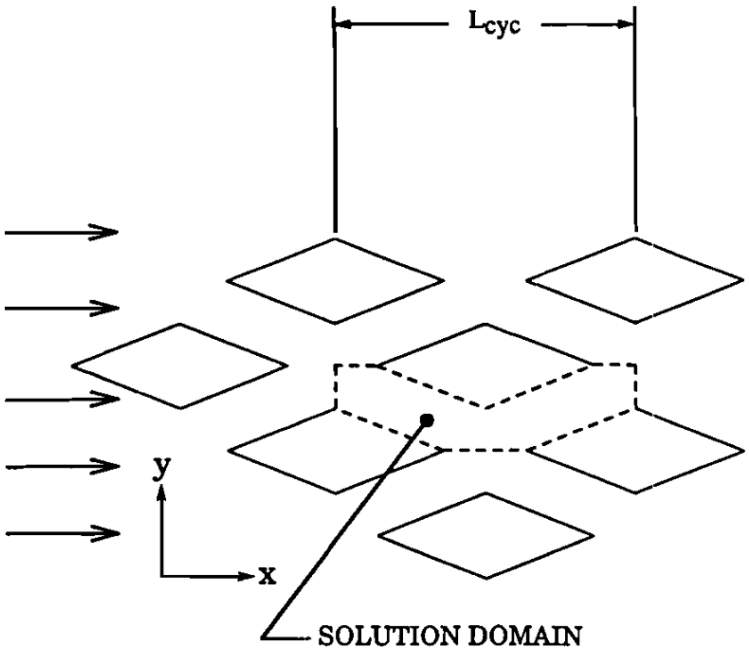


Figure 2.3. Defined solution domain for the periodic flow around diamond shaped elements (Sparrow and Grannis, 1990; Grannis and Sparrow, 1991)

Waheed et al. (2018) made a numerical study of diamond shaped tubes at constant volume to determine tube spacing using Bejan's constructal theory. Study was made for the Raylegh number in the range of 10^3 to 10^5 and axis ratio range of 0 to 0.5 for Pr number of 0.71 at constant volume. Results showed that optimum tube spacing which doesn't rely on the axis ratio decreases with increasing Rayleigh number. Additionally, the highest heat transfer values was obtained for flat tube (axis ratio=0).

Mustafa (2019) implemented a numerical study on heat transfer characteristics of single row diamond shaped tubes. Dimensionless pressure drop which was defined as Bejan number (10^3 to 10^5), and vertical axis (0.2 to 2) were used as parameters ranged from and, respectively. Results indicated that heat transfer increases with decreasing vertical axis (attack angle) and increasing Bejan number. It was also determined that rear vortices formation occurred at the Bejan number of 10^4 and vertical axis of 0.4 for optimum spacing.

Sayed Ahmed et al. (2014a) experimentally and numerically investigated a wing-shaped staggered tube bank for different angles of attack in the Re range from 1800 to 9700. It was found that the highest values of Nu number were obtained at angles of attack 45, 135, 225 and 315˚. Correlations for Nu St and the heat transfer rate for one unit of pumping power as a function of the parameters used in the design are also presented.

Sayed Ahmed et al. (2016a) presented a numerical study on heat transfer and entropy generation of a wing shaped finned tube bank in cross flow for the Re range of 1800 to 9700. Fin height and thickness were varied in a range of 2 to 12 mm and 1.5 to 3.5 mm, respectively. Numerical outcomes showed that an increment in fin length resulted in an increment in Nu number up to 36%

compared to geometry without fin. Predominated irreversibilities were obtained 1800 to 4200 and 6950 to 9700 for irreversibilities in heat transfer and friction, respectively.

2.3. Tube Bank Optimization Studies

Matos et al. (2001) carried out an optimization study to maximize the heat transfer of circular and elliptic tube banks in equilateral triangular staggered arranged. They used the finite element method for the given flow and volume for the Re range from 300 to 800. For the studied parameter range, a 13% heat transfer enhancement was obtained for 0.6 ellipses eccentricity at Re=465 compared to a circular one.

Rocha and Bejan (2001) conducted an optimization study on the flow and heat transfer characteristics of a circular tube bank. Two types of pulsating flow were considered, namely stop-and-go and back-and-forth flow assuming a fully developed periodic flow. It was found that the optimum geometry is independent of the frequency of pulsation and the type of flow.

Matos et al. (2004) carried out an optimization study on finned circular and elliptic tube banks in cross flow. Both experimental and numerical methods were applied on 3D geometries to find out the geometry with maximum heat transfer at constant volume. Determined optimum elliptic geometry showed a 19% increment in heat transfer and a 32% mass reduction was obtained compared to optimum circular one.

Ranut et al. (2014) made a shape optimization study of a tube bank in cross-flow. The 2-D geometry shape was drawn by using spline curve with 4 control points as optimization parameter. Two different genetic algorithm which were NSGA-II and FMOGA-II were used and compared. Aerodynamically efficient geometries showed low pressure drop at shell side with lower heat transfer and higher pressure drop value at tube side. Whereas, geometries with upper part are bulky showed opposite behavior for three optimization parameters.

Yilmaz and Yilmaz (2016) made an optimization study for an inline arranged circular tube bank at constant wall temperature. Gnielinski-Gaddis and Zukauskas methods were applied to calculate the heat transfer coefficient and pressure loss. By the help of prescribed optimization method heat exchanger dimensions can be determined for a given heat transfer rate.

Zeeshan et al. (2017) made an optimization study on fin tube heat exchanger with circular, oval and flat cross-sections. Multi-objective optimization on the basis of ratio analysis (MOORA) was used as optimization method. Results indicated that oval shaped tube banks have the optimum configuration with 14% heat transfer coefficient increment and nearly 40% pressure drop reduction compared to circular one.

Khan et al. (2007) carried out an optimization study on inline and staggered arranged tube bank using entropy generation minimization method. Tube diameter, tube length, dimensionless pitch ratios, heat load and frond sectional area are used as parameters to minimize generated entropy. For each condition optimum approaching velocity was determined. It was determined that lower

approaching velocities and longer tubes were better for staggered arrangement compared to inline arrangement.

Sahamifar et al. (2019) made a numerical optimization study on cross flow around staggered tube bank using a generalized pattern search algorithm (GPSA). A simulation was carried out to reach the optimum transverse and longitudinal pitch ratios for various Reynolds and Pr number. It was verified that optimum transverse and longitudinal pitch ratios, which were independent from Re and Pr were roughly 1 and 1.3, respectively.

Ge et al. (2021) investigated an optimization study on staggered arranged five tubes with 25 polar radii as design variables using MOGA and CFD software coupled to each other. TOPSIS (The Technique for Order of Preference by Similarity to Ideal Solution) was preferred as optimization algorithm. Compared to circular one optimum configuration showed 7.6% heat flux increment or 27% pressure drop reduction for the same heat flux.

Erdinc et al. (2021) carried out an optimization study on thermal and flow behavior of staggered arranged circular and diamond shaped elements using MOGA. Initially, optimum circular configuration was obtained using the objective of minimum pressure loss and maximum total heat transfer. In the second section optimum diamond shaped designs were determined with the same objectives in the first section using the heat transfer and pressure loss values of optimum circular design as constraint. Results indicated that Nusselt number of optimum shaped elements was 10.11% higher and pressure loss value was 11.9% lower than the optimum circular configuration. Moreover, 52.76% of total volume reduction was obtained with the optimum diamond shaped elements. (The details about this study are given in the Appendix section.)

3. MATERIAL AND METHOD

3.1. Description of Methodology

In order to carry out the numerical analysis following assumptions are made for the flow:

- Steady state, incompressible and turbulent flow
- Constant thermophysical properties of the fluid
- Uniform fluid inlet velocity
- Radiation and conduction heat transfer are neglected

To make the definition of the problem, all three governing equations must be solved.

Over the computation domain, implemented turbulence equations, as well as conservation equations, are given below (Ansys Fluent User's Guide, 2013):

The conservation of mass is given by:

$$\frac{\partial}{\partial \mathrm{x_i}}\left(\rho u_j\right) = 0 \tag{1}$$

The conservation of Momentum equation

$$\frac{\partial}{\partial \mathrm{x_j}}\left(\rho u_i u_j\right) = -\frac{\partial p}{\partial \mathrm{x_i}} + \frac{\partial}{\partial \mathrm{x_j}}\left[\mu\left(\frac{\partial \mathrm{u_i}}{\partial \mathrm{x_j}} + \frac{\partial \mathrm{u_j}}{\partial \mathrm{x_i}}\right)\right] + \frac{\partial}{\partial \mathrm{x_j}}(\mu_\mathrm{t}\left(\frac{\partial \mathrm{u_i}}{\partial \mathrm{x_j}} + \frac{\partial \mathrm{u_j}}{\partial \mathrm{x_i}}\right)) \tag{2}$$

The Energy Conservation is written as follows:

$$\frac{\partial}{\partial \mathrm{x_j}}(\rho u_i T) = \frac{\partial}{\partial \mathrm{x_j}}\left(\frac{\mu}{Pr}\frac{\partial \mathrm{T}}{\partial \mathrm{x_j}} + \frac{\mu}{Pr_t}\left(\frac{\partial \mathrm{T}}{\partial \mathrm{x_j}}\right)\right) \tag{3}$$

Turbulent flow is fairly complicated phenomenon and representation of flow characteristics is not easy. Therefore, modeling of turbulence is one of the most important subjects of fluid dynamics. Although, Reynolds averaged Navier-Stokes (RANS) equations can also define the turbulent flow, but it is not possible to give the all details of turbulent flow. Today there are numerous turbulent models described in numerical solution packages. Some of them are much closer to experimental results than the others. In this study RNG k-ε model is preferred which includes two equations to make the prediction of flow behavior realistically. It contains a novel formulation for the viscosity of turbulence. It accurately estimates the characteristics of flow with boundary layers

under strong adverse pressure gradients, recirculation, and (Ansys Fluent User's Guide, 2013). The equations for the turbulence kinetic energy (k) and energy dissipation rate (ε) are as follows:

$$\frac{\partial}{\partial \mathrm{x_j}}(\rho \mathrm{k u_i}) = \frac{\partial}{\partial \mathrm{x_j}}\left[\alpha_k(\mu + \mu_t)\frac{\partial k}{\partial x_j}\right] + \mathrm{G_k} - \rho\varepsilon \tag{4}$$

$$\frac{\partial}{\partial \mathrm{x_i}}(\rho \epsilon \mathrm{u_i}) = \frac{\partial}{\partial \mathrm{x_j}}\left[\alpha_e(\mu + \mu_t)\frac{\partial \varepsilon}{\partial x_i}\right] + \mathrm{C_{1\varepsilon}}\frac{\varepsilon}{k}\mathrm{G}_k - \mathrm{C_{2\varepsilon\rho}}\frac{\varepsilon^2}{k} - \frac{C_\mu \rho \eta^3(1-\eta/\eta_0)}{1+\beta\eta^3}\frac{\varepsilon^2}{k} \tag{6}$$

Here, α_k and α_ε represents Prandtl numbers of k and ε. The term $\mathrm{G_k} = \mu_\mathrm{t} S^2$ defines the generation of turbulent kinetic energy as a result of buoyancy (Ibrahim and Gomaa, 2009). Here, S stands for the mean tensor modulus of the strain-rate. Also, $C_{1\varepsilon} = 1.42$, $C_{2\varepsilon} = 1.68$, $\eta = S\frac{k}{\varepsilon}$ and $S = \sqrt{2S_{ij}S_{ij}}$, $\eta_0 = 4.38$, $\beta = 0.012$. μ_t denotes the turbulent viscosity,

$$\mu_\mathrm{t} = \rho \mathrm{C_\mu}\frac{\mathrm{k}^2}{\varepsilon} \tag{7}$$

$$\mathrm{C_\mu} = 0.0845 \tag{8}$$

3.2. Data Analysis

Following definitions are presented to make the comparison of heat transfer and pumping power of the studied three tube bank geometries.

3.3. Definition of the Tube Bank Geometries

Cross section of three-dimensional longitudinal section of cross flow tube bank of three different geometries: circular, diamond and enhanced are demonstrated in Figure 3.1 and 3.2 for inline and staggered arrangement, respectively. Air with specified inlet velocity V_in, temperature T_in, flows over the tubes. Also, constant wall temperature T_w is assigned to the tube surfaces. For circular tubes, geometric parameters are streamwise tube spacing S_L and transverse tube spacing S_T with constant diameter D. Besides, in addition to these parameters attack angle θ is prescribed for diamond tube bank. Whereas, for enhanced geometry, there are two attack angles which are: front θ_1 and rear θ_2 attack angle.

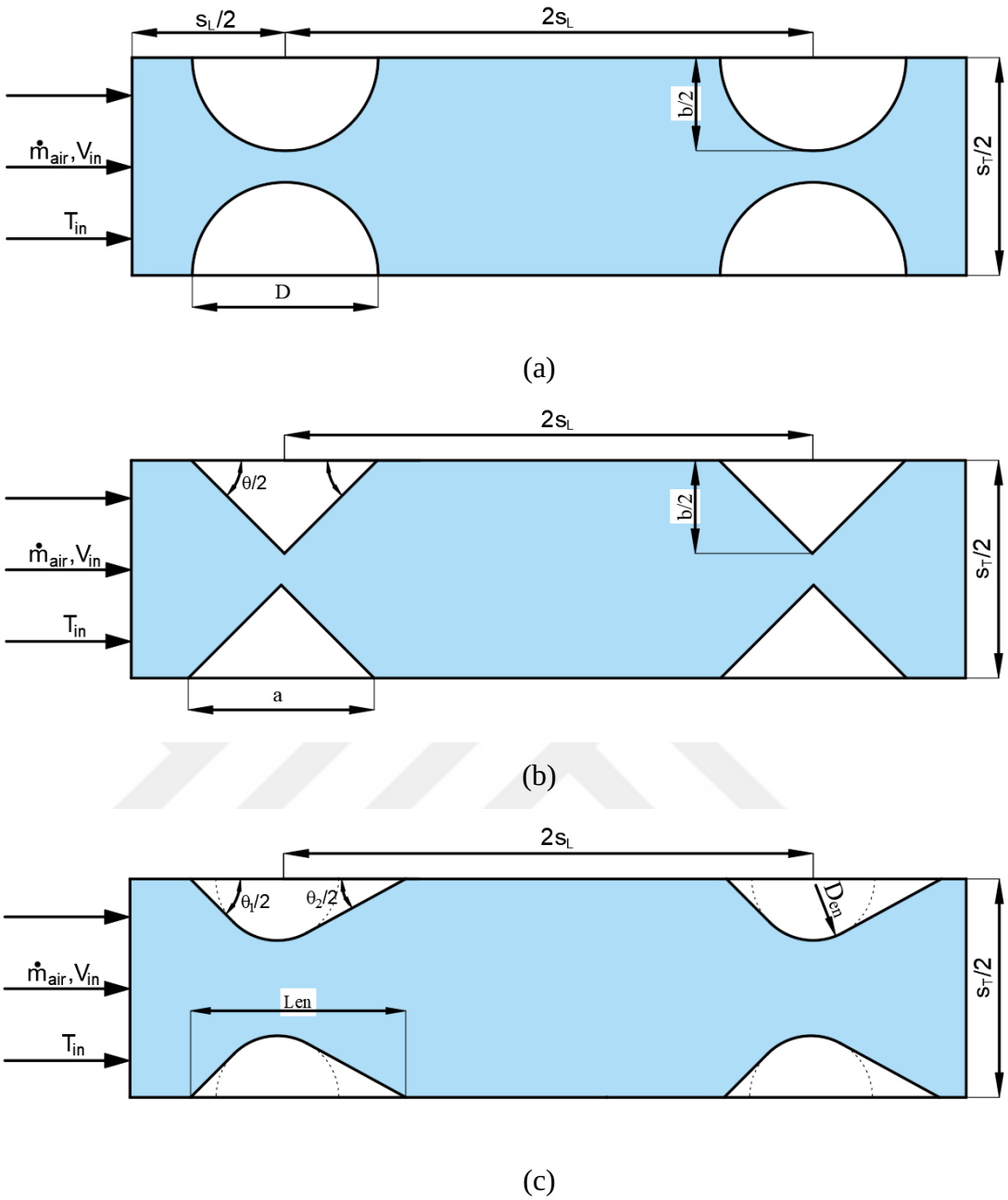


Figure 3.1. Solution domain for inline (a) circular (b) diamond (c) enhanced shaped tube banks

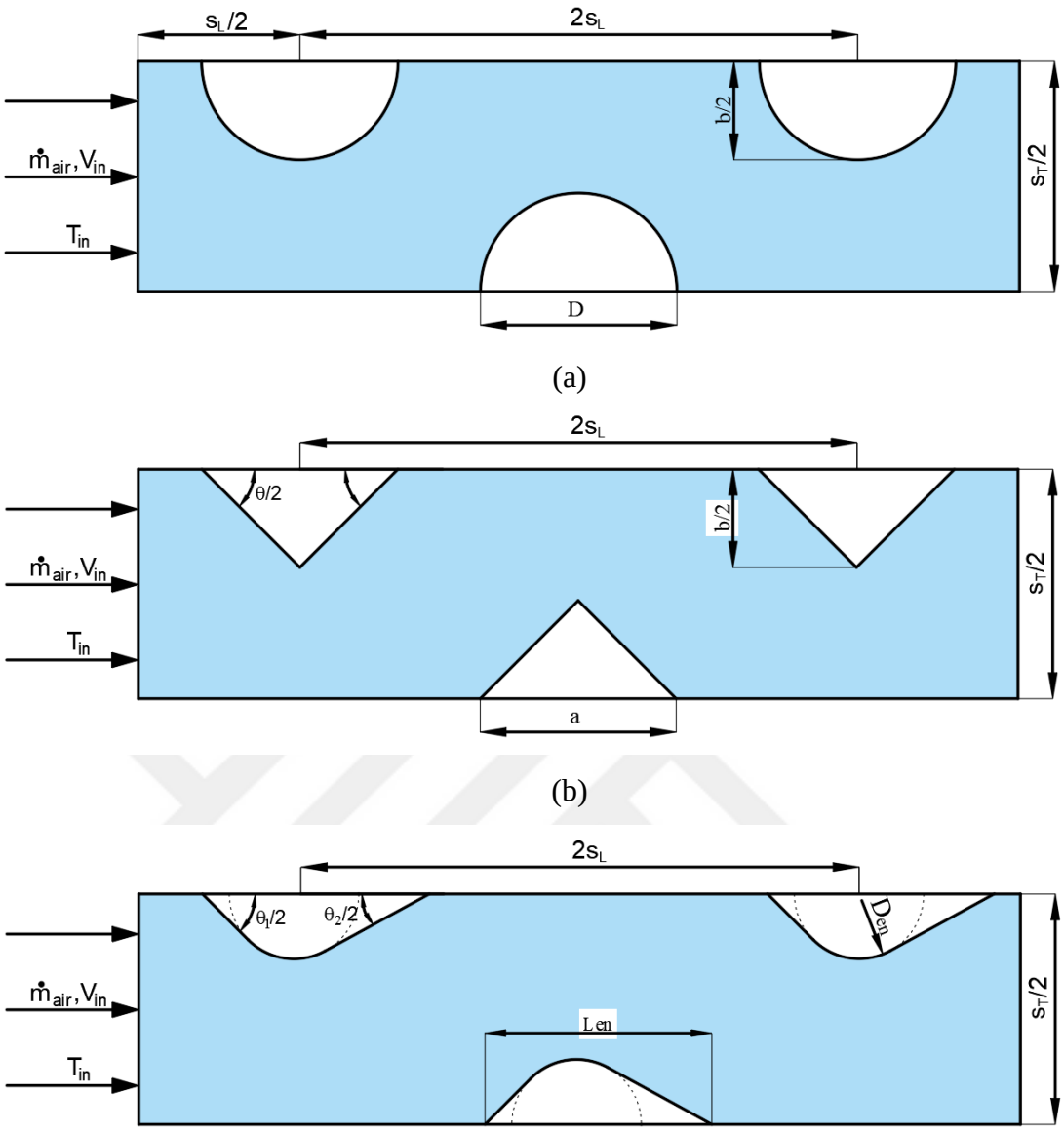


Figure 3.2. Solution domain for staggered (a) circular (b) diamond (c) enhanced shaped tube banks

Geometries are considered here in a three-dimensional form for both inline and staggered arranged tube banks.

For circular tube bank, dimensionless longitudinal and transversal pitch ratios, S_L^* and S_T^* are defined as follow:

$$S_L = S_L^* \cdot \mathrm{D} \tag{9}$$

$$S_T = S_T^* \cdot \mathrm{D} \tag{10}$$

However, for diamond shaped geometry in addition to S_L and S_T, attack angle θ should be also defined.

$$S_L = S_L^* \cdot a \tag{11}$$

$$S_L = S_L^* \cdot b \tag{12}$$

$$a = \sqrt{\frac{\pi^2 \cdot D^2}{4 \cdot \left[1 + \left(\tan\frac{\theta}{2}\right)^2\right]}} \tag{13}$$

$$b = \sqrt{\frac{\pi^2 \cdot D^2}{4} - a^2} \tag{14}$$

Where a, b and θ are longitudinal length, transversal length and attack angle of the diamond shaped tube. P is periphery which is equal for the all three geometries can be defined as follows:

$$P = \pi \cdot D \tag{15}$$

For enhanced geometry, there are two attack angles which are front θ_1 and rear θ_2, D_{en} and L_{en} are diameter of curvature and longitudinal length of the enhanced geometry.

$$D_{en} = \frac{P}{\pi\left(\frac{\theta_1 + \theta_2}{360}\right) + \frac{1}{\tan(\frac{\theta_1}{2})} + \frac{1}{\tan(\frac{\theta_2}{2})}} \tag{16}$$

$$L_{en} = \frac{D_{en}}{2 \cdot \sin\left[\frac{\theta_1}{2}\right]} + \frac{D_{en}}{2 \cdot \sin\left[\frac{\theta_2}{2}\right]} \tag{17}$$

Therefore, S_L and S_T can be easily calculated by the following equations.

$$S_L = S_L^* \cdot L_{en} \tag{18}$$

$$S_T = S_T^* \cdot D_{en} \tag{19}$$

Tube length L_D, can be calculated by the following formula.

$$L_D = \frac{2 \cdot Volume}{N_L \cdot S_L \cdot S_T} \tag{20}$$

Here, N_L is the number of the tube within the tube bank.

In order to determine the total heat transfer $\dot{Q}_{total}$, heat transfer area A_{heat} should be calculated:

$$A_{heat} = 0.5 \cdot \pi \cdot D \cdot L_D \cdot N_L \tag{21}$$

Therefore, $\dot{Q}_{total}$ can be calculated as follows:

$$\dot{Q}_{total} = \dot{q} \cdot A_{heat} \tag{22}$$

Heat flux $\dot{q}$, is assessed by the Ansys Fluent Software (Ansys Fluent User's Guide, 2013). Cross section area A_{cross}, and volumetric flow rate $\dot{V}$ of the flow domain are calculated from the following equations:

$$A_{cross} = 0.5 \cdot S_T \cdot L_D \tag{23}$$

$$\dot{V} = V_{in} \cdot A_{cross} \tag{24}$$

Required pump power $\dot{W}_{pump}$, is calculated by the following equation.

$$\dot{W}_{pump} = \dot{V} \cdot (P_{in} - P_{out}) \tag{25}$$

Inlet and outlet pressures of the flow domain P_{in} and P_{out} are also obtained from the Ansys Fluent Software ("Ansys Fluent User's Guide," 2013).

3.4. Boundary Condition

Fluid Domain of the given three-dimensional tube bank problem is shown in the Figure 3.3 representing enhanced shaped staggered tube bank. Since all three geometries are drawn in the similar flow domain only enhanced shaped one is demonstrated here. Four tube rows of staggered and inline arrangements are defined. Three-dimensional model is taken as symmetric to save the computation time. As seen from the figure, the flow field is divided into three regions which are entrance, tube bank and exit section. Length of the entrance section is 6xD to be sure that the flow is

uniform before the tube bank section. Besides, the length of the exit section is drawn as long as 12xD to prevent backflow at the outlet. Boundary condition of the inlet, outlet, wall and symmetry zone are given in Table 3.1.

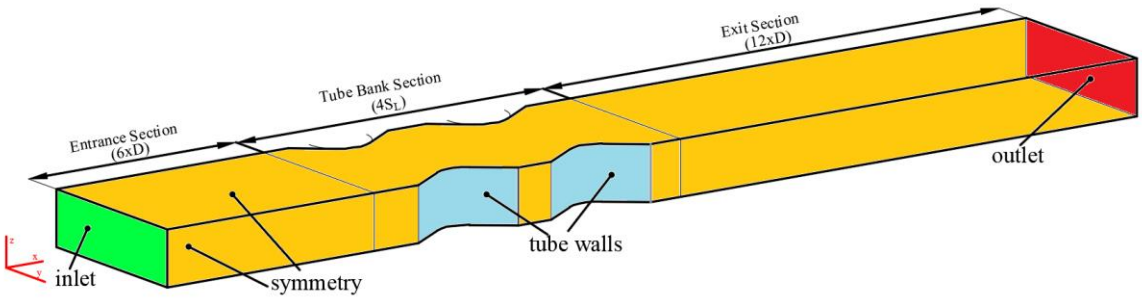


Figure 3.3. Computational domain and boundaries

Table 3.1. Boundary conditions for computational domains

Location	Description	
Inlet	• Velocity inlet	$u = u_{inlet}, v = w = 0$ $T = T_{inlet} = constant$
Symmetry	• Symmetry condition	$\frac{\partial u}{\partial y} = \frac{\partial w}{\partial y} = v = 0$ $\frac{\partial u}{\partial z} = \frac{\partial v}{\partial z} = w = 0$ $\frac{\partial T}{\partial y} = \frac{\partial T}{\partial z} = 0$
Tube Walls	• Wall • No-slip conditions	$u = v = w = 0,$ $T = T_{wall}$
Outlet	• Pressure outlet	$P = P_{atm}$ $\frac{\partial u}{\partial x} = \frac{\partial v}{\partial x} = \frac{\partial w}{\partial x}$ $\frac{\partial T}{\partial x} = 0$

3.5. Optimization Problem

In the current study, MOGA-II is used to maximize $\dot{Q}_{total}$ and minimize $\dot{W}_{pump}$ as objectives to determine the optimum designs. Multidisciplinary design optimization software modeFRONTIER is applied to solve the given optimization problems. In order to reach the optimum designs, optimization studies are implemented in two steps for inline and staggered geometry, respectively.

In the first step, comparison of circular and diamond tube banks are made with the objective functions of maximizing $\dot{Q}_{total}$ and minimizing $\dot{W}_{pump}$ for the constant volume and constant

perimeter. Formulation of the multi-objective design problem for inline and staggered arranged tube banks belong to first optimization step can be given as follows:

Input Data		T_{in} , T_w, Perimeter , Volume
Optimization Variables	Circular	$\dot{V}_{in}, S_L^*$, S_T^*
	Diamond	$\dot{V}_{in}, S_L^*$, S_T^* , θ
Objective Functions		Maximize $\dot{Q}_{total}$, Minimize $\dot{W}_{pump}$

In the second optimization step for inline arranged tube banks diamond and enhanced shaped geometries are compared with the same objective functions as the first step. For both geometries same length constraints are applied as $L_{D,max}$=1 m. Formulation of the multi-objective design of the diamond and enhanced shaped tube banks belong to second optimization step can be given as follows:

Input Data	T_{in} , T_w, Perimeter , Volume
Optimization Variables	$\dot{V}_{in}, S_L^*$, S_T^* , θ (for diamond shaped geometry), θ_1, θ_2 (for enhanced shaped geometry)
Objective Functions	Maximize $\dot{Q}_{total}$, Minimize $\dot{W}_{pump}$
Constraint	$L_D \leq 1$ m

Whereas, for the second step of staggered arranged diamond shaped tube bank optimization study is realized with a constraint of tube length $L_{D,max}$=1 m which is required to prevent unreasonable tube bank dimensions. Formulation of the multi-objective design of the diamond shaped tube bank belong to second optimization step can be given as follows:

Input Data	T_{in} , T_w, Perimeter , Volume
Optimization Variables	$\dot{V}_{in}, S_L^*$, S_T^* , θ
Objective Functions	Maximize $\dot{Q}_{total}$, Minimize $\dot{W}_{pump}$
Constraint	$L_D \leq 1$ m

For enhanced shaped staggered tube bank since L value kept constant as 1 m, volume of the tube is set free as an output parameter. Formulation of the multi-objective design of enhanced tube bank belong to second optimization step can be given as follows:

Input Data	T_{in} , T_w, D , L_D
Optimization Variables	$\dot{V}_{in}, S_L^*$, S_T^* , θ_1, θ_2
Objective Functions	Maximize $\dot{Q}_{total}$, Minimize $\dot{W}_{pump}$

3.6. Computational Details

Three-dimensional flow domain of all three geometries is created in Ansys Design Modeler. All domains including inflation layers on the tube surfaces are meshed with hexahedron construction by the help of Ansys Meshing Module. Flow and heat transfer properties are specified by solving the governing equations using Ansys Fluent Software. COUPLED algorithm is applied to resolve the coupling between pressure and velocity. Second order upwind scheme is used for energy, momentum, pressure, turbulent dissipation rate, and turbulent kinetic energy. For momentum and continuity equations, residuals are set at 10^{-5} whereas for energy equation it is set at 10^{-8}. modeFRONTIER software is coupled to Ansys Workbench to solve the optimization problems.

Process flow of the optimization problem is depicted in Figure 3.4. MOGA-II is preferred as optimization algorithm. If the defined constraints are fulfilled the results are classified as feasible, otherwise they are classified as unfeasible.

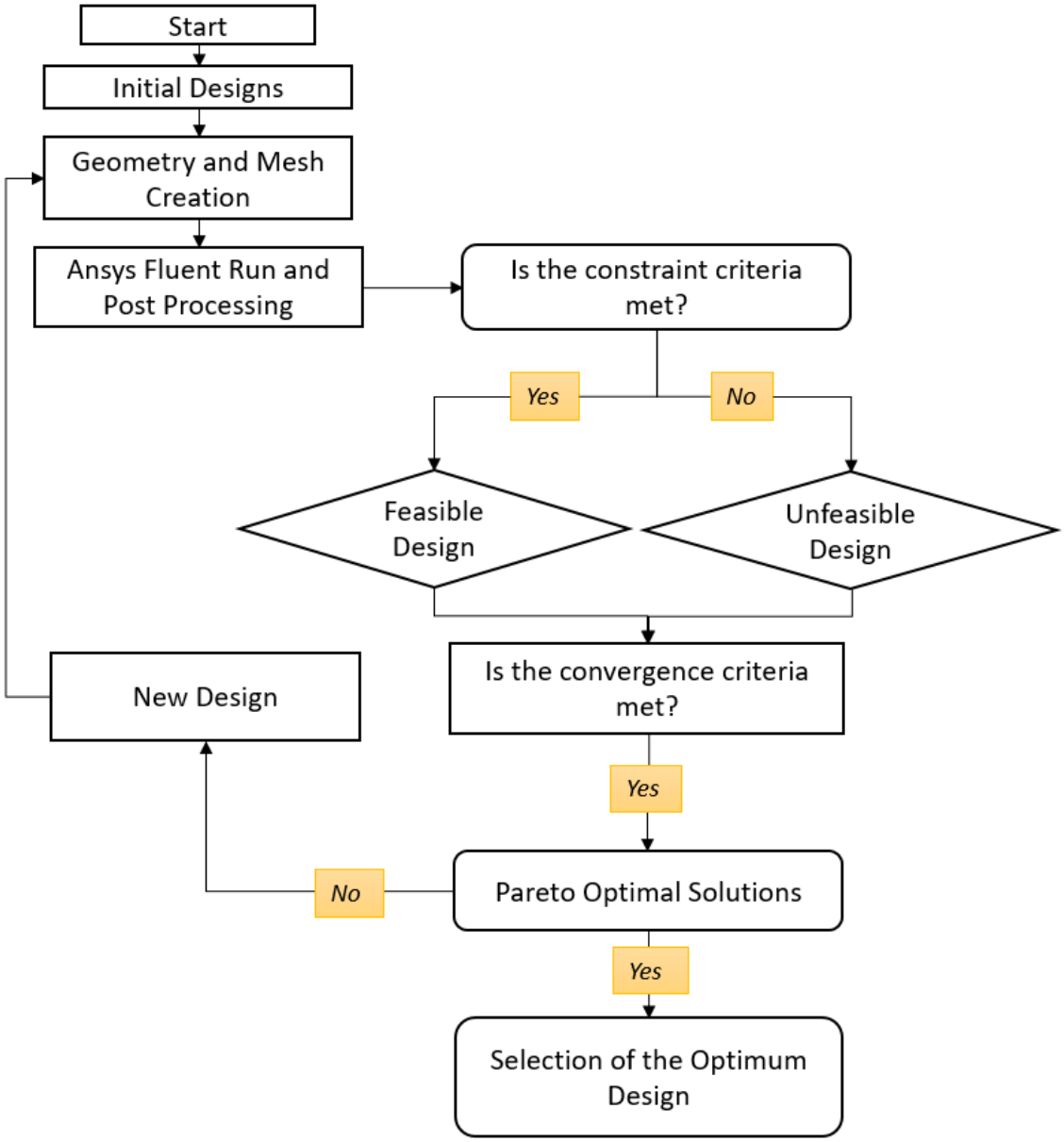


Figure 3.4. Optimization algorithm flowchart

Since formulations of the current optimization studies include more than one objective function, it is called a multi-objective optimization problem. When a set of solutions do not dominate each other and at the same time are better than other solutions, it is called a Pareto front. After that, the designer can decide the optimum design among those solutions. Designs of experiments (DOEs) which are the starting population should be designated at the first step of the optimization study. These are the input variables of the Ansys Workbench. Batch script automatically fulfills a design for the specified parametric configuration. Following the calculation, the results of the CFD analysis are used as output files for the optimization software.

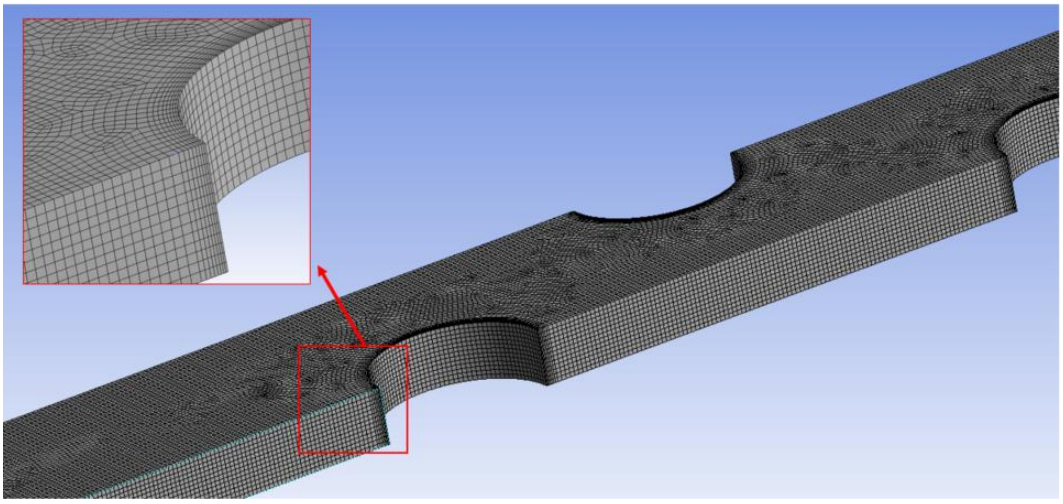


Figure 3.5. Computational mesh created for circular staggered tube bank

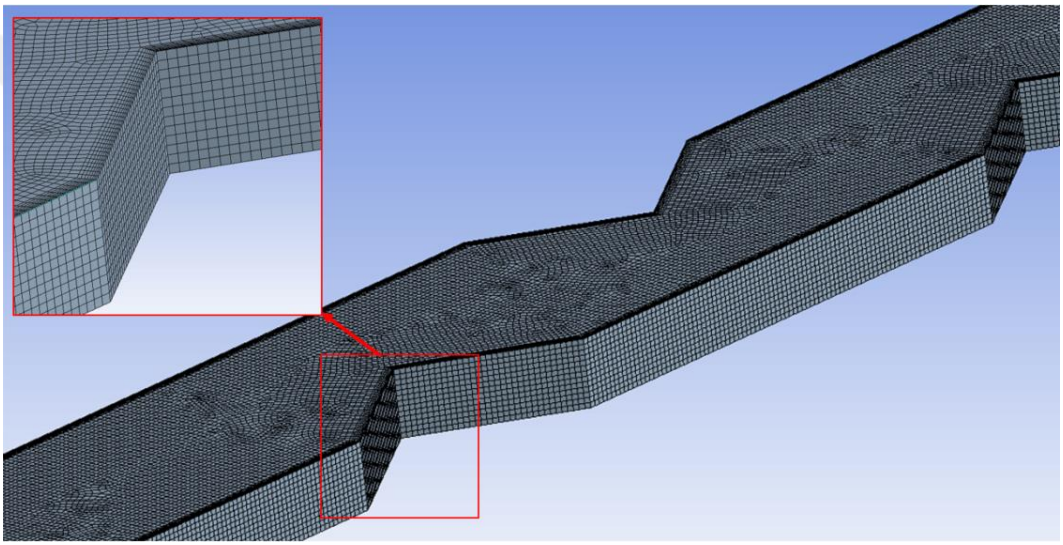


Figure 3.6. Computational mesh created for diamond shaped staggered tube bank

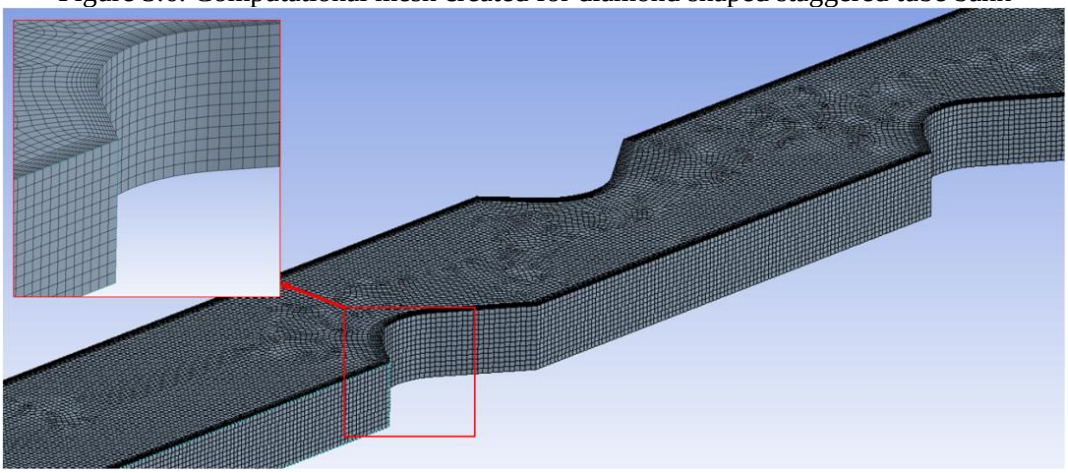


Figure 3.7. Computational mesh created for enhanced shaped staggered tube bank

As seen from Figures 3.5-3.7 hexahedron meshes are used throughout the solution domains for all three geometries using ANSYS Mesher. Around the tube wall inflation layers are created with the growth rate of 1.15.

3.7. Grid Independence Study

Four different grid numbers are used for circular staggered tube bank geometry with S_L=22.5 mm and S_T=30 mm at V_{in}=3 m/s to select suitable grid number. Obtained grid numbers for cases I, II, III and IV are 193248, 278733, 385756 and 842904, respectively as demonstrated in Figure 3.8. Differences between grid numbers I to II, II to III and III to IV are -1.907%, -1.342% and 0.097% respectively. Therefore, in order to minimize the computing resource, grid numbers of III with a good accuracy is adopted. The y+ values are kept in the range of 1 to 5.

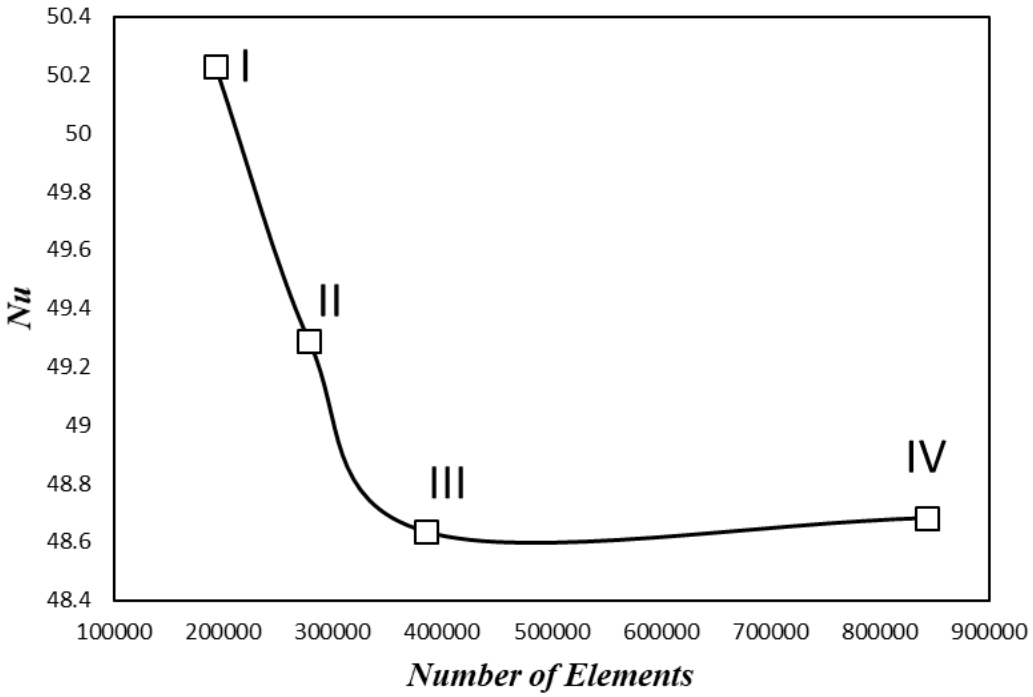


Figure 3.8. Grid independence study (Number of grids)

4. RESULTS AND DISCUSSIONS

4.1. Validation Studies

To prove the validity and accuracy of the solution model comparison of the numerical results with experimental study from must be done. In this section, pressure drop and Nusselt number values are compared with experimental studies from the literature. Since its results are closest to compared experimental results, RNG k-ε model is used to verify the relevant experimental studies. Additionally, convergence criteria are set to $1x10^{-8}$ for energy and $1x10^{-5}$ for other equations.

4.1.1. Validation of Circular Shaped Tube Bank with In-line and Staggered Arrangement

A prominent Zukauskas (1987) Nu correlation and experimental results are preferred to compare the current numerical outcomes. Input parameters for the validation study is given in Table 4.1. In these validation studies the case of flow over tube bank for 4 cylinders in flow direction is simulated. Nu correlation for inline tube arrangement is as follows:

$$\overline{Nu} = F_{in}\ 0.27\ Re^{0.63}\ Pr^{0.36}\ \left(\frac{Pr}{Pr_w}\right)^{0.25} \tag{4}$$

Where correction factor F_{in} is taken as 0.90 for 4 rows of inline tube arrangement. Similarly, Nu correlation for staggered tube arrangement is as follows:

$$\overline{Nu} = F_{st}\ 0.35\ \left(\frac{S_T}{S_L}\right)^{0.2}\ Re^{0.6}\ Pr^{0.36}\ \left(\frac{Pr}{Pr_w}\right)^{0.25} \tag{5}$$

Table 4.1. Input values for the validation study of inline and staggered tube bank

	inline	staggered
D (mm)	15	15
S_L/D	1.25	1.5
S_T/D	1.25	1.5
Fluid	Air	Air
Definition of Re	in the minimum cross-section area	in the minimum cross-section area
Number of rows	4	4
T_{in}	300 ˚C	300 ˚C
T_w	350 ˚C	350 ˚C

Where correction factor for staggered arrangement is taken as $F_{st} = 0.89$. Uncertainty of these correlations derived by Zukauskas (1987) are ± 15%. Simulations are made for Pr=0.7276 and Pr_w=0.7163 within the Re range of 3000 to 8000 for both inline and staggered tube arrangements.

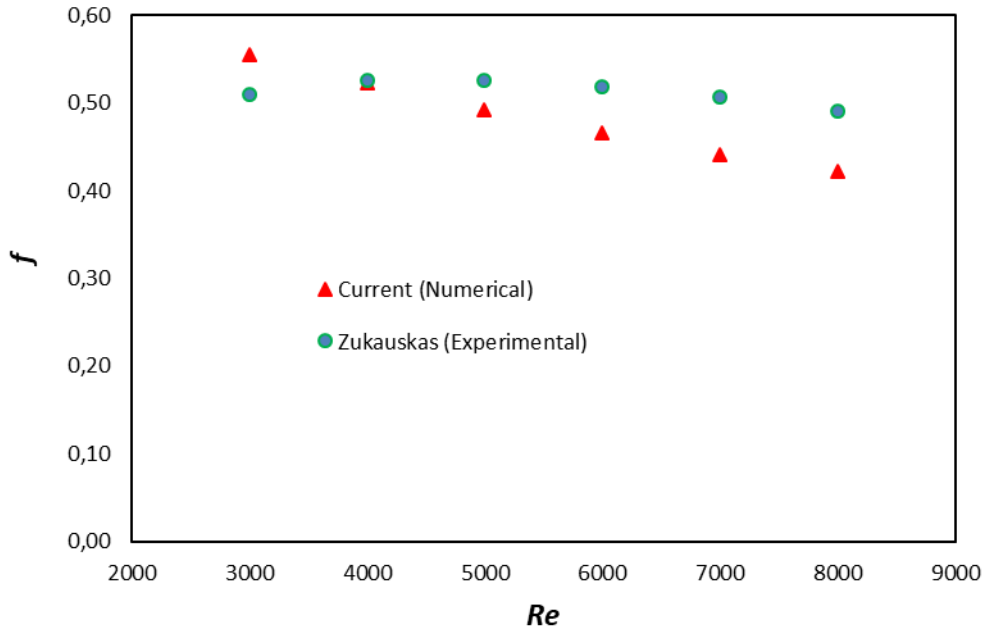


Figure 4.1. Friction Factor Comparison of Current Numerical Results with Experimental of Zukauskas (1987) for Inline Arrangement

Figure 4.1 and 4.2 show variation of friction factor and Nusselt number as a function of Re number for inline tube bank arrangement. As Re number increases friction factor decreases and Nu number increases due to increment in turbulence level resulting in enhancement in heat transfer rate. Figures indicate that there is an agreement between numerical results and experimental correlation. Difference between the numerical and experimental values of friction factor is 9.05% (at Re=3000) to -13.96% (at Re=8000) and for Nusselt number it is 8.77% (at Re=3000) to 18.78% (at Re=8000).

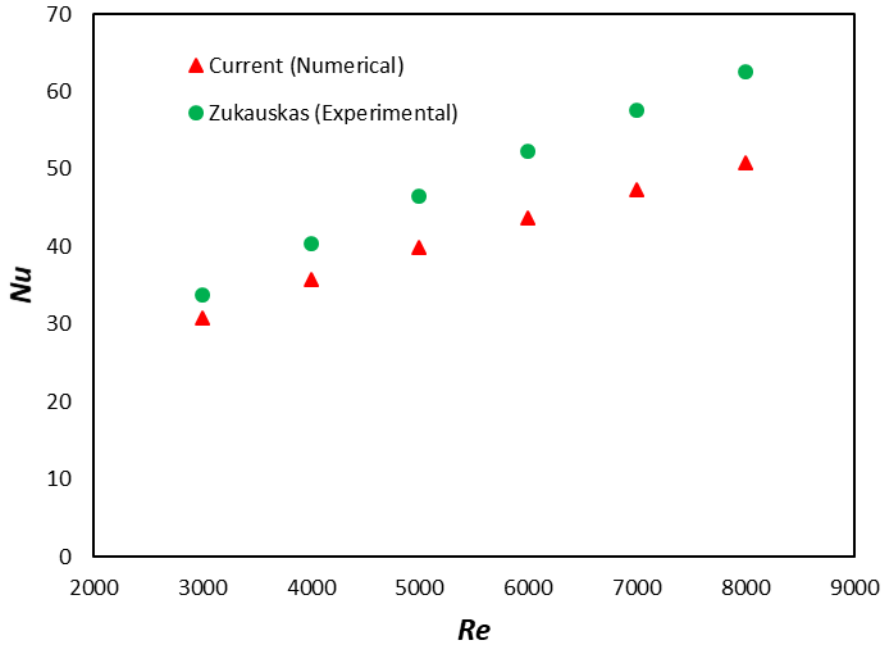


Figure 4.2. Nusselt Number Comparison of Current Numerical Results with Experimental of Zukauskas (1987) for Inline Arrangement

Figure 4.3 and 4.4 present variation of friction factor and Nusselt number with respect to Re number for staggered tube bank arrangement. Figures indicate that simulation results of the staggered tube arrangement are in good agreement with Zukauskas's experimental results. Difference between the numerical and experimental values of friction factor is -10.42% (at Re=3000) to 3.65 (at Re=7000) and for Nusselt number it is -1.97 (at Re=3000) to 5.27 (at Re=8000).

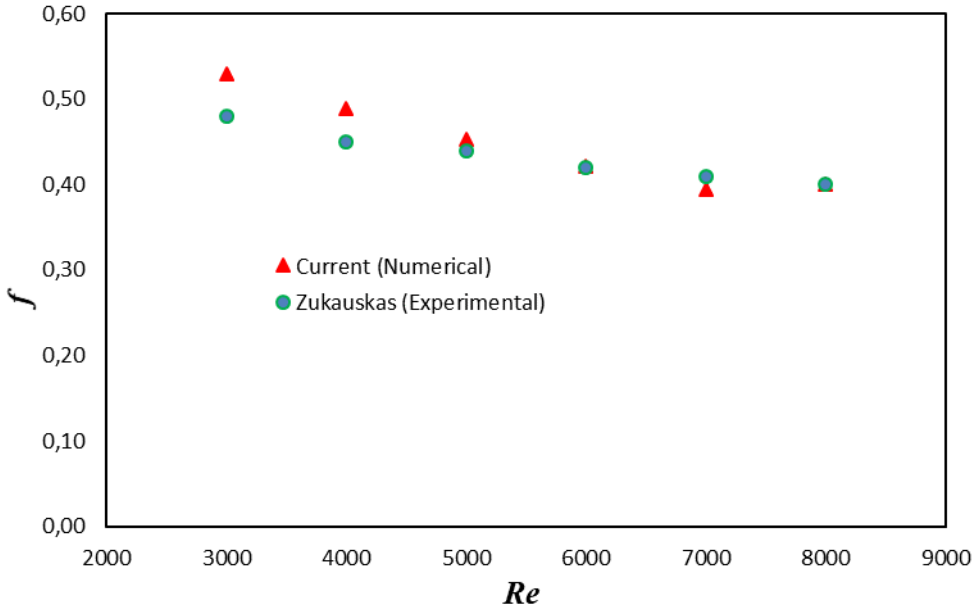


Figure 4.3. Friction Factor Comparison of Current Numerical Results with Experimental of Zukauskas (1987) for Staggered Arrangement

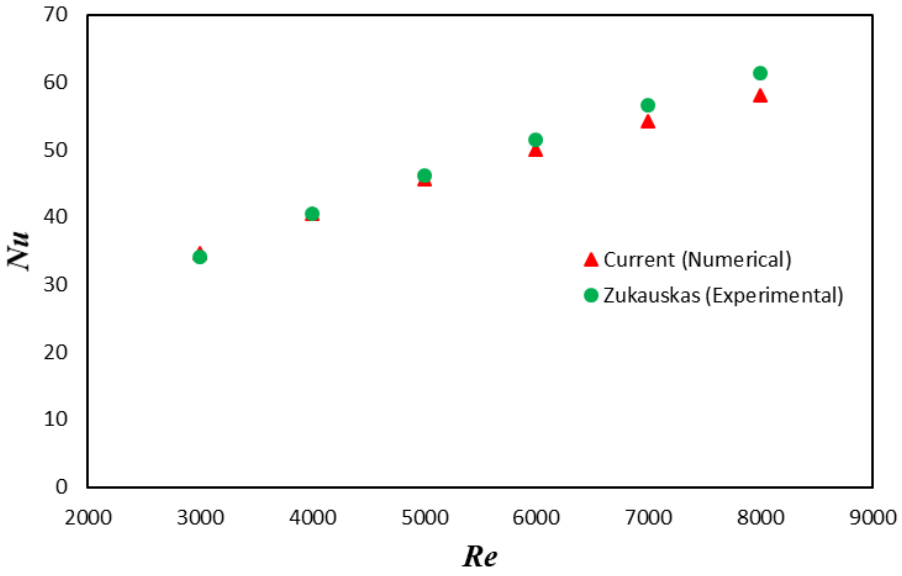


Figure 4.4. Nusselt Number Comparison of Current Numerical Results with Experimental of Zukauskas (1987) for Staggered Arrangement

4.1.2. Validation of Diamond Shaped Tube Bank with Staggered Arrangement

After the survey of literature one can see that the most similar geometry to the thesis geometry is the diamond shape. From this aspect, Sparrow and Grannis's experimental study of diamond shaped pin fin study is chosen to validate. In this data only flow characteristics around the staggered arranged diamond shaped geometries are given. Input data of the validation study is given in Table 4.2. Figure 4.5 presents variation of friction factor as a function of Re number for staggered tube bank arrangement. Figure verified that there is a good agreement between numerical result and experimental data. Difference between the numerical and experimental values of friction factor is 5.11% (at Re=546), 1.44% (at Re=902) 4.35% (at Re=1204), 7.74% (at Re=1987) and 7.41% (at Re=2222).

Table 4.2. Validation data from Sparrow and Grannis (1990; 1991)

	Sparrow and Grannis
Arrangement	Staggered
a (mm)	36.21
b (mm)	15
S_L/ b	1.73
S_T/ b	2
Vertex Angle	45
Fluid	Air
Definition of Re	in the minimum cross-section area
Re number Range	546-2222

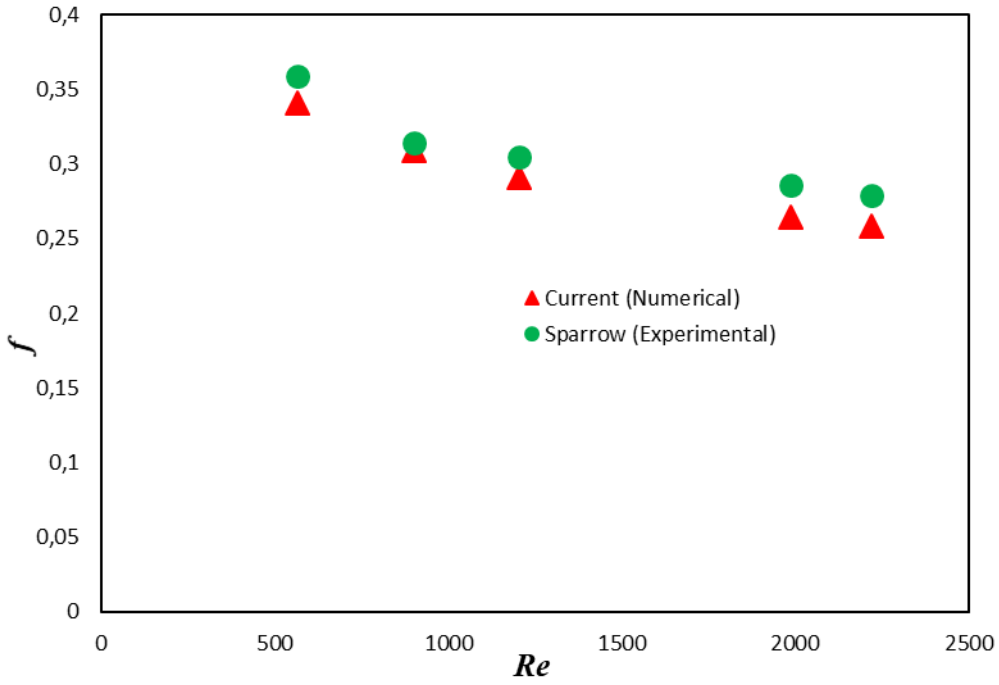


Figure 4.5. Friction factor Comparison of Current Numerical Results with Experimental of Sparrow and Grannis (1990; 1991) for Staggered Arrangement

4.2. Optimization of Tube Bank with Inline Arrangement

After reviewing the literature, it can be seen that the geometry most similar to the geometry of the thesis is the diamond shape. Therefore, optimization studies for circular, diamond and enhanced shaped geometries for staggered and inline arrangement are presented and discussed in detail.

Air with constant thermophysical properties is used as the working fluid for all optimization studies. These data were taken from (Cengel and Ghajar, 2014) for T=300 K, as given in Table 4.3. Additionally, for all optimization studies, $T_{in,}$ $T_{w,}$ V_{in} and Perimeter were kept identical and these are given in Table 4.4.

Table 4.3. Thermo-physical properties of air at T=300 K (Cengel and Ghajar, 2014)

Property	Value
ρ [kg/m^3]	1.177
Cp [kJ/kg.K]	1.005
μ [N.s/ m^2]	1.857 X 10^{-5}
k [W/m.K]	0.02565
Pr	0.7276

Table 4.4. Problem data for optimization studies of circular, diamond and enhanced-shaped tube banks

Variable	Value
T_{in} [K]	300
T_w [K]	350
$\dot{V}$ [m/s]	1-6 m/s
D [mm]	15
P [mm]	47.12

4.2.1. Comparison of Optimum Circular and Diamond Shaped Tube Bank with Inline Arrangement

Two conflicting objective functions are taken for the optimization procedure. These are maximization of heat transfer and minimization of pump power. In the current study, optimization studies are divided into two sections. In the first section, optimum geometrical configuration of inline arranged circular and diamond shaped tube banks are determined and compared to each other. Afterwards, optimum inline geometrical configuration of diamond and enhanced shaped geometries are obtained and compared.

The workflow for inline circular tube bank to be created and carried out using modeFRONTIER software.

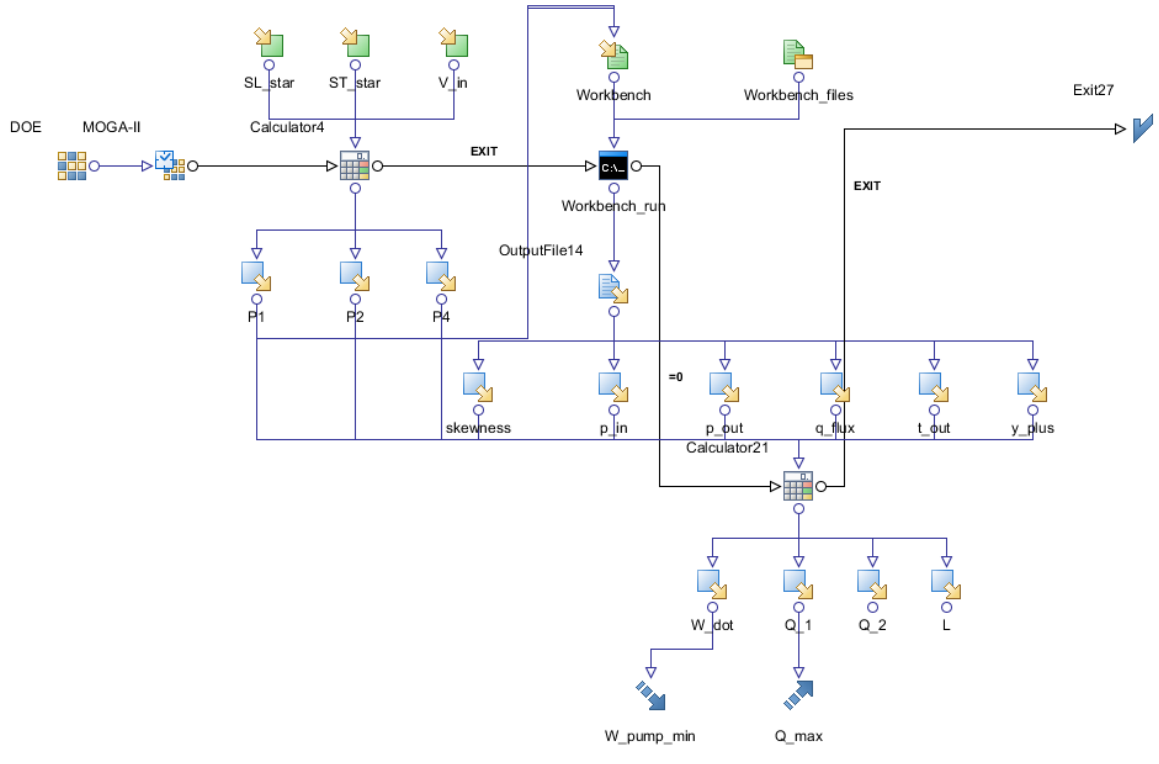


Figure 4.6. Optimization workflow for inline arranged circular geometry

Table 4.5. Multi-objective design optimization problem for circular shaped inline tube bank

Objective Functions	(1)	Maximum $\dot{Q}_{total}$		
	(2)	Minimum $\dot{W}_{pump}$		
Optimization Variables		***Lower Bound***	***Upper Bound***	***Step Size***
	V_{in} [m/s]	1	6	0.5
	S_L^*	1.2	3.0	0.1
	S_T^*	1.2	3.0	0.1

Initially, a 3D parametric geometry and mesh are generated in the Ansys Workbench environment. Afterward, the model is coupled to the optimization software to obtain designs. Figure 4.6 and 4.7 describe the optimization algorithm, design of experiments, variables of optimization, workbench files, transfer file which govern the numerical simulation, output files, input/output variables, objective functions, and constraints. Optimization problem is composed of two objective functions which are minimization pumping power ($\dot{W}_{pump}$) and maximization heat transfer ($\dot{Q}_{total}$). S_L^*, S_T^* and V_{in} are selected as optimization variables for circular arrangement. Whereas, S_L^*, S_T^*, V_{in} and attack angle θ are taken as input parameter for diamond shaped inline tube bank. Upper and lower limits and step sizes of those parameters are given in Table 4.5 and 4.6 for circular and diamond shaped inline tube banks.

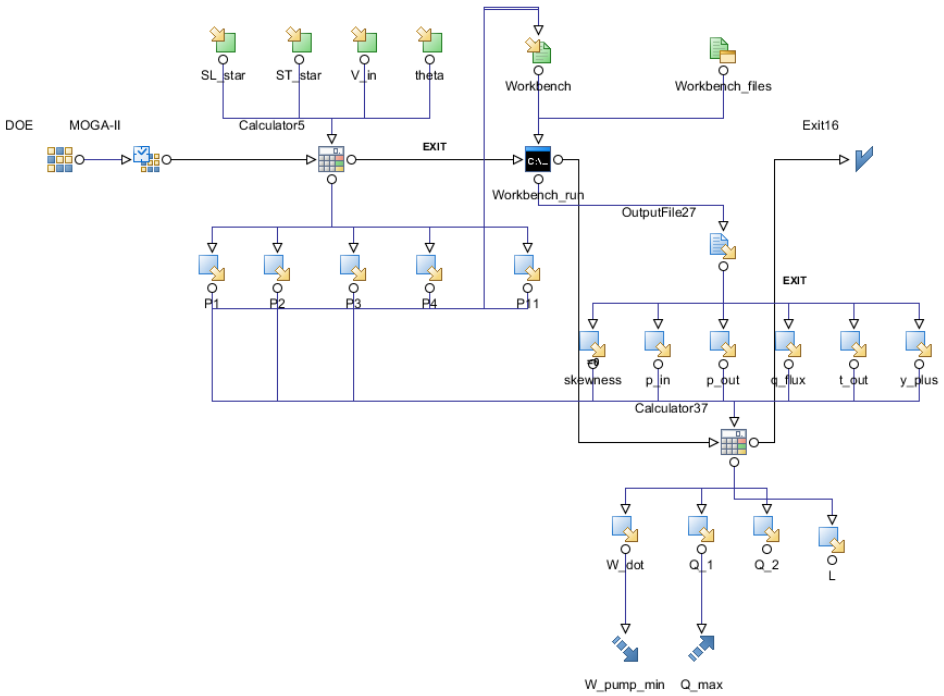


Figure 4.7. Optimization workflow for diamond shaped inline tube bank

Table 4.6. Multi-objective design optimization problem for diamond shaped inline tube bank

Objective Functions	(1)	Maximum $\dot{Q}_{total}$		
	(2)	Minimum $\dot{W}_{pump}$		
Optimization Variables		***Lower Bound***	***Upper Bound***	***Step Size***
	V_{in} [m/s]	1	6	0.5
	S_L^*	1.2	3.0	0.1
	S_T^*	1.2	3.0	0.1
	θ [˚]	10	170	5

Outlet temperature, inlet pressure, heat flux, y+ value, and skewness are prescribed as output files which are achieved from Ansys Fluent postprocessor. All these data are edited by the Phyton programming language which is integrated to modeFRONTIER environment.

The heat flux $\dot{q}$, the pressure at inlet P_{in} and outlet P_{out}, the temperatures at the outlet T_{out}, y+ value and the skewness are written to output files using the postprocessor of the Ansys Fluent program. We can use modeFRONTIER to retrieve the values from the output files and Python scripting language is used for the file operations. Heat transfer area, cross section area, logarithmic mean temperature difference, total heat transfer, mass flow rate, total pressure drop, and tube length of the parametric model are obtained for each design point using the 'Calculator' of the script of the optimization software for comparison. The Design of Experiments (DOEs) method is used to generate initial designs in the design space of the optimization problem, so that it is possible to obtain Pareto designs around DOEs. The Sobol sequence method is chosen in this study for the distribution of optimization variables in the design space. 20 DOEs are generated to obtain the optimal design. At the end of the optimization run, for the circular staggered tube bank, a total of 483 designs are obtained. Among these 87 designs are identified as Pareto designs in these results. For diamond inline arrangement, 647 of total design and 84 of Pareto designs among these are determined.

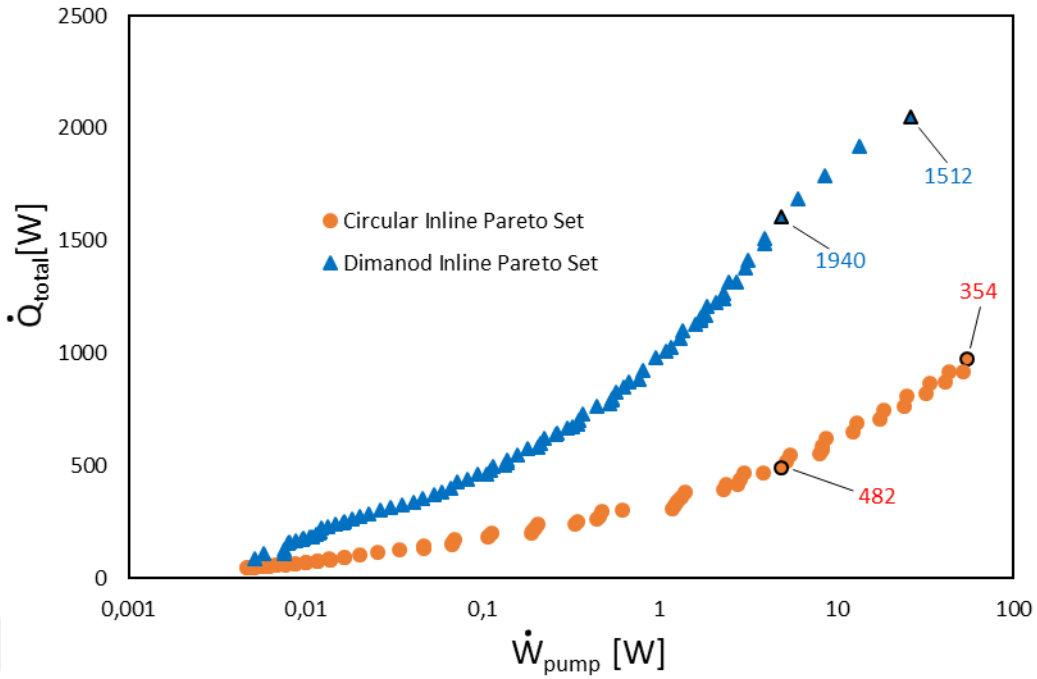


Figure 4.8. Scatter of $\dot{Q}_{total}$ vs $\dot{W}_{pump}$

Figure 4.8 demonstrates the relationship between $\dot{Q}_{total}$ and $\dot{W}_{pump}$, for all feasible designs of circular and diamond inline tube banks. Due to no constraints in the optimization setup, all obtained designs are feasible. It is seen that increment in $\dot{Q}_{total}$ results in higher $\dot{W}_{pump}$ for both geometries. For the calculated Pareto designs, diamond shaped geometries have higher $\dot{Q}_{total}$ than circular ones for identical $\dot{W}_{pump}$ value and those differences gradually increases with increasing $\dot{W}_{pump}$ value. For instance, ID 1940 within the diamond Pareto set has a $\dot{Q}_{total}$=1601W and ID 482 within the circular Pareto set has a $\dot{Q}_{total}$=491 W for identical $\dot{W}_{pump}$=4.9 W, which is higher than 3 times. Maximum $\dot{Q}_{total}$ is found to be 970 W at $\dot{W}_{pump}$=54.55 W among circular Pareto set with ID 1940. However, maximum $\dot{Q}_{total}$ is obtained as 2047 W (more than 2 times higher than that of circular one) at $\dot{W}_{pump}$=26.53 W (less than half of circular one). These 4 designs are given detailed in Table 4.7 for comparison.

Table 4.7. Selected designs of circular and diamond shaped inline tube banks from the first step optimization study.

Design ID	Pareto Design	$\dot{Q}_{total}$ [W]	$\dot{W}_{pump}$ [W]	V_{in} [m/s]	S_L^*	S_T^*	θ [°]	L_D [m]
354	Circ.	969.86	54.55	6	1.2	1.2	-	1.16
482	Circ.	490.51	4.93	2.5	1.4	1.2	-	0.99
1512	Dia.	2046.6	26.53	6	1.2	1.2	10	5.40
1940	Dia.	1601.3	4.87	6	1.2	1.6	10	4.05

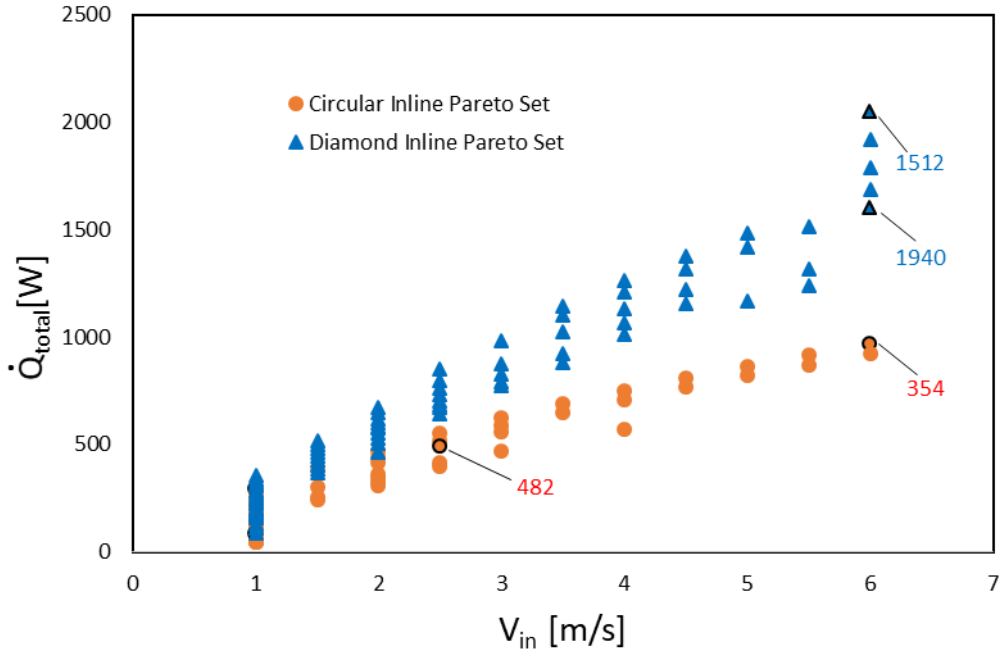


Figure 4.9. Scatter of $\dot{Q}_{total}$ vs V_{in}

Figure 4.9 demonstrates the Pareto set comparison of $\dot{Q}_{total}$ values as a function of V_{in} for circular and diamond inline tube bank. It is evident that, with increase of V_{in}, greater $\dot{Q}_{total}$ value is obtained for both geometries in general. Maximum $\dot{Q}_{total}$ value is achieved at 6 m/s for circular (ID 1512) and diamond shaped (ID 354) inline arrangement.

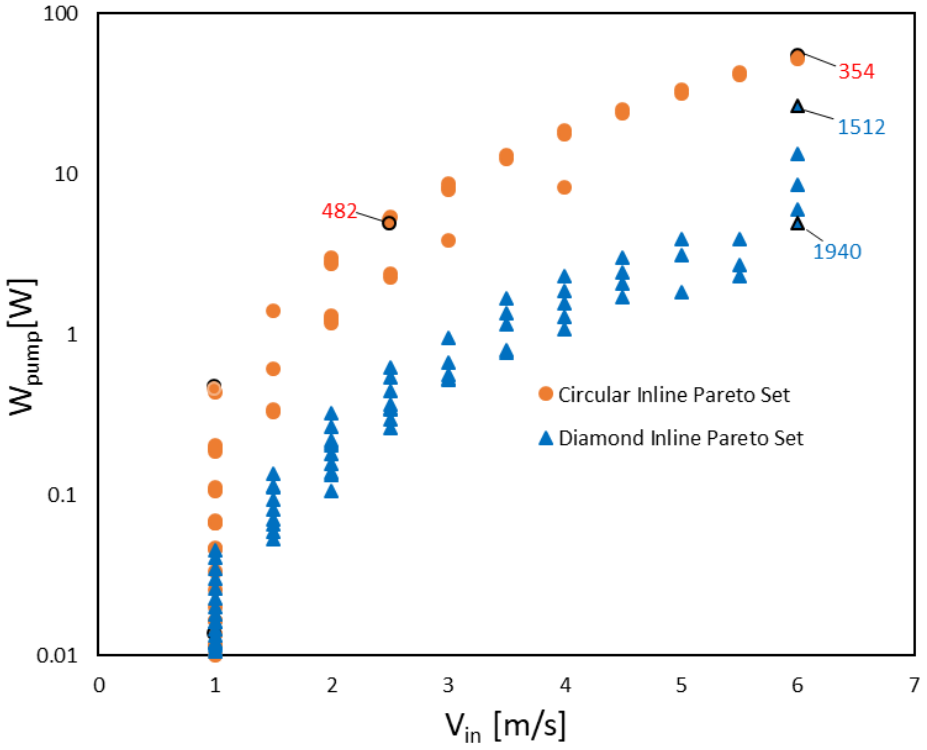
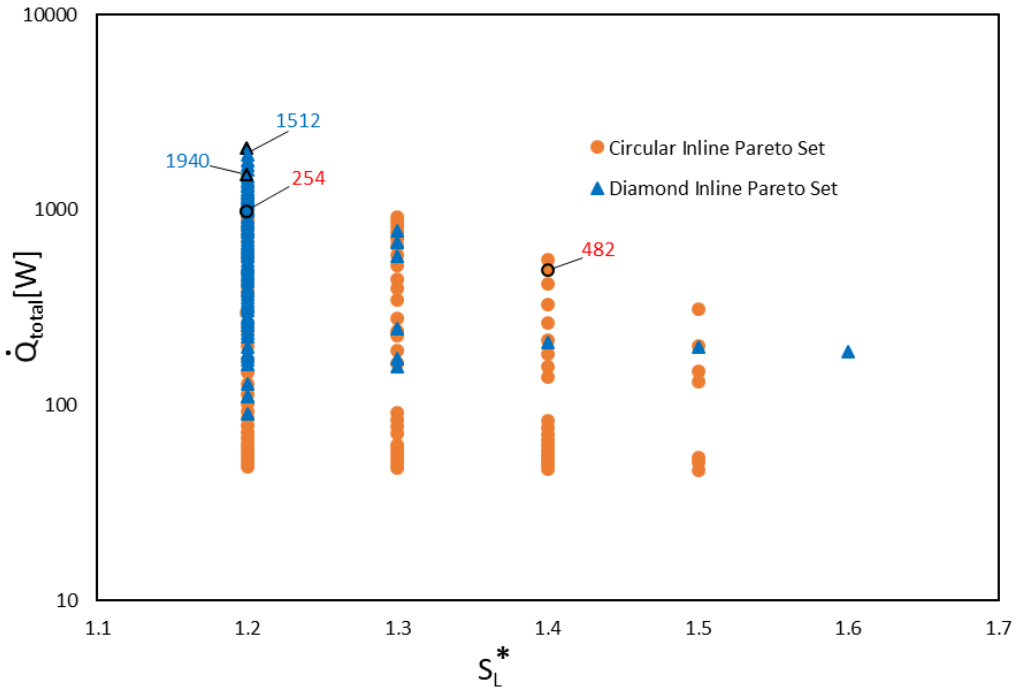
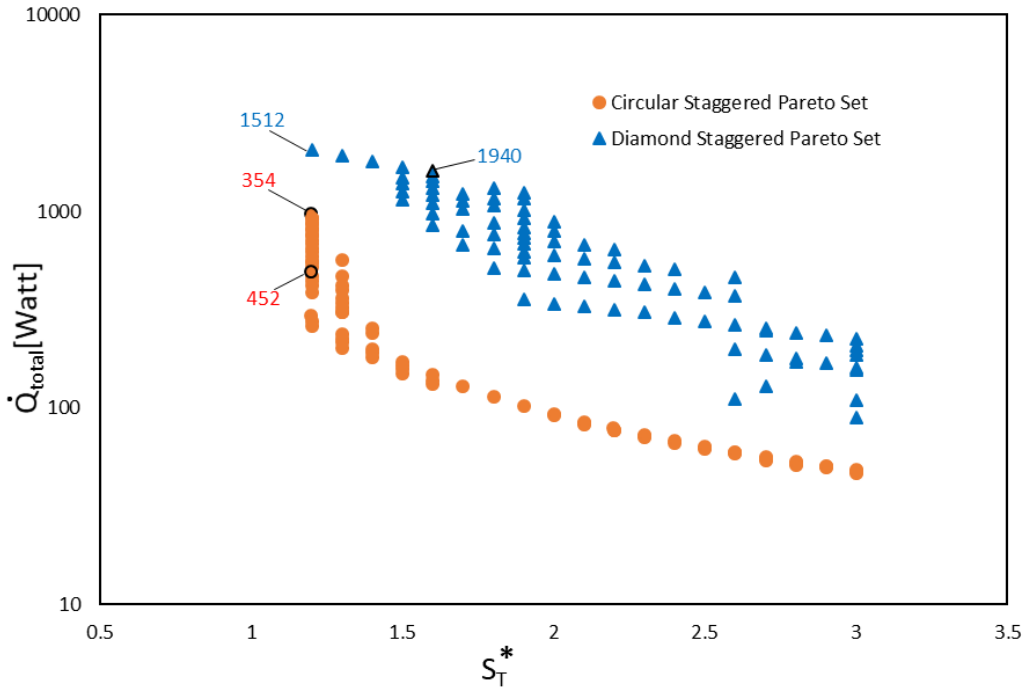


Figure 4.10. Scatter of $\dot{W}_{pump}$ vs V_{in}

Figure 4.10 shows the relationship between V_{in} and $\dot{W}_{pump}$, for circular and diamond inline tube bank. $\dot{W}_{pump}$ value shows a growth trend with increasing V_{in} for both inline tube banks. It is seen that required power is higher for circular tube bank compared to inline one for most of the Pareto set.



(a)



(b)

Figure 4.11. (a) Scatter of $\dot{Q}_{total}$ vs S_L^* (b) Scatter of $\dot{Q}_{total}$ vs S_T^*

Figure 4.11 (a) and (b) demonstrate the behavior of $\dot{Q}_{total}$ to the S_L^* and S_T^* for inline arranged circular and diamond shaped tube banks. It is seen that, Pareto $\dot{Q}_{total}$ values of circular inline tube bank is distributed in the S_L^* range of 1.2 to 1.5. Whereas, these values are mostly obtained when S_L^*=1.2 for diamond shaped inline tube bank. On the other hand, $\dot{Q}_{total}$ values gradually decreases with increasing S_T^* for both geometries. It is also observed that, Pareto designs are obtained for all S_T^* range (1.2 – 3.0). Maximum $\dot{Q}_{total}$ values are achieved where S_L^*=S_T^*=1.2 for both geometries.

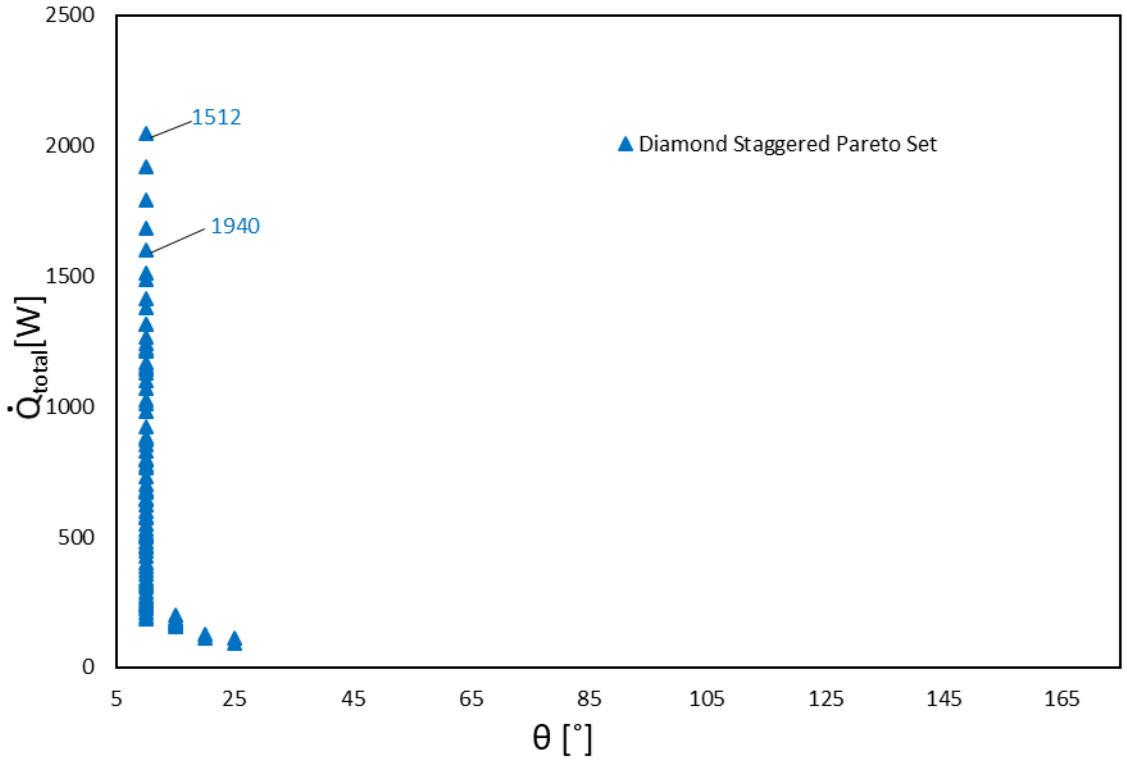


Figure 4.12. Scatter of $\dot{Q}_{total}$ vs θ

Figure 4.12 illustrates the $\dot{Q}_{total}$ value as a function of attack angle, θ which is the parameter of diamond shaped inline tube bank. All Pareto designs are achieved between 10 to 25˚. Maximum value is obtained where θ is 10˚.

4.2.2. Comparison of Optimum Diamond and Enhanced Shaped Tube Bank with Inline Arrangement

In the first optimization step, inline arranged circular and diamond tube banks were compared based on the objective functions of maximum $\dot{Q}_{total}$ and minimum $\dot{W}_{pump}$ for the identical constant volume condition. In the current section, Pareto designs of diamond and enhanced shaped inline tube banks are obtained. In both studied same objective functions of maximum $\dot{Q}_{total}$ and minimum $\dot{W}_{pump}$ are set and maximum tube length L_D is limited to 1 m. Formulation of the second step diamond and enhanced shaped inline optimization study is given in Table 4.8 and 4.9. At the end of the second optimization run, for the diamond staggered tube bank, a total of 422 designs are obtained as feasible. Among these 55 designs (see Table 4.10) are identified as Pareto designs in these results. For enhanced staggered arrangement, 1757 of total designs and 117 (see Table 4.11) of Pareto designs among these are determined.

Table 4.8. Second step multi-objective design optimization problem for diamond shaped inline tube bank

Objective Functions	(1)	Maximum $\dot{Q}_{total}$		
	(2)	Minimum $\dot{W}_{pump}$		
Optimization Variables		Lower Bound	Upper Bound	Step Size
	V_{in} [m/s]	1	6	0.5
	S_L^*	1.2	3.0	0.1
	S_T^*	1.2	3.0	0.1
	θ	10	170	5
Constraints	$L_D \leq 1\ m$			

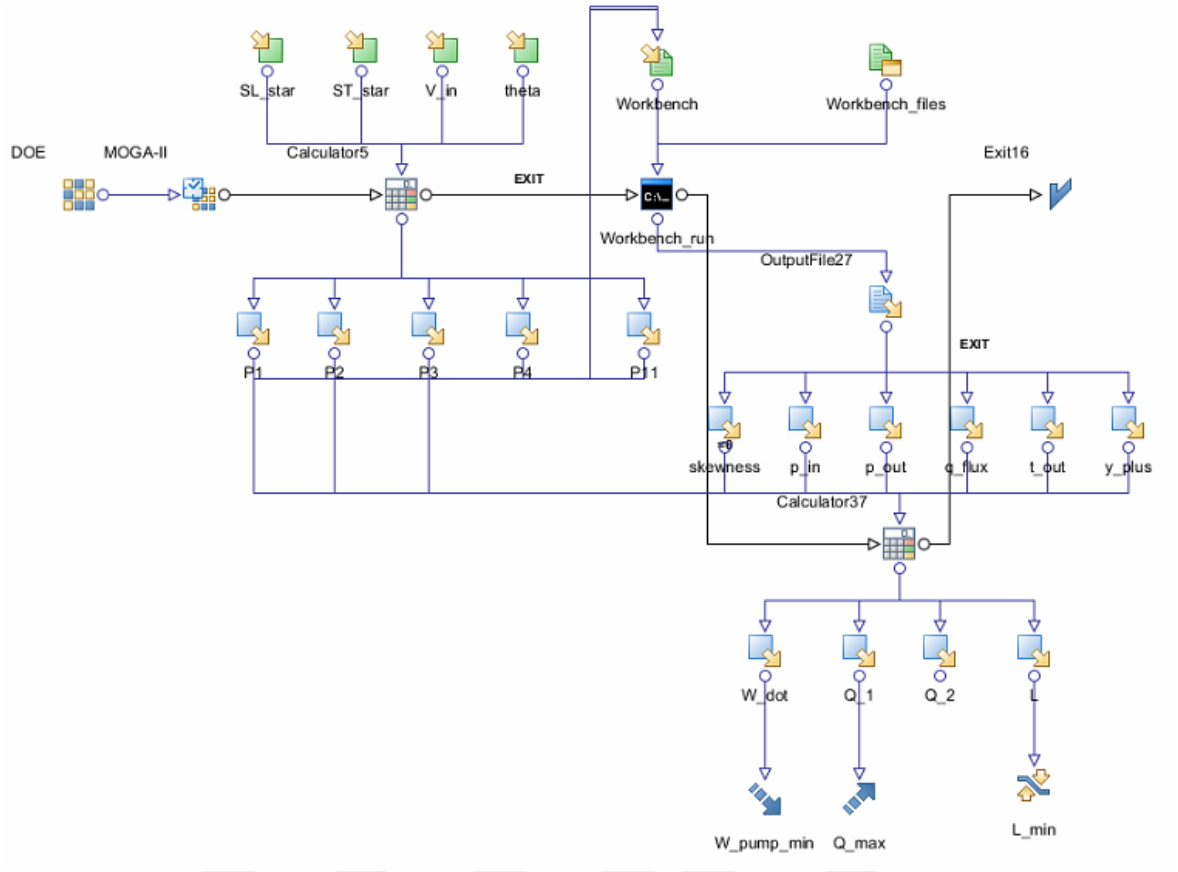


Figure 4.13. Optimization workflow for diamond shaped inline tube bank of the second optimization step.

Table 4.9. Second step multi-objective design optimization problem for enhanced shaped inline tube bank

Objective Functions	(1)	Maximum $\dot{Q}_{total}$		
	(2)	Minimum $\dot{W}_{pump}$		
Optimization Variables		Lower Bound	Upper Bound	Step Size
	V_{in} [m/s]	1	6	0.5
	S_L^*	1.2	3.0	0.1
	S_T^*	1.2	3.0	0.1
	θ_1	10	170	5
	θ_2	10	170	5
Constraint	$L_D \leq 1\ m$			

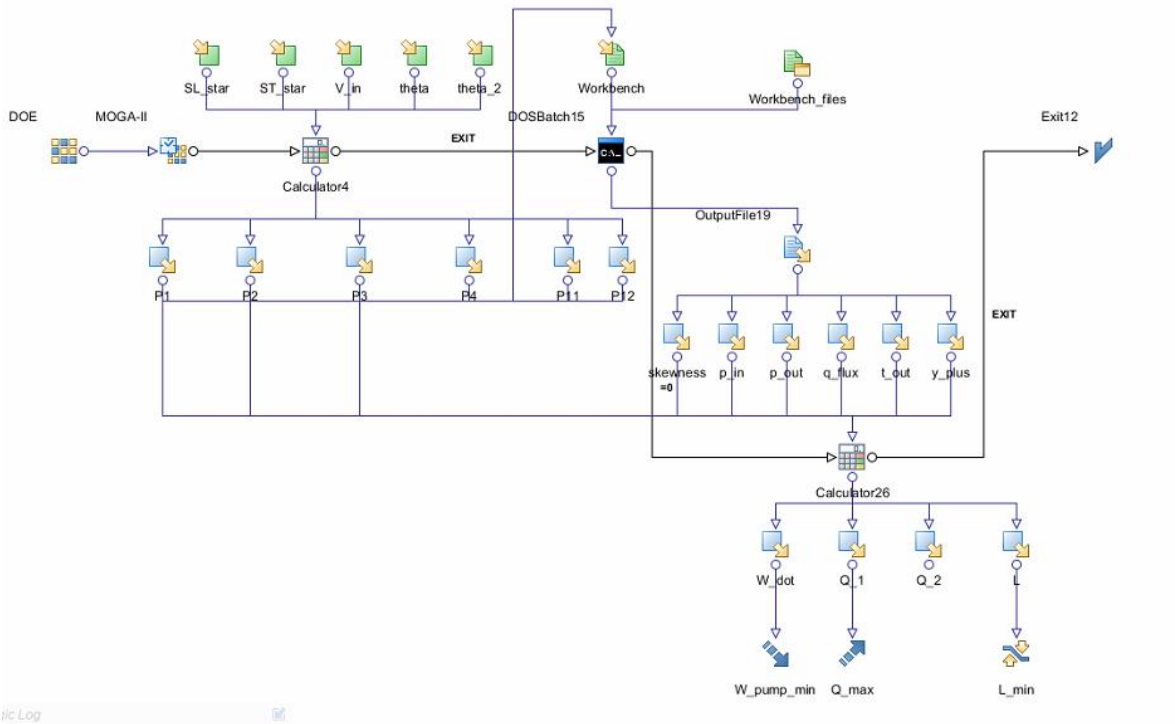


Figure 4.14. Optimization workflow for enhanced shaped inline tube bank of the second optimization step.

Table 4.10. Pareto designs for inline arranged diamond shaped tube bank

Design ID	S_L^*	S_T^*	V_{in} [m/s]	θ [°]	L_D [m]	$\dot{Q}_{total}$ [W]	$\dot{W}_{pump}$ [W]
31	2.7	1.2	5	30	0.833919	442.8729	10.05068
168	2.7	1.2	4.5	30	0.833919	411.012	7.507099
186	2.6	3	6	10	0.997411	398.1498	0.533646
692	2.7	3	6	10	0.96047	384.1491	0.514646
237	2.6	3	5.5	10	0.997411	376.7942	0.435603
600	2.7	3	5.5	10	0.96047	363.5095	0.419594
539	2.6	3	5	10	0.997411	354.1021	0.348449
557	2.7	3	5	10	0.96047	341.7252	0.335461
356	2.6	3	4.5	10	0.997411	330.2735	0.271549
499	2.7	3	4.5	10	0.96047	318.7744	0.261862
535	2.8	3	4.5	10	0.926167	307.8944	0.250163
280	2.6	3	4	10	0.997411	305.7294	0.204771
553	1.9	3	4	15	0.915731	297.4917	0.198671
413	2.7	3	4	10	0.96047	294.9298	0.197769
328	2.8	3	4	10	0.926167	284.8565	0.188783
381	2.6	3	3.5	10	0.997411	280.6563	0.148212
325	2.7	3	3.5	10	0.96047	270.2827	0.14358
1716	1.8	3	3	15	0.966605	268.0403	0.103877
291	2.6	3	3	10	0.997411	254.9822	0.102136
1646	1.9	3	3	15	0.915731	254.7151	0.09891
1583	2	3	3	15	0.869944	242.439	0.093999
873	1.8	3	2.5	15	0.966605	241.0784	0.067343

Design ID	S_L^*	S_T^*	V_{in} [m/s]	θ [°]	L_D [m]	$\dot{Q}_{total}$ [W]	$\dot{W}_{pump}$ [W]
1306	1.9	3	2.5	15	0.915731	229.0423	0.064009
1384	2	3	2.5	15	0.869944	217.9627	0.060934
1476	2.1	3	2.5	15	0.828519	207.771	0.058106
1586	1.8	3	2	15	0.966605	206.1652	0.03937
1116	1.9	3	2	15	0.915731	195.852	0.037368
1054	2	3	2	15	0.869944	186.1861	0.035606
1128	2.1	3	2	15	0.828519	177.7405	0.033979
944	2.2	3	2	15	0.790859	169.46	0.032419
1370	1.8	3	1.5	15	0.966605	164.5284	0.018675
1280	1.9	3	1.5	15	0.915731	156.2449	0.01772
1335	2	3	1.5	15	0.869944	148.4517	0.01687
1055	2.1	3	1.5	15	0.828519	141.5255	0.016094
964	2.2	3	1.5	15	0.790859	134.9081	0.015359
1196	2.3	3	1.5	15	0.756473	129.2358	0.01469
1132	1.8	2.9	1	15	0.999936	128.5695	0.006951
1712	1.8	3	1	15	0.966605	123.6234	0.006414
618	1.9	3	1	15	0.915731	117.5088	0.006094
1424	2	3	1	15	0.869944	111.6462	0.005801
885	2.1	3	1	15	0.828519	106.4157	0.005532
731	2.2	3	1	15	0.790859	101.5045	0.005281
814	2.3	3	1	15	0.756473	97.15217	0.00505
935	2.4	3	1	15	0.724954	93.13486	0.004831
869	2.5	3	1	15	0.695956	89.26832	0.004632
886	2.6	3	1	15	0.669188	85.83058	0.004464
629	2.7	3	1	15	0.644403	82.6693	0.004296
630	2.9	2.9	1	15	0.62065	80.14451	0.004277
393	2.8	3	1	15	0.621389	79.80341	0.004145
782	2.9	3	1	15	0.599962	76.91497	0.003992
758	3	3	1	15	0.579963	74.38493	0.003874
1964	2.6	3	1	20	0.506399	62.85897	0.003497
878	2.8	3	1	20	0.470227	58.33788	0.003246
1247	3	3	1	20	0.438879	54.41492	0.003035
1890	3	3	1	25	0.35518	44.1491	0.002809

Table 4.11. Pareto designs for inline arranged enhanced shaped tube bank

Design ID	S_L^*	S_T^*	V_{in} [m/s]	θ_1 [°]	θ_2 [°]	L_D [m]	$\dot{Q}_{total}$ [W]	$\dot{W}_{pump}$ [W]
1402	2	1.2	6	80	25	0.998199	623.3426	19.1473
964	2	1.2	5.5	50	30	0.97642	575.998	16.25851
1578	2	1.2	5	80	25	0.998199	550.0391	11.56816
853	1.9	1.2	4.5	50	35	0.955082	508.97	10.22042
1491	2	1.2	4.5	50	30	0.97642	503.7361	9.278256
948	2	1.3	5.5	50	35	0.837534	455.433	7.742561
1570	2.2	1.2	4.5	50	30	0.887655	454.1808	7.622334
1030	1.8	1.4	5.5	65	30	0.87992	436.1274	4.827297
582	2	1.2	3.5	50	35	0.907328	407.2518	4.665114
1067	2	1.3	4	40	30	0.962135	405.7773	3.025826
1684	2.3	1.4	5	85	20	0.854366	387.8444	2.672882
1890	1.7	1.7	6	50	30	0.810868	361.0659	2.395143
4120	1.8	2.8	6	40	10	0.99401	348.1128	0.610134
923	1.9	2.8	6	30	10	0.995874	345.4671	0.56359
3758	1.9	3	6	25	10	0.971729	329.0314	0.49293
2504	2	2.7	5.5	30	10	0.98112	323.855	0.463179
108	1.9	2.8	5.5	35	10	0.964458	318.0486	0.45672
2748	2.1	2.9	5.5	20	10	0.97022	312.3803	0.395255
2443	2	2.7	5	30	10	0.98112	303.7117	0.364131
4335	2.2	3	5	15	10	0.990366	301.2099	0.297128
2210	2.3	2.6	4.5	20	10	0.988066	283.4309	0.277613
2527	2	3	4.5	20	10	0.984773	279.6546	0.237991
3576	2.1	2.5	4	35	10	0.977318	268.7595	0.237979
2408	2	2.7	4	30	10	0.98112	264.6482	0.207845
2966	2.4	2.2	3.5	15	15	0.996909	262.2663	0.202489
2803	2.2	2.4	3.5	15	15	0.996909	260.1148	0.177083
3866	1.9	2.6	3.5	50	10	0.981846	250.1629	0.174346
2524	2.3	2.4	3.5	15	15	0.953565	249.5873	0.170413
2660	2.2	2.5	3.5	15	15	0.957033	249.1334	0.162263
3869	2.2	3	3.5	10	15	0.990366	248.5502	0.132176
959	2	2.9	3.5	25	10	0.954975	235.255	0.131761
2606	1.9	2.5	3	20	15	0.975997	233.627	0.117197
2410	2.3	2.4	3	15	15	0.953565	229.4439	0.116732
1821	2	2.7	3	30	10	0.98112	224.3726	0.101533
4223	2	2.8	3	25	10	0.989081	223.3235	0.096154
4056	1.9	2.9	3	30	10	0.961533	218.4878	0.091674
2727	2.3	2.3	2.5	15	15	0.995025	216.7401	0.082811
946	2.2	2.4	2.5	15	15	0.996909	216.4673	0.077759
1208	2.2	2.5	2.5	15	15	0.957033	207.4741	0.071511
3784	2.2	3	2.5	10	15	0.990366	207.046	0.059305
3567	1.8	3	2.5	30	10	0.98112	199.7992	0.057361
3371	1.9	3	2.5	25	10	0.971729	197.9828	0.056338
3329	1.9	3	2.5	30	10	0.929482	189.5689	0.054429

Design ID	S_L^*	S_T^*	V_{in} [m/s]	θ_1 [°]	θ_2 [°]	L_D [m]	$\dot{Q}_{total}$ [W]	$\dot{W}_{pump}$ [W]
1194	1.7	3	2	10	40	0.982316	188.9057	0.044157
2177	2.1	2.6	2	15	15	0.964044	184.425	0.039654
2888	1.9	2.8	2	30	10	0.995874	179.9944	0.036347
3178	2.2	3	2	15	10	0.990366	179.1403	0.032576
4107	2.3	3	2	15	10	0.947307	171.1087	0.031211
3917	2	3	2	15	15	0.87728	166.6589	0.030616
1059	1.9	2.6	1.5	10	45	0.995821	165.8857	0.026438
990	1.6	3	1.5	10	160	0.965336	161.8135	0.025072
1096	2.2	2.4	1.5	15	15	0.996909	161.6523	0.022604
3820	1.9	2.8	1.5	15	15	0.989414	159.8637	0.018501
4060	1.8	3	1.5	15	15	0.974756	156.5156	0.016867
2459	2.2	3	1.5	15	10	0.990366	151.4284	0.016342
1458	1.8	3	1.5	30	10	0.98112	148.5947	0.016304
1727	1.9	3	1.5	25	10	0.971729	147.7267	0.016231
2372	2.3	3	1.5	15	10	0.947307	144.5785	0.015649
2751	2.1	3	1.5	20	10	0.937879	142.6139	0.015649
3461	2	3	1.5	15	15	0.87728	141.3642	0.015172
4014	2.4	3	1.5	15	10	0.907836	138.5034	0.014983
1946	2.2	3	1.5	20	10	0.895248	136.1512	0.014948
3446	2.1	3	1.5	15	15	0.835505	134.7463	0.014443
3112	2.5	3	1.5	15	10	0.871522	132.8032	0.014377
2342	2.3	3	1.5	20	10	0.856324	130.1414	0.014297
1156	1.9	2.6	1	10	45	0.995821	128.7967	0.009487
1702	1.9	2.7	1	10	45	0.958938	124.031	0.008681
3849	1.8	3	1	15	15	0.974756	123.0533	0.006181
2110	2.2	3	1	15	10	0.990366	118.4798	0.006153
2785	2	3	1	20	10	0.984773	117.5252	0.006126
3040	1.6	3	1	20	15	0.96583	117.4762	0.006056
1583	1.8	3	1	30	10	0.98112	116.8443	0.006012
3478	1.9	3	1	15	15	0.923453	116.8368	0.005878
1497	1.8	3	1	35	10	0.95017	113.0088	0.005845
3140	1.7	3	1	20	15	0.909017	112.1348	0.00578
3448	2	3	1	15	15	0.87728	111.2969	0.005577
1645	1.9	3	1	35	10	0.900161	107.5636	0.005536
3438	1.8	3	1	20	15	0.858516	106.9282	0.005514
3615	2.1	3	1	15	15	0.835505	106.2639	0.005317
1589	2	3	1	35	10	0.855153	102.5883	0.005304
3404	1.9	3	1	20	15	0.813331	101.7639	0.005249
2852	2.2	3	1	15	15	0.797527	101.1524	0.005087
1511	2.1	3	1	35	10	0.814432	97.79147	0.00506
2577	2	3	1	20	15	0.772664	97.13631	0.004993
2498	2.3	3	1	15	15	0.762852	96.7019	0.004867
1267	2.2	3	1	35	10	0.777412	93.37639	0.004843
1961	2.8	3	1	15	10	0.778145	92.82221	0.00483

Design ID	S_L^*	S_T^*	V_{in} [m/s]	θ_1 [°]	θ_2 [°]	L_D [m]	$\dot{Q}_{total}$ [W]	$\dot{W}_{pump}$ [W]
1915	2.4	3	1	15	15	0.731067	92.69608	0.004663
2702	2.6	2.9	1	15	15	0.698101	89.74887	0.004644
2190	2.9	3	1	15	10	0.751312	89.54485	0.004643
2296	2.3	3	1	35	10	0.743611	89.34078	0.004633
2276	2.5	3	1	15	15	0.701824	88.72596	0.004474
1351	2.4	3	1	35	10	0.712628	85.55953	0.004434
1340	2.6	3	1	15	15	0.674831	85.4581	0.004309
1977	2.7	3	1	15	15	0.649837	82.34991	0.004141
2725	2.8	3	1	15	15	0.626629	79.46156	0.003988
3080	2.9	3	1	15	15	0.605021	77.40078	0.003813
2925	3	3	1	15	15	0.584853	73.8399	0.003712
2144	3	3	1	30	10	0.588672	70.59914	0.003641
2189	2.8	3	1	20	15	0.551903	69.37303	0.003585
1612	3	3	1	35	10	0.570102	68.28946	0.003545
2302	2.9	3	1	20	15	0.532872	67.02128	0.00346
1819	2.6	3	1	30	15	0.516103	65.18317	0.003432
2842	3	3	1	20	15	0.515109	64.71815	0.003345
1692	2.7	3	1	30	15	0.496988	62.76638	0.003305
2049	2.9	3	1	25	15	0.490379	61.42478	0.00324
2174	2.8	3	1	30	15	0.479238	60.48708	0.003185
2432	3	3	1	25	15	0.474033	59.34745	0.003133
2192	2.9	3	1	30	15	0.462713	58.38183	0.003075
2496	3	3	1	30	15	0.447289	56.44022	0.002974
1443	3	3	1	35	15	0.428733	54.0862	0.002891
1663	3	3	1	40	15	0.415291	52.20811	0.002831
1551	3	3	1	45	15	0.405256	50.76723	0.002804
1659	3	3	1	50	15	0.397603	49.64678	0.002788
1742	2.9	3	1	45	20	0.34717	43.73314	0.002769
1523	3	3	1	40	20	0.345615	43.67008	0.002699
1640	3	3	1	45	20	0.335597	42.27853	0.002678

Figure 4.13 and 4.14 illustrate the workflow of second step optimization study of diamond and enhanced shaped inline tube bank. Differently from first step optimization studies maximum tube length L_D is limited to 1 m which is constructed as constraint in the workflow. Unlike diamond shaped geometry enhanced geometry has two distinct attack angles as input parameters.

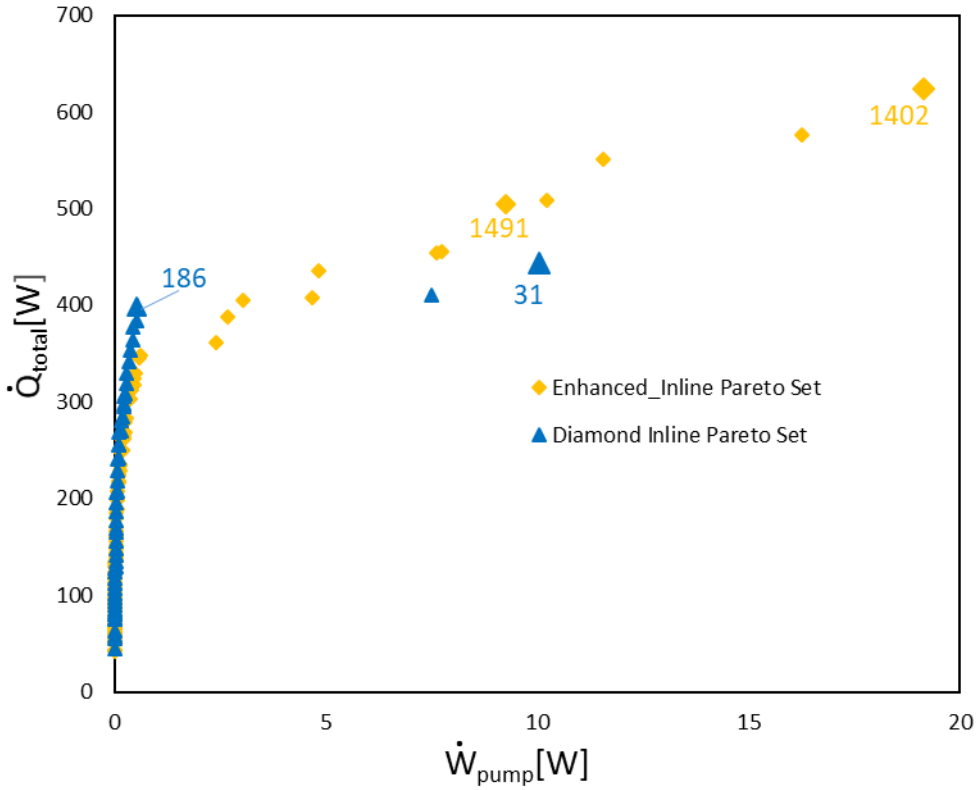


Figure 4.15. Scatter of $\dot{Q}_{total}$ vs $\dot{W}_{pump}$

Figure 4.15 shows the relationship between $\dot{Q}_{total}$ and $\dot{W}_{pump}$. for all Pareto designs of diamond and enhanced inline tube banks. It is seen that increment in $\dot{Q}_{total}$ cause higher $\dot{W}_{pump}$ for both geometries. In the zone $\dot{W}_{pump} < 0.7\ W$ diamond geometries show higher $\dot{Q}_{total}$ values than enhanced geometry for the same $\dot{W}_{pump}$. However, in the zone $\dot{W}_{pump} > 0.7\ W$ opposite is true. It should be noted that there are 12 Pareto designs for enhanced and only two Pareto designs for diamond geometry in this zone. Maximum $\dot{Q}_{total}$ is found to be 442.87 W at $\dot{W}_{pump}$=10.05 W among diamond Pareto set with ID 31. However, Maximum among enhanced Pareto set $\dot{Q}_{total}$ is obtained as 623.34 W (41% higher than that of diamond one with ID 31) at $\dot{W}_{pump}$=19.147 W 41% higher than that of diamond one with ID 31) with ID 1402. For diamond geometry design with ID 31 is selected as optimum. However, ID 1402 isn't preferred as optimum due to the higher $\dot{W}_{pump}$ requirement. Instead. Pareto design ID 1491 with $\dot{Q}_{total}$=503.74 W (14% higher than that of diamond one with ID 31) and $\dot{W}_{pump}$ =9.28 W (8% lower than that of diamond one with ID 31) is selected as optimum design. If $\dot{W}_{pump}$ is not significant diamond design with ID 1402 can be considered as optimum. Also among inline Pareto diamond results, as an alternative to design with ID 31 design with ID 186 can be selected as optimum with $\dot{Q}_{total}$=398.15 W (only 11% lower than that of diamond one with ID 31) and $\dot{W}_{pump}$ =0.53 W (18 times lower than that of diamond one with ID 31). These 4 designs are given detailed in Table 4.12 for comparison.

Table 4.12. Selected designs of diamond and enhanced shaped inline tube bank from the second step optimization study.

Design ID	Pareto Design	$\dot{Q}_{total}$ [W]	$\dot{W}_{pump}$ [W]	V_{in} [m/s]	S_L^*	S_T^*	θ_1 [°]	θ_2 [°]	L_D [m]
1402	Enh.	623.34	19.147	6	2	1.2	80	25	0.998
1491	Enh.	503.74	9.28	4.5	2	1.2	50	30	0.976
31	Dia.	442.87	10.05	5	2.7	1.2	30	30	0.833
186	Dia.	398.15	0.533	6	2.6	3	10	10	0.997

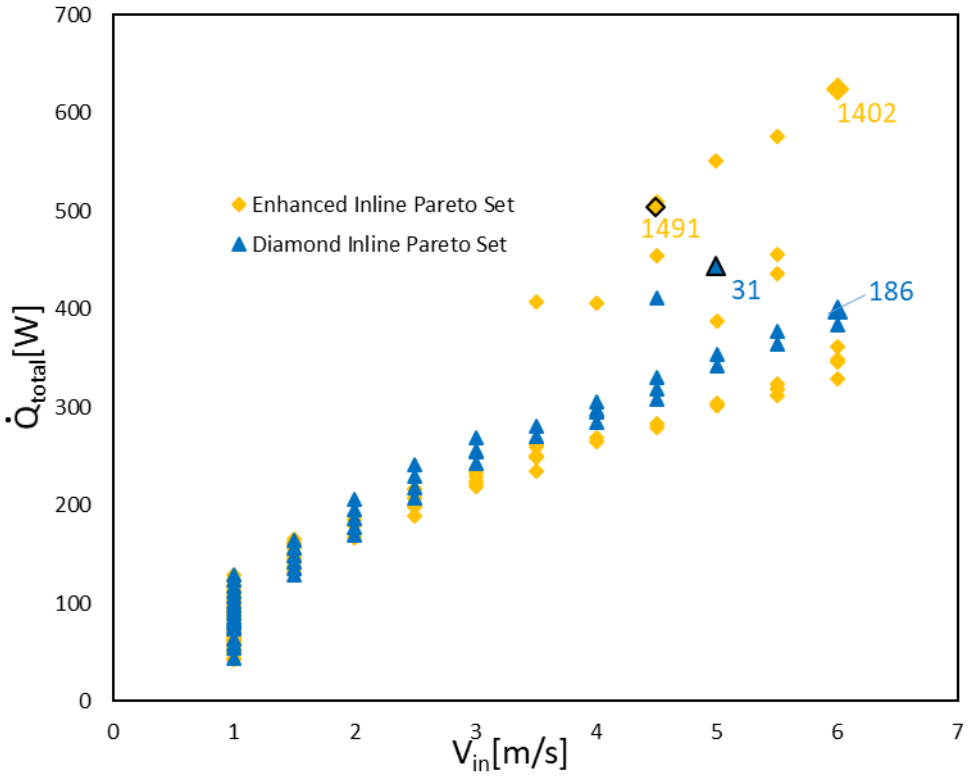


Figure 4.16. Scatter of V_{in} vs $\dot{Q}_{total}$

Figure 4.16 shows the Pareto set comparison of $\dot{Q}_{total}$ values as a function of V_{in} for diamond and enhanced inline tube bank. It is seen that, with increase of V_{in} greater $\dot{Q}_{total}$ value is obtained for both geometries in general. For the zone $\dot{W}_{pump} < 0.7\,W$ these increment happens more uniformly for both geometry. However, designs obtained for the zone $\dot{W}_{pump} > 0.7\,W$ shows irregular increment with higher $\dot{Q}_{total}$ values. Maximum $\dot{Q}_{total}$ value is achieved at 5 m/s and 6 m/s for diamond (ID 31) and enhanced shaped (ID 1402) inline arrangement, respectively.

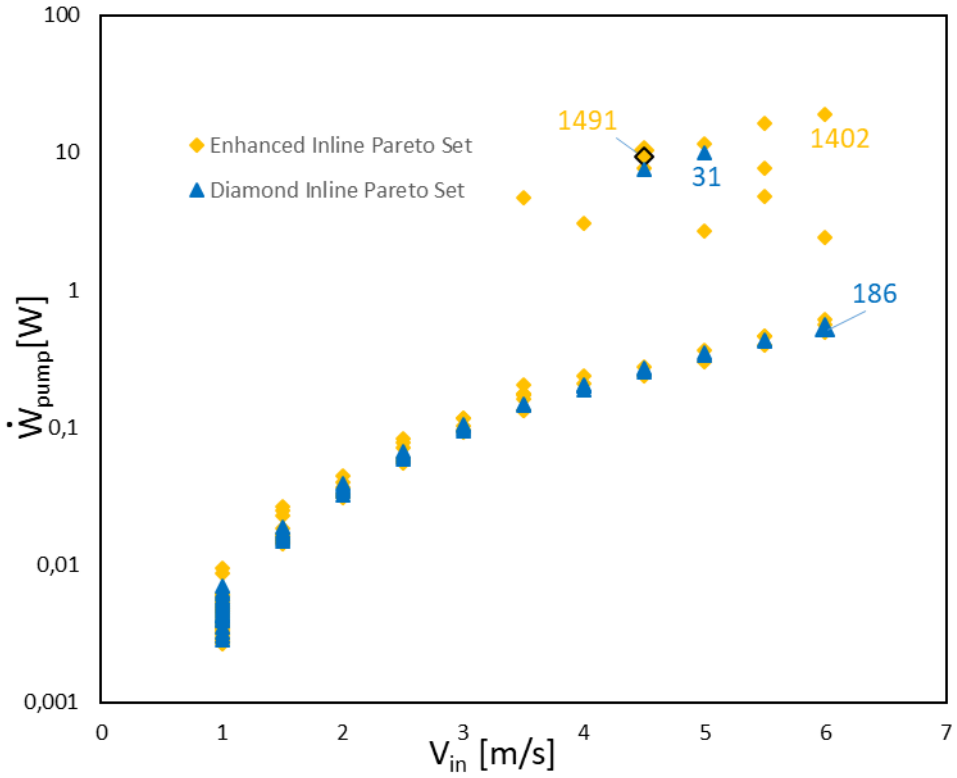
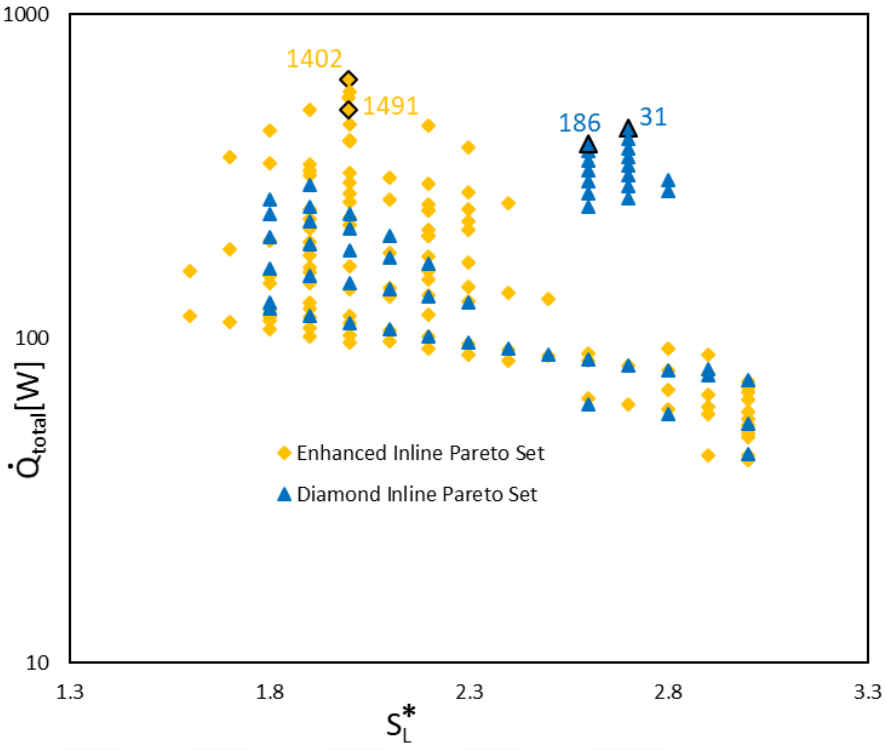
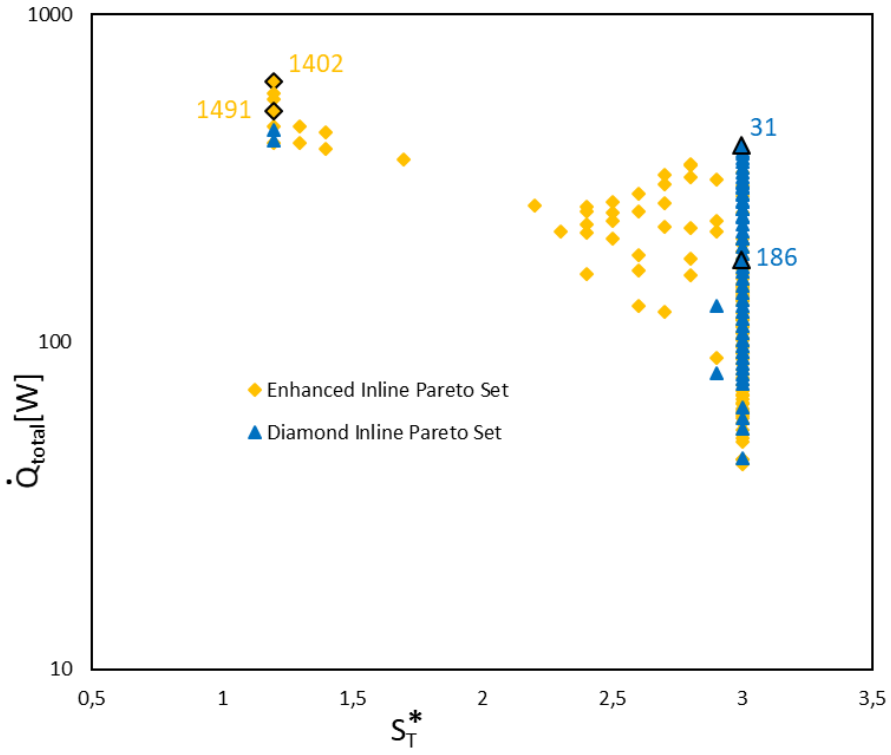


Figure 4.17. Scatter of V_{in} vs $\dot{W}_{pump}$

Relationship between V_{in} and $\dot{W}_{pump}$ is shown in Figure 4.17 for diamond and enhanced shaped inline tube bank. $\dot{W}_{pump}$ value shows a similar growth trend with increasing V_{in} for both inline tube banks for the zone $\dot{W}_{pump} < 0.7\ W$. However, these obtained Pareto values show uneven distribution for the zone $\dot{W}_{pump} > 0.7\ W$ in the range of V_{in}=3.5 - 6 m/s. Maximum $\dot{W}_{pump}$ value is achieved at 6 m/s and 5 m/s for diamond (ID 31) and enhanced shaped (ID 1402) inline arrangement, respectively.



(a)

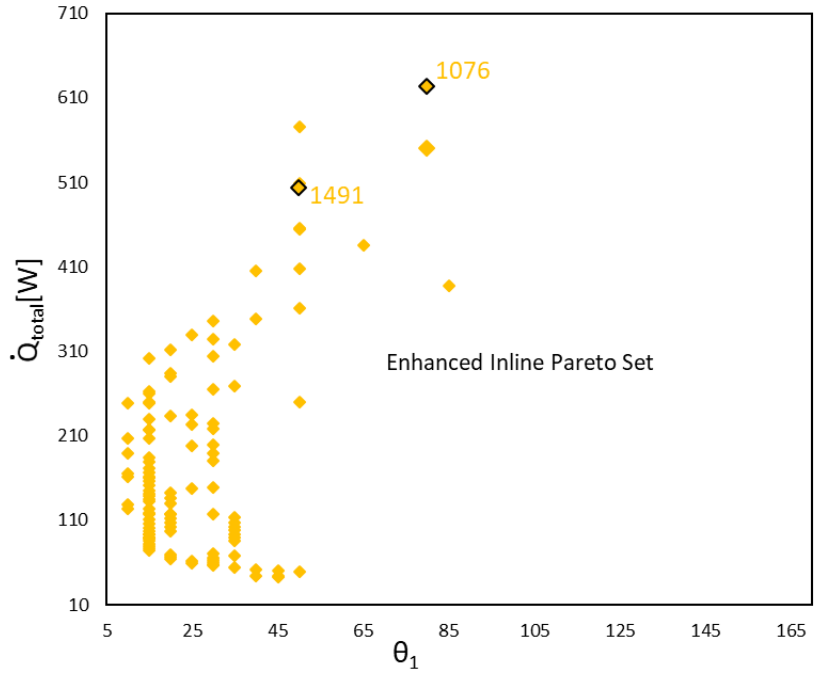


(b)

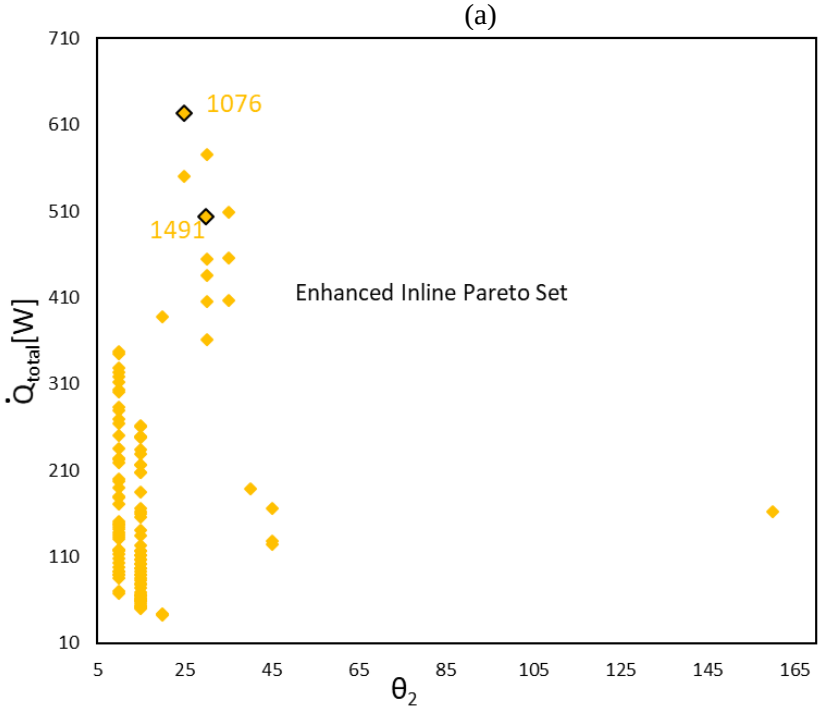
Figure 4.18. (a) Scatter of $\dot{Q}_{total}$ vs S_L^* (b) Scatter of $\dot{Q}_{total}$ vs S_T^*

Figure 4.18 (a) and (b) demonstrate $\dot{Q}_{total}$ as a function of S_L^* and S_T^*, respectively. Generally, $\dot{Q}_{total}$ value shows increasing trend with decreasing S_L^* for both geometries. However, 17 diamond Pareto designs which are located S_L^* =2.6-2.8 behave different from this trend. For diamond tube

bank, all Pareto designs are obtained within the range of S_L^* =1.8 - 3. Whereas, enhanced geometries are obtained within the range of S_L^* =1.6 - 3. Maximum $\dot{Q}_{total}$ is obtained at S_L^* =2.7 and S_L^* =2 for diamond (ID 31) and enhanced (ID 1402) designs, respectively. On the other hand, Pareto designs of diamond geometries are obtained at S_T^* =1.6 (only two exceptional designs are achieved at S_T^* = 2.9) which are the limit parameters of S_T^*. Pareto designs of enhanced geometry are located in the all ranges of S_L^* and S_T^*. Maximum $\dot{Q}_{total}$ is achieved at S_L^* = 2.7 and S_L^* = 1.2 for (ID 31) and achieved at S_L^* =2 and S_L^* = 1.2 for enhanced (ID 1402) geometry, respectively.



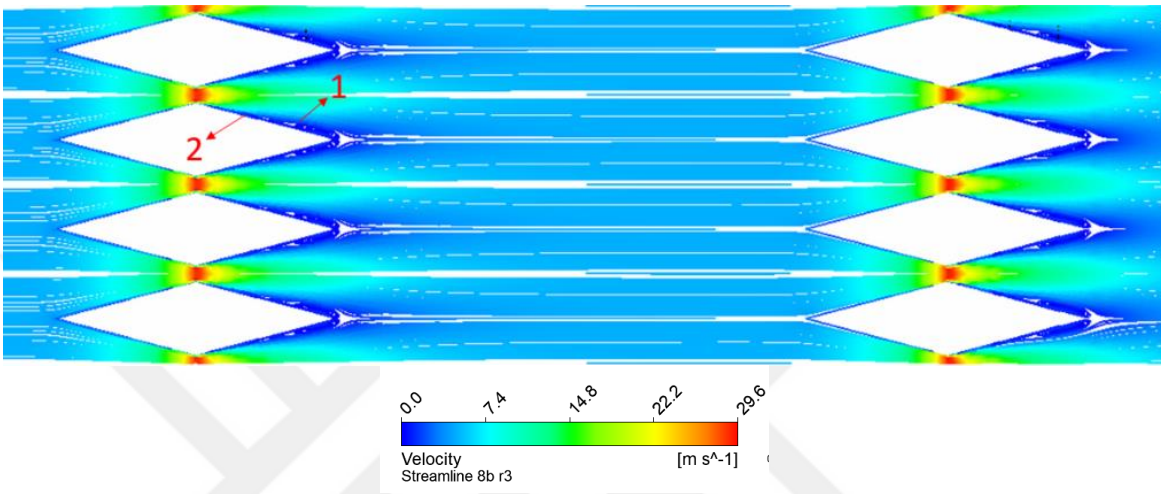
(a)



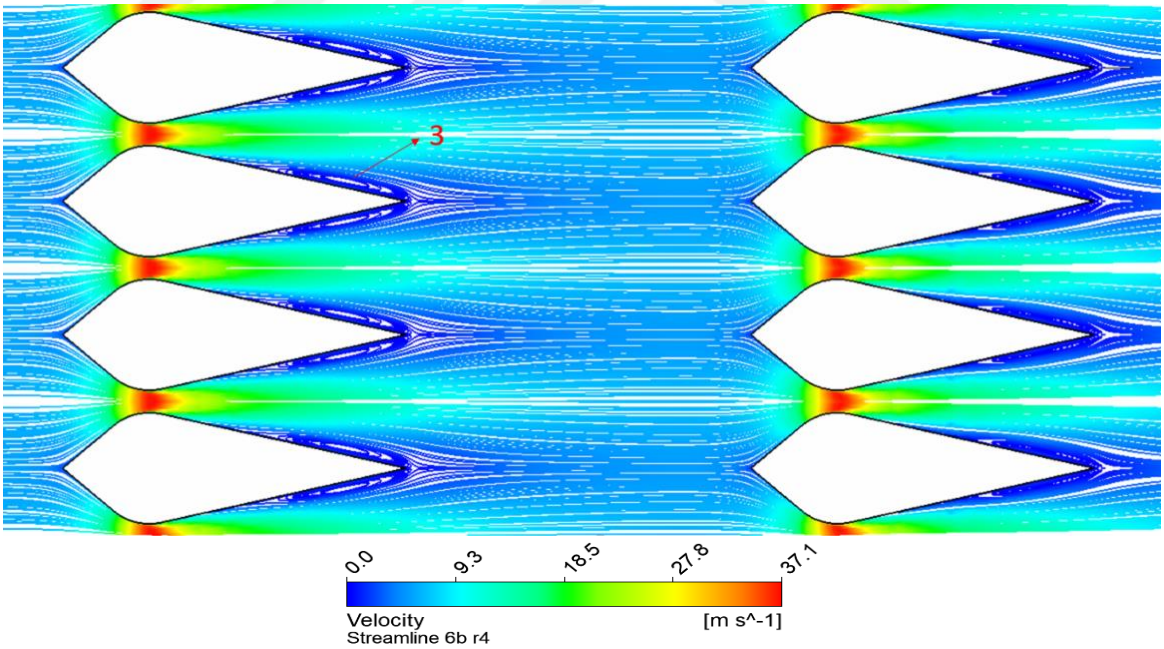
(b)

Figure 4.19. (a) Scatter of $\dot{Q}_{total}$ vs θ_1 (b) Scatter of $\dot{Q}_{total}$ vs θ_2

Figure 4.19 (a) and (b) demonstrate $\dot{Q}_{total}$ as a function of θ_1 and θ_2 for enhanced inline tube bank, respectively. It can be inferred from the figures that Pareto designs are obtained θ_1 =10-85˚ and θ_2 =10-45˚ (only one exceptional design at θ_2 =160˚). In general, number of Pareto designs tend to decrease with increasing attack angle θ. However, opposite is true for Pareto designs with highest $\dot{Q}_{total}$ value for each angle. Maximum $\dot{Q}_{total}$ value of inline arranged enhanced tube bank (ID 1076) is achieved at θ_1 =80˚ and θ_2 = 25˚, respectively.



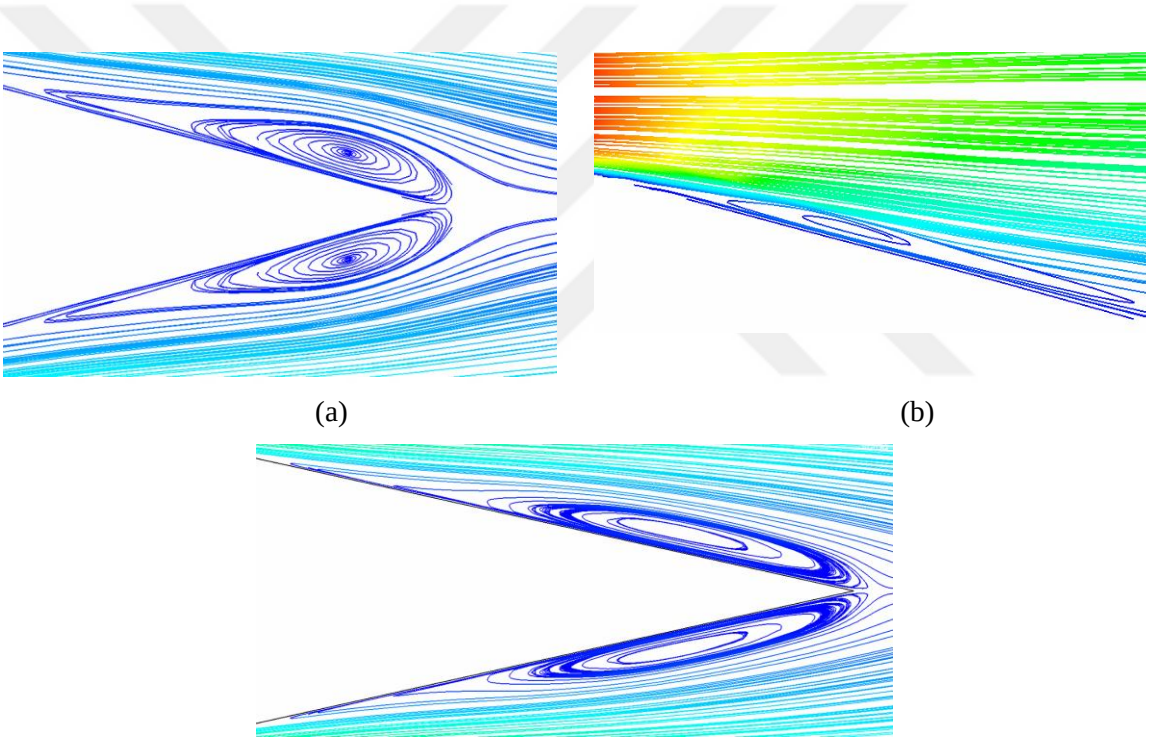
(a)



(b)

Figure 4.20. Streamlines of optimum a) diamond b) enhanced shaped inline tube banks

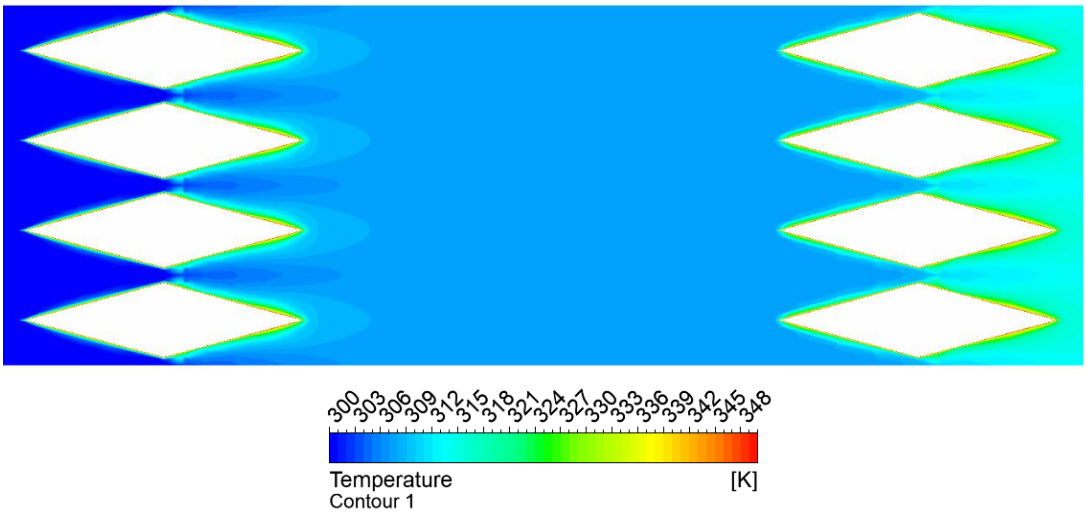
Figure 4.20 shows the streamlines of the optimum diamond (ID 31) and enhanced (ID 1491) shaped inline tube banks. Wake zone is created at the rear side of the tubes of both geometries due to the adverse pressure gradient. Therefore, flow separations are observed. For the optimum diamond tube bank, there are two couple of separated recirculation zones exist. However, there is a couple of recirculation zone for optimum enhanced tube bank observed (See Figure 4.21). Figure 4.22 depicts the temperature distribution of optimum inline diamond and enhanced tube bank geometries. Temperature value increases in the flow direction due to higher temperature of the tubes. Thin boundary layer observed near the upstream of the tubes where high gradient occurs. In the wake zone, temperature gradient becomes lower. Figure 4.23 shows the pressure contours of the optimum inline diamond and enhanced tube banks. Minimum static pressure is observed at the rear side of the tubes where flow separation occurs. At the stagnation point in the front side of the tubes, maximum local static pressure is observed.



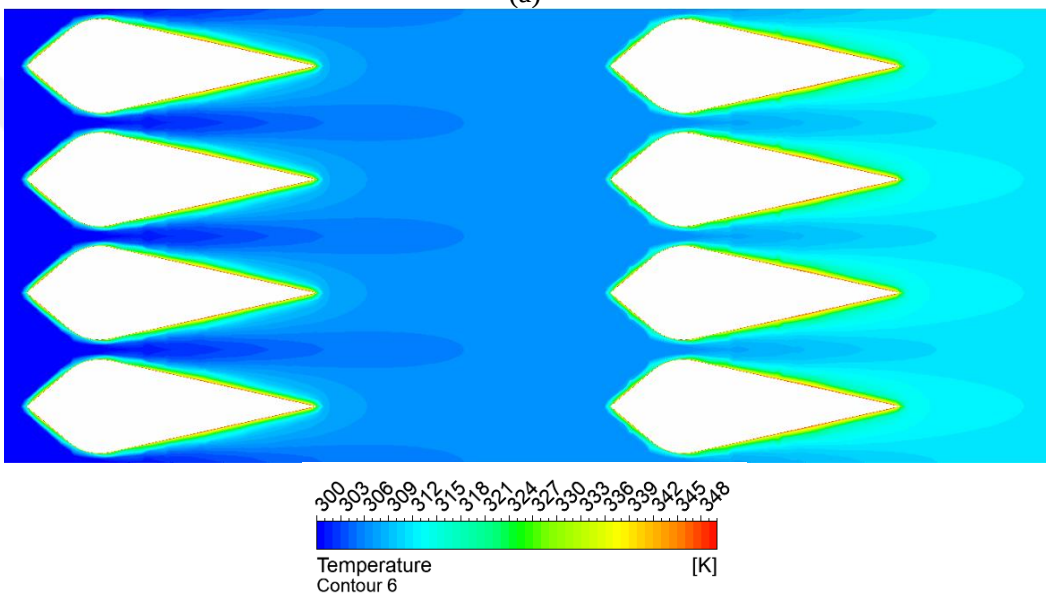
(a) (b)

(c)

Figure 4.21. Enlarge view of optimum diamond a. b (1.2) and enhanced inline c (3) shaped geometry streamlines

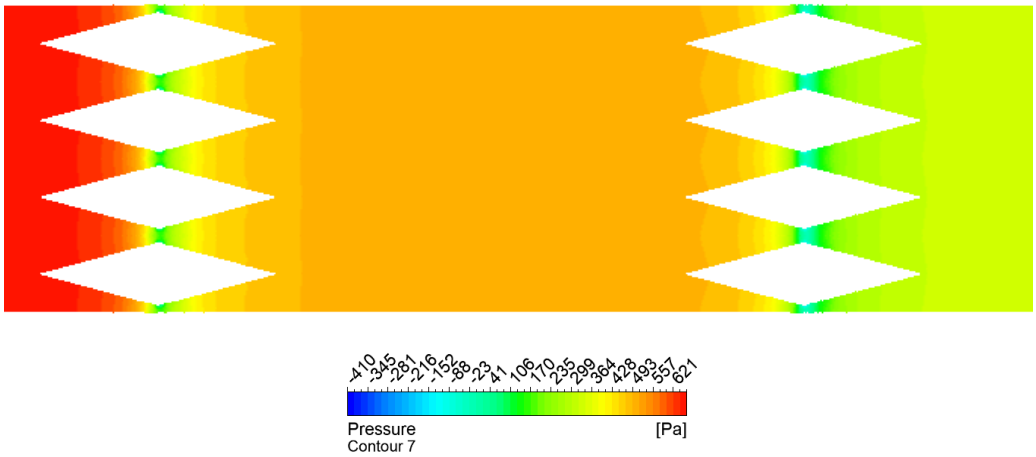


(a)

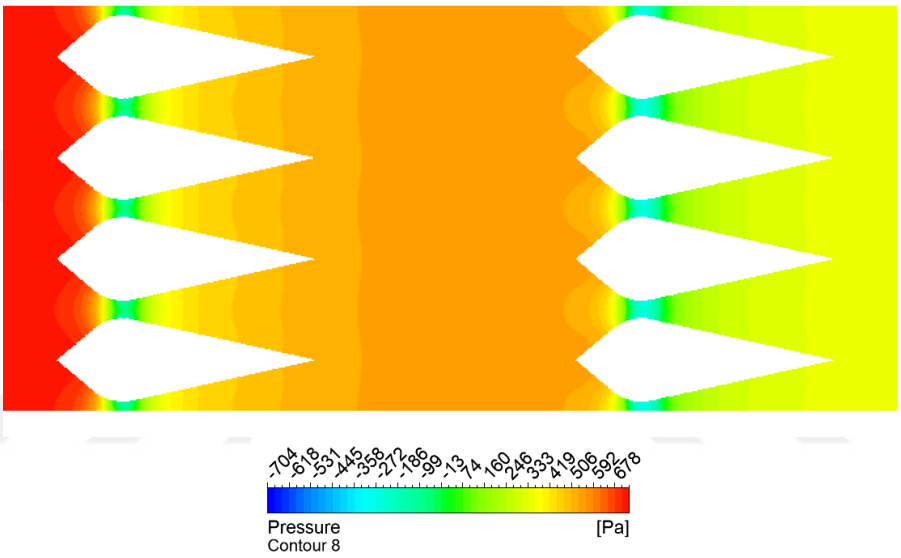


(b)

Figure 4.22. Temperature contours of optimum a) diamond b) enhanced shaped inline tube banks



(a)



(b)

Figure 4.23. Pressure contours of optimum a) diamond b) enhanced shaped inline tube banks

4.3. Optimization of Tube Bank with Staggered Arrangement (Aktas et al., 2023)

4.3.1. Comparison of Optimum Circular and Diamond Shaped Tube Bank with Staggered Arrangement

In the optimization problems for the staggered arrangement, two objective functions are chosen which are contradictory to each other, namely maximizing the heat transfer and minimizing the pump power. And the objective of the study is to determine the optimal condition for a given parameter ranges. Since the objective of this study is to obtain optimal geometrical configurations of staggered arranged circular, diamond and enhanced shaped tube banks, an optimization study for circular tube bank is firstly conducted. Then, using the same objectives optimum staggered enhanced arrangement designs are determined.

The optimization problem is studied using the commercial software modeFRONTIER.

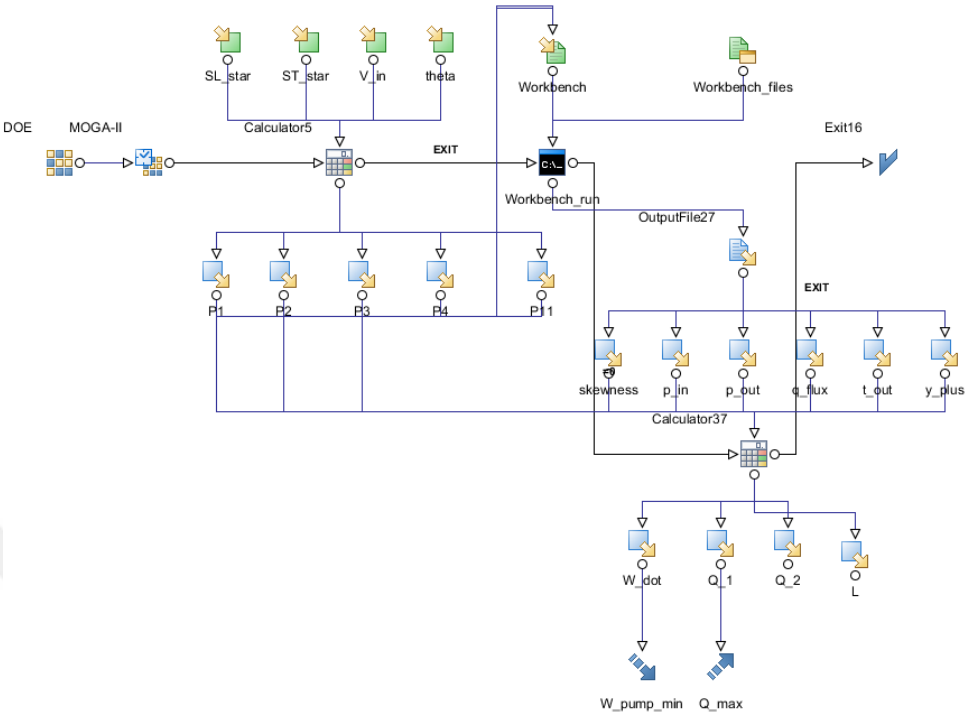


Figure 4.24. Optimization workflow for circular geometry

Table 4.13. Multi-objective design optimization problem for circular shaped staggered tube bank

Objective Functions	(1)	Maximum $\dot{Q}_{total}$		
	(2)	Minimum $\dot{W}_{pump}$		
Optimization Variables		***Lower Bound***	***Upper Bound***	***Step Size***
	V_{in} [m/s]	1	6	0.5
	S_L^*	1.2	3.0	0.1
	S_T^*	1.2	3.0	0.1

Firstly, a parametric model is created, and grids are applied to the model in ANSYS Workbench software. Then the model is integrated into an optimization program to obtain designs. As can be seen in Figure 4.24 and 4.25 the optimization algorithm, design of experiments, optimization variables, workbench files using the parametric model, controlling the numerical simulation, output files, variables, objective functions, and constraints are described for staggered circular and diamond shaped tube banks. It can be seen that the optimization problem has two objectives: The first is to obtain the total heat transfer ($\dot{Q}_{total}$) and the other is to minimize the

pressure drop ($\dot{W}_{pump}$). For this purpose, two non-dimensional optimization variables are chosen, namely S_L^*, S_T^* and V_{in} for circular arrangement. For diamond shaped staggered tube bank, in addition to S_L^*, S_T^* and V_{in} attack angle θ also prescribed as input parameter. Identical lower and upper bounds are limited to 1.2 and 3.0 for S_L^* and S_T^*, respectively, with a step size of 0.1. For the inlet velocity, the step size is set to 0.5 within the bounds of 1 to 6 m/s. Attack angle is limited in the 10 to 170˚ with the step size of 5˚. The optimization problem of staggered arranged circular and diamond geometry for the multi-objective design is given in Table 4.13 and 4.14 as follows:

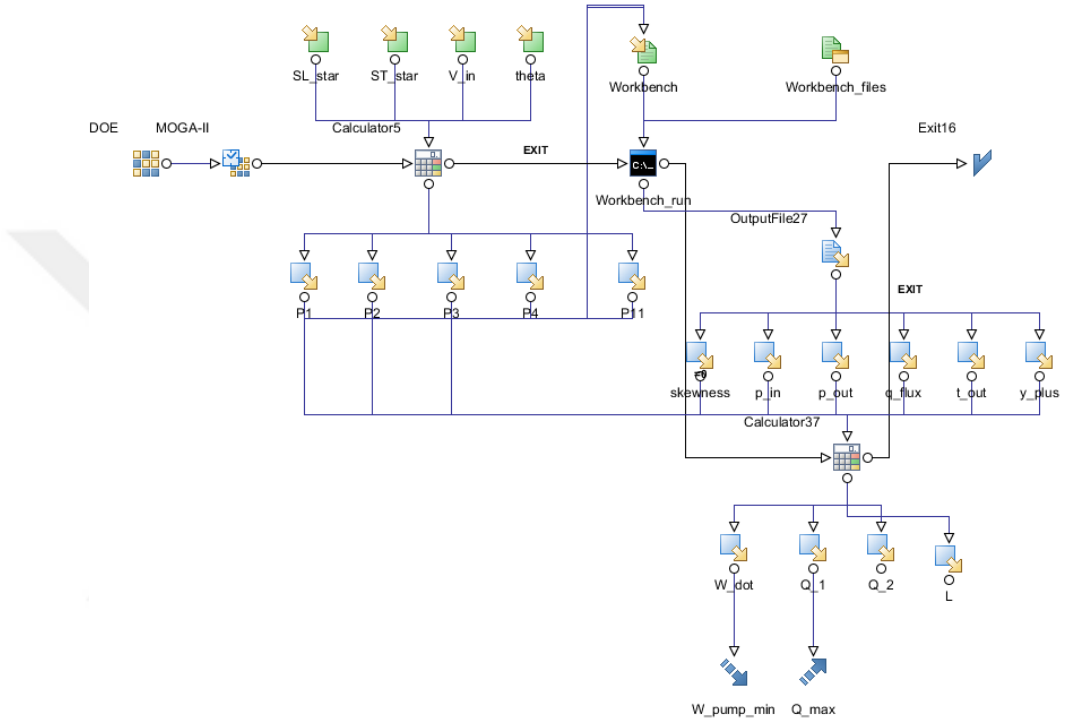


Figure 4.25. Optimization workflow for diamond shaped staggered tube bank

Table 4.14. Multi-objective design optimization problem for diamond shaped staggered tube bank

Objective Functions	(1)	Maximum $\dot{Q}_{total}$		
	(2)	Minimum $\dot{W}_{pump}$		
Optimization Variables		***Lower Bound***	***Upper Bound***	***Step Size***
	V_{in} [m/s]	1	6	0.5
	S_L^*	1.2	3.0	0.1
	S_T^*	1.2	3.0	0.1
	θ [˚]	10	170	5

The heat flux $\dot{q}$, the pressure at inlet P_{in} and outlet P_{out}. the temperatures at inlet T_{in} and outlet T_{out}. y+ value and the skewness are written to output files using the postprocessor of the Ansys Fluent software. We can use modeFRONTIER to retrieve the values from the output files and Python scripting language is used for the file operations. Heat transfer area, cross section area, logarithmic mean temperature difference, total heat transfer, mass flow rate, total pressure drop, and tube length of the parametric model are obtained for each design point using the 'Calculator' of the script of the optimization software for comparison. DOEs method is used to generate initial designs in the design space of the optimization problem, so that it is possible to obtain Pareto designs around DOEs. The Sobol sequence method is chosen in this study for the distribution of optimization variables in the design space. At the end of the optimization run, for the circular staggered tube bank, a total of 477 designs are obtained. Among these 108 designs are identified as Pareto designs in these results. For diamond staggered arrangement. 736 of total designs and 99 of Pareto designs among these are determined. These selected designs are given in Table 4.15.

Table 4.15. Selected designs of circular and diamond shaped staggered tube banks from the first step optimization study.

Design ID	Pareto Design	$\dot{Q}_{total}$ [W]	$\dot{W}_{pump}$ [W]	V_{in} [m/s]	S_L^*	S_T^*	θ [°]
863	Circ.	1089.88	61.36	6	1.2	1.2	-
1832	Circ.	741.50	19.78	4	1.3	1.2	-
233	Dia.	6161.32	1472.3	4	1.4	1.3	170
1020	Dia.	1895.84	19.79	5.5	1.2	1.2	10

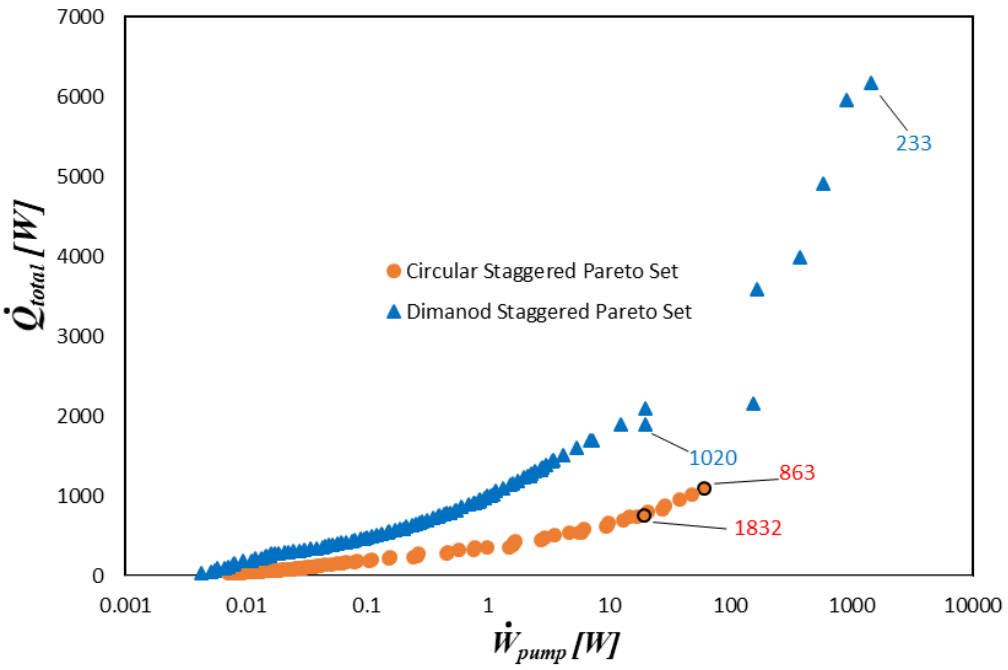


Figure 4.26. Scatter of $\dot{Q}_{total}$ vs $\dot{W}_{pump}$

Figure 4.26 shows the relationship between $\dot{Q}_{total}$ and $\dot{W}_{pump}$. for circular and diamond staggered tube banks for all feasible designs. Since there is no constraint, there is no unfeasible design in the design space. It can be observed that $\dot{Q}_{total}$ increases with increasing $\dot{W}_{pump}$. Moreover, in Pareto designs, maximizing $\dot{Q}_{total}$ is improved while minimizing $\dot{W}_{pump}$ is worsened. Within the Pareto designs, one can easily observe that diamond designs are always yields higher $\dot{Q}_{total}$ than circular design for the same $\dot{W}_{pump}$. For example, ID 1020 of diamond geometry has the $\dot{Q}_{total}$ value of 1895.84 W and ID 1832 of circular geometry has 741.5 W $\dot{Q}_{total}$ for the same $\dot{W}_{pump}$ of 19.8 W, which is 2.5 times higher. It is also observed that there is no feasible design for $\dot{W}_{pump}$ value higher than 72.22. However, there are 6 designs above that $\dot{W}_{pump}$ value for diamond tube bank. Highest obtainable $\dot{Q}_{total}$ are 1089.9 and 6161.3 for circular and diamond shaped tube bank, respectively.

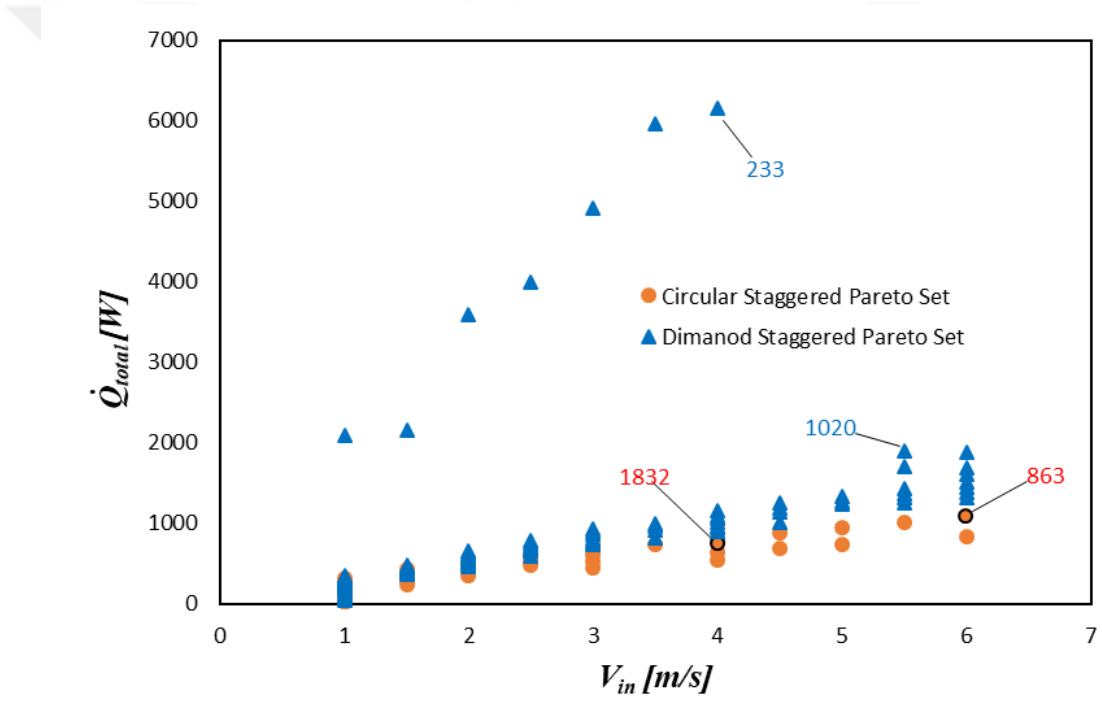


Figure 4.27. Scatter of $\dot{Q}_{total}$ vs V_{in}

Figure 4.27 displays the relationship between $\dot{Q}_{total}$ and V_{in}, for circular and diamond staggered tube banks for all feasible designs. It is seen that $\dot{Q}_{total}$ values show an increasing trend with increasing inlet velocity V_{in} as expected. Most of the designs are gathered in the zone below the 2000 W of $\dot{Q}_{total}$ value. Whereas, all the 6 designs above the 2000 W of $\dot{Q}_{total}$ are belong to the diamond shaped staggered tube bank. Highest $\dot{Q}_{total}$ are obtained at 6 m/s and 4 m/s for circular (ID 863) and diamond (ID 233) shaped tube bank, respectively.

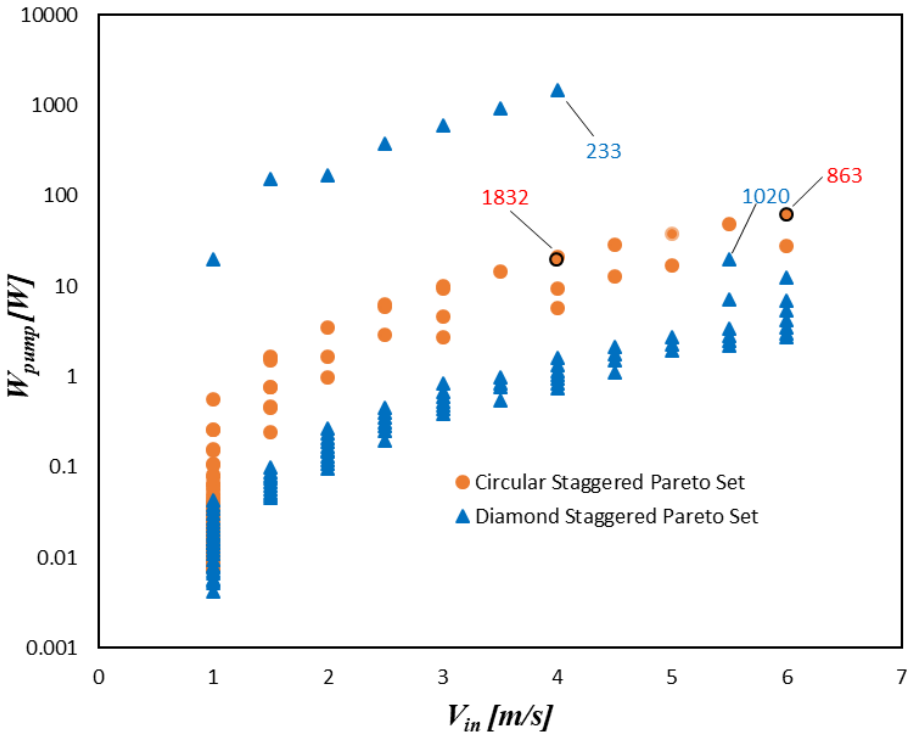
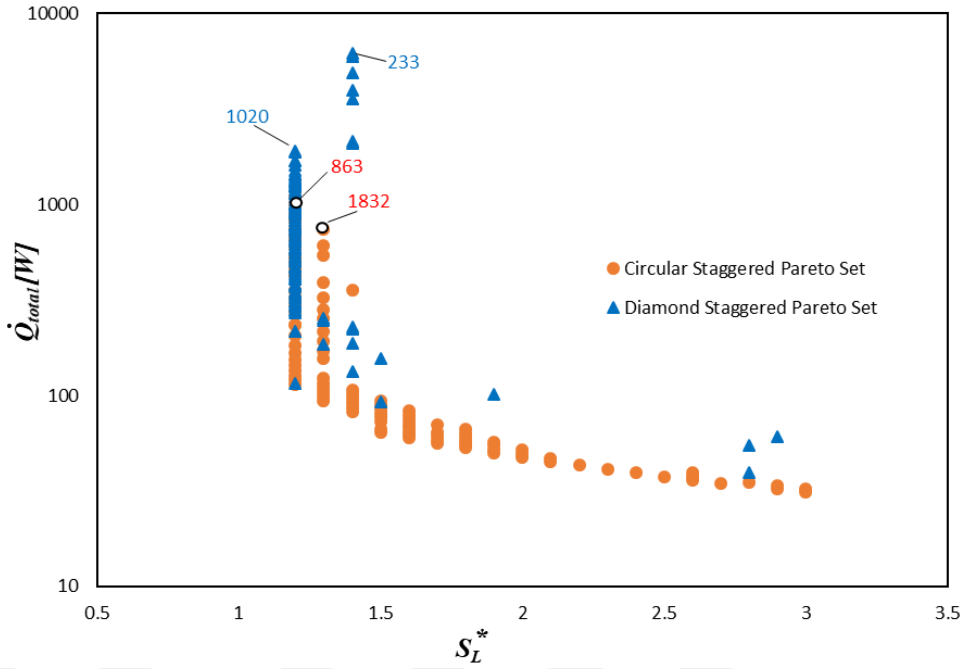
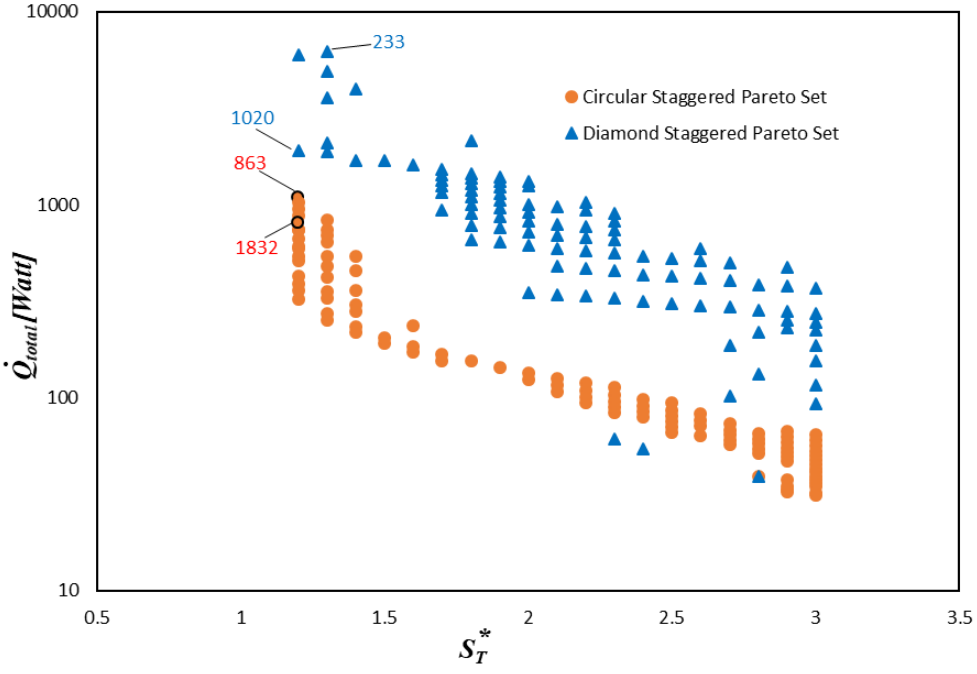


Figure 4.28. Scatter of $\dot{W}_{pump}$ vs V_{in}

Figure 4.28 demonstrates the behavior of $\dot{W}_{pump}$ against to inlet velocity V_{in} for Pareto designs. It can be observed that $\dot{W}_{pump}$ tends to increase with increasing V_{in}. For most of the Pareto designs, power requirement is lower for circular staggered arranged tube bank. For the 6 exceptional designs, power requirements are slightly higher for diamond staggered arranged tube bank.



(a)



(b)

Figure 4.29. (a) Scatter of $\dot{Q}_{total}$ vs S_L^* (b) Scatter of $\dot{Q}_{total}$ vs S_T^*

Figure 4.29 (a) and (b) present scatter of $\dot{Q}_{total}$ as a function of S_L^* and S_T^*, respectively. It can be observed that, generally $\dot{Q}_{total}$ has a decreasing trend with increasing S_L^* and S_T^*. Most of the designs are gathered in the low S_L^* region. Only 3 Pareto diamond designs have S_L^* value above 1.9. Others are in the region of 1.2 to 1.5. Highest obtained $\dot{Q}_{total}$ value for circular and diamond geometry where S_L^* is 1.2 (ID 863) and 1.4 (ID 233), respectively. Whereas, Pareto designs are located in whole S_T^* range a more homogeneous way for both geometries. Highest obtained $\dot{Q}_{total}$ value for circular and diamond geometry where S_T^* is 1.2 (ID 863) and 1.3 (ID 233), respectively.

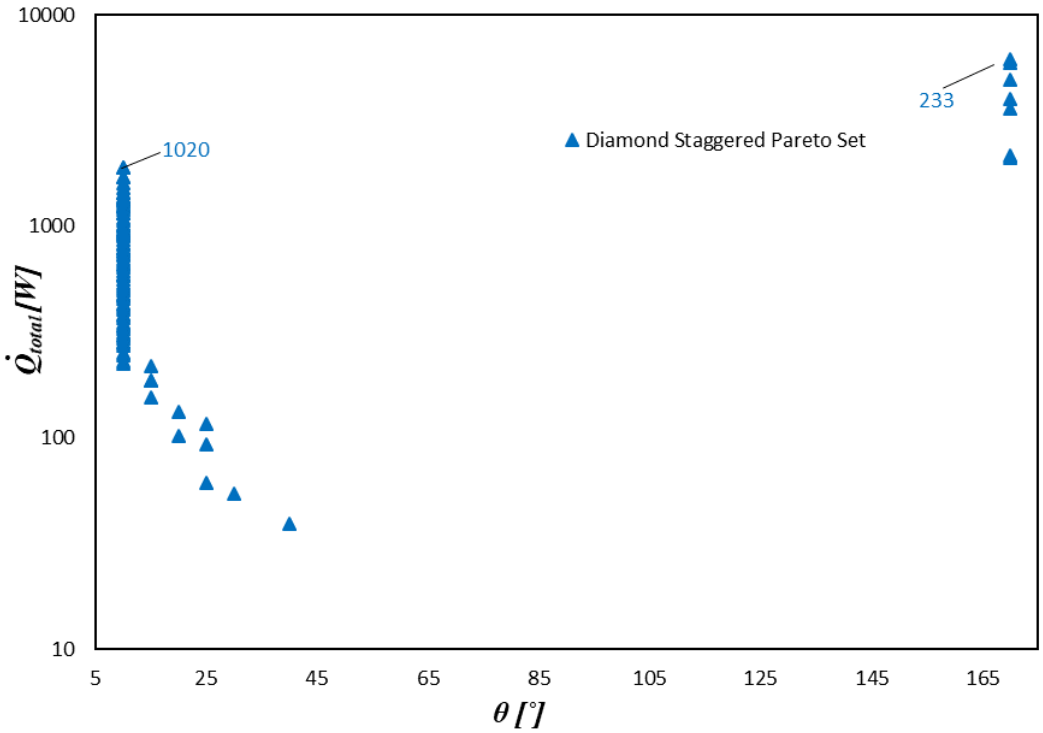


Figure 4.30. Scatter of $\dot{W}_{pump}$ vs θ

Figure 4.30 shows the scatter of $\dot{Q}_{total}$ as a function of attack angle. θ for diamond staggered tube bank. Since, attack angle cannot be a variable for circular geometry it is not involved in the graph. It is seen that most of the designs are gathered in the region of 10 to 40˚ and only 5 of them are at 170˚. Highest $\dot{Q}_{total}$ (ID 233) is obtained where attack angle is 170˚.

4.3.2. Comparison of Optimum Diamond and Enhanced Shaped Tube Bank with Staggered Arrangement

In the first section, circular and diamond shaped staggered tube banks were compared with objective functions of maximum $\dot{Q}_{total}$ and minimum $\dot{W}_{pump}$ for the same constant volume condition. In this section there will be again 2 optimization studies: Firstly, optimum diamond shaped staggered tube bank is determined. In this optimization problem in addition to two objective functions of maximum $\dot{Q}_{total}$ and minimum $\dot{W}_{pump}$ also length of the tube is limited to prevent unreasonable tube bank dimensions. Multi-objective optimization of diamond shaped geometry for second optimization step is formulated in Table 4.16. At the end of the second optimization run for the diamond staggered tube bank, a total of 229 (see Table 4.18) designs are obtained as feasible. Among these 28 designs are identified as Pareto designs in these results. For enhanced staggered arrangement. 1642 of total design and 146 (see Table 4.19) of Pareto designs among these are determined.

Table 4.16. Multi-objective design optimization problem for diamond shaped staggered tube bank

Objective Functions	(1)	Maximum $\dot{Q}_{total}$		
	(2)	Minimum $\dot{W}_{pump}$		
Optimization Variables		***Lower Bound***	***Upper Bound***	***Step Size***
	V_{in} [m/s]	1	6	0.5
	S_L^*	1.2	3.0	0.1
	S_T^*	1.2	3.0	0.1
Constraint	$L \leq 1\ m$			

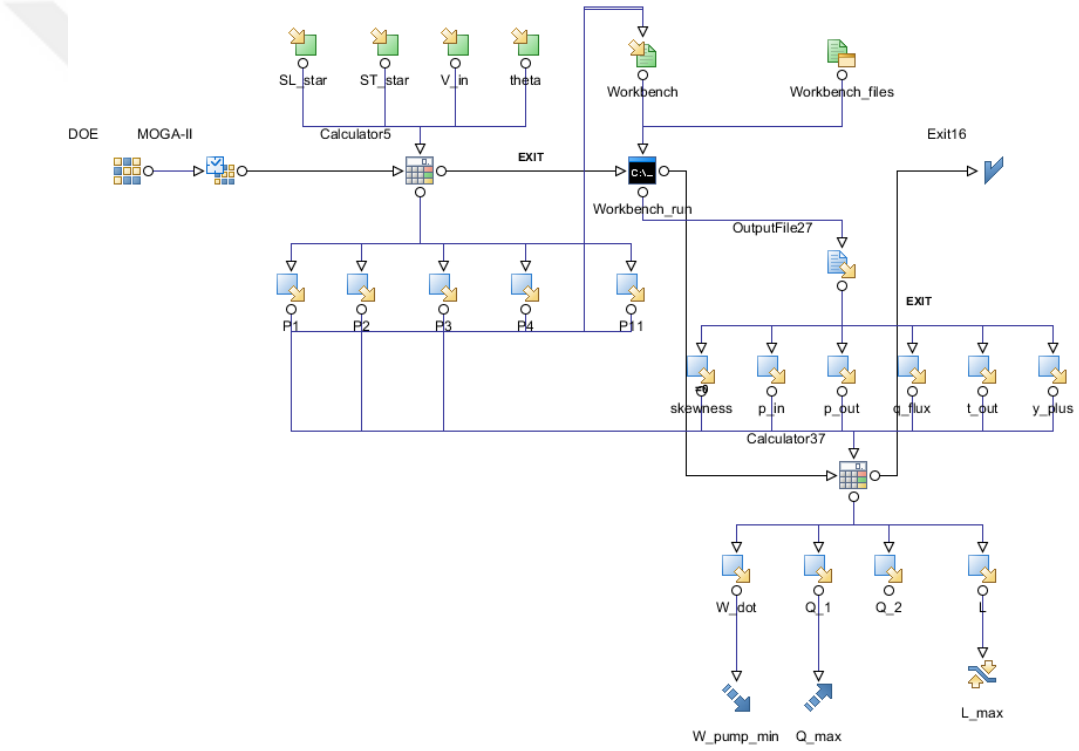


Figure 4.31. Optimization workflow for diamond shaped staggered tube bank of the second optimization step.

As seen from the figure 4.31, unlike the first step diamond optimization study tube bank length L is limited as constraint.

Table 4.17. Multi-objective design optimization problem for enhanced shaped staggered tube bank

Objective Functions	(1)	Maximum $\dot{Q}_{total}$		
	(2)	Minimum $\dot{W}_{pump}$		
Optimization Variables		***Lower Bound***	***Upper Bound***	***Step Size***
	V_{in} [m/s]	1	6	0.5
	S_L^*	1.2	3.0	0.1
	S_T^*	1.2	3.0	0.1
	θ_1	10	170	5
	θ_2	10	170	5
Constraint	$L = 1\ m$			

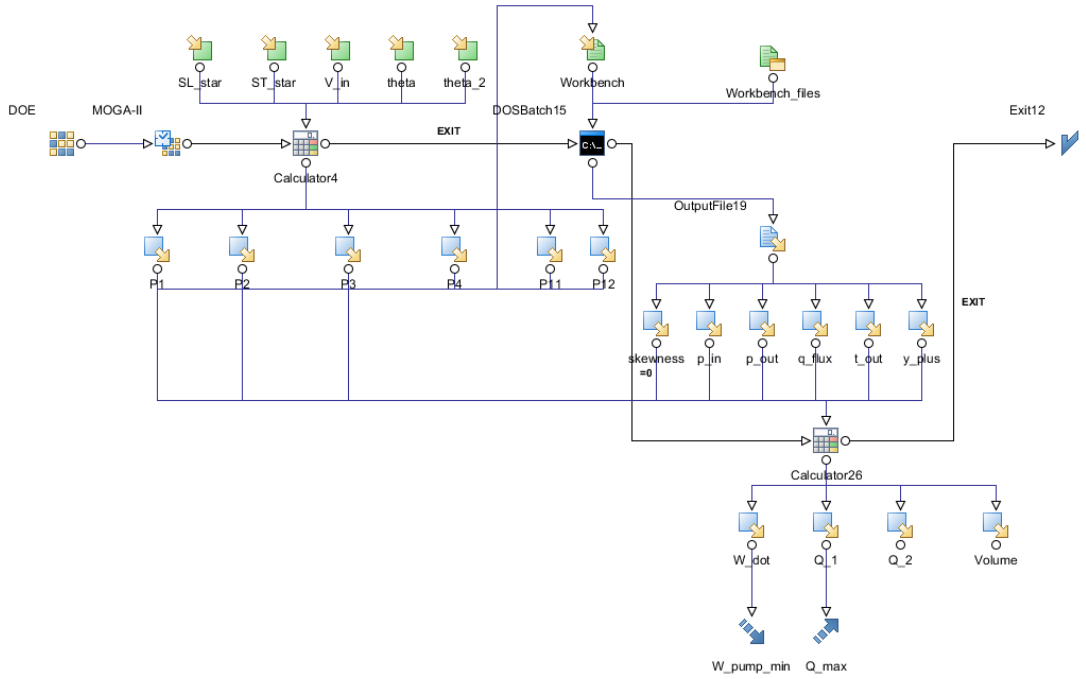


Figure 4.32. Optimization workflow for enhanced staggered tube bank of the second optimization step.

Figure 4.32 demonstrates the workflow employed for the optimization of the enhanced staggered tube bank. This workflow is constructed similar to second optimization step of staggered diamond tube bank. However, due to the independent front and rear attack angle definition of the geometry. 2 angles θ_1 and θ_2 are defined as input parameters as given in the Table 4.17. Maximizing heat transfer and minimizing pressure drop at the constant tube bank length are the objective functions of this case, apart from case 1. Therefore, we will be able to obtain an optimum design at a smaller volume.

Table 4.18. Pareto designs for staggered arranged diamond shaped tube bank

Design ID	S_L^*	S_T^*	V_{in} [m/s]	θ [°]	$\dot{W}_{pump}$ [W]	$\dot{Q}_{total}$ [W]	L_D [m]
32	1.7	1.2	3	125	43.35561	613.4289	0.808434
43	1.7	1.2	3	120	38.46686	567.0995	0.764677
49	1.5	2.3	3	25	0.191764	249.1053	0.926556
60	1.3	1.2	3	120	51.92422	766.7726	0.999963
82	2.1	2.6	6	15	0.66214	413.2129	0.955983
103	2.8	2.8	1	40	0.004495	39.20252	0.268074
111	2.3	2.8	6	15	0.532513	348.7539	0.810507
121	2.2	1.8	3.5	20	0.434912	298.3099	0.997452
125	2.7	3	6	10	0.545648	385.5812	0.96047
221	1.4	2.1	1	30	0.016055	135.4004	0.919013
230	2.4	1.7	3	20	0.29607	294.6171	0.968115
270	1.5	2.1	1	30	0.014968	124.8424	0.857745
654	2.9	2.3	1	25	0.005795	61.05234	0.479253
659	2.3	2.7	2.5	15	0.070048	213.5325	0.840526
685	1.4	2	2.5	30	0.206093	255.2587	0.964964
827	2.8	2.9	4	10	0.213645	293.4239	0.958104
941	2.8	2.1	2	15	0.057438	197.0893	0.887698
946	2.8	2.4	1	30	0.005444	54.52489	0.402068
1027	2.6	2.2	1.5	15	0.029566	162.8962	0.912529
1450	1.9	2.7	1	20	0.006994	101.3572	0.769963
1495	2	2.8	2.5	15	0.074654	237.265	0.932083
1499	1.5	2.4	1	25	0.010242	119.6149	0.887949
1643	1.2	2.3	1	35	0.015658	132.8097	0.853372
1653	1.5	3	1	25	0.006098	92.95839	0.71036
1662	1.2	3	1	25	0.007426	116.0101	0.887949
1712	1.2	2.8	2	30	0.056503	171.1988	0.804136
1815	1.2	1.9	6	40	3.862483	469.3828	0.9218
2008	1.7	2.5	2	20	0.05769	212.3156	0.929391

Table 4.19. Pareto designs for staggered arranged enhanced shaped tube bank

Design ID	S_L^*	S_T^*	V_{in} [m/s]	θ_1 [°]	θ_2 [°]	Volume [m^3]	$\dot{W}_{pump}$ [W]	$\dot{Q}_{total}$ [W]
148	1.4	1.4	6	130	15	0.000438	5.2464	526.644
156	2.5	1.3	5.5	105	15	0.000727	5.7070	531.4076
157	1.4	2.6	2	15	100	0.000814	0.0864	234.948
167	1.6	2.2	6	105	35	0.001346	2.2278	448.1252
175	2	1.7	5.5	95	35	0.001296	2.9333	472.2955
179	2.5	1.3	6	140	15	0.000726	7.3728	562.3053
189	2.5	1.2	6	70	15	0.000657	13.5647	604.0787
191	2.4	1.4	6	140	15	0.000751	5.0636	520.2877
219	2.9	1.3	6	60	15	0.000812	6.3952	549.0195
250	2.3	1.5	6	140	15	0.000771	3.6303	493.3421
270	1.2	2.6	1	15	90	0.000695	0.0137	158.9668
318	1.2	1.7	5.5	60	20	0.000536	1.8984	440.5487
328	1.4	1.5	6	65	20	0.000558	3.9258	495.077
352	1.2	1.2	5	65	65	0.000652	24.5394	675.9381
379	1.3	1.2	5.5	85	50	0.000684	32.4839	689.7845
385	1.2	1.2	5.5	45	20	0.000358	10.7405	573.8616
395	1.9	1.6	6	40	15	0.00061	2.2723	449.4913
409	1.2	1.6	6	40	70	0.000755	6.2217	537.6874
419	1.2	1.3	5.5	80	60	0.000717	16.1482	629.3526
435	1.2	1.3	5	80	60	0.000717	12.3561	590.856
459	1.2	1.3	5.5	85	70	0.000745	16.6380	642.7312
461	1.2	2.8	5.5	60	10	0.00053	0.5930	361.2528
506	1.5	1.6	6	110	10	0.00039	2.4015	454.1164
513	1.3	1.2	6	40	85	0.000628	36.2863	741.878
522	1.5	1.6	6	125	10	0.00039	2.5052	456.5561
1076	1.3	1.2	6	50	85	0.000684	42.6528	771.3055
1084	2.8	1.6	6	70	10	0.000716	2.1086	440.6143
1121	1.3	3	1	25	35	0.001022	0.0106	144.4879
1122	1.2	1.2	6	40	65	0.000559	35.1517	729.8145
1127	2.5	1.4	6	75	15	0.000771	4.4833	514.1979
1132	1.3	2.8	1	35	35	0.001112	0.0130	152.3617
1138	2.4	1.6	6	75	15	0.000846	2.6662	465.7428
1204	1.3	2.9	1	30	30	0.001014	0.0106	143.572
1237	1.3	2.6	1	35	50	0.001164	0.0176	162.9249
1284	1.2	2.6	1	40	55	0.001167	0.0198	166.2298
1295	1.2	2.5	1	30	65	0.001015	0.0190	164.2965
1356	1.6	2.6	1.5	45	50	0.001585	0.0589	208.6513
1362	1.2	2.9	1	55	15	0.00074	0.0079	132.4432
1448	1.2	2.7	1.5	40	35	0.001041	0.0400	194.5773
1531	1.2	2.5	1	35	15	0.000583	0.0091	137.278
1573	1.2	2.7	3	35	15	0.00063	0.1299	254.2417
1604	1.3	2.7	1	30	25	0.000869	0.0102	139.2145

Design ID	S_L^*	S_T^*	V_{in} [m/s]	θ_1 [°]	θ_2 [°]	Volume [m^3]	$\dot{W}_{pump}$ [W]	$\dot{Q}_{total}$ [W]
1628	1.2	2.6	6	85	10	0.000504	0.8869	400.6182
1640	1.3	2.6	1	30	15	0.00063	0.0086	136.4221
1681	1.2	2.6	4	30	15	0.000581	0.2701	297.0598
1683	1.2	2.3	6	60	15	0.000594	1.1070	414.4851
1692	1.2	2.6	6	70	15	0.000683	0.9849	404.4547
1702	1.2	2.7	1.5	30	30	0.000871	0.0322	184.9043
1714	1.3	2.7	6	30	10	0.000497	0.6382	376.147
1725	1.2	2.6	4.5	10	15	0.000358	0.3122	308.4466
1738	1.2	2.6	5	20	10	0.000396	0.3923	328.1271
1741	1.2	2.7	4.5	40	15	0.00065	0.3748	320.0359
1745	1.2	2.7	2	30	35	0.000927	0.0749	224.833
1751	1.3	2.4	1.5	30	15	0.000581	0.0259	173.9815
1760	1.2	2.7	1.5	20	25	0.000668	0.0262	175.9271
1761	1.2	2.7	1	30	35	0.000927	0.0126	151.0621
1767	1.2	2.6	5	15	15	0.000445	0.4117	336.6241
1774	1.2	2.7	1.5	20	30	0.000715	0.0289	182.4336
1776	1.2	2.7	3.5	30	10	0.000459	0.1640	263.7867
1783	1.2	2.6	2	30	35	0.000892	0.0783	226.6361
1794	1.2	2.7	4	30	20	0.000715	0.2904	297.9136
1815	1.2	2.7	5.5	20	10	0.000411	0.4797	350.7118
1819	1.2	2.7	2	20	30	0.000715	0.0596	214.2469
1827	1.2	2.6	6	30	10	0.000442	0.6678	381.0273
1837	1.2	2.6	6	25	10	0.000422	0.6500	376.4807
1839	1.2	2.7	4.5	30	10	0.000459	0.3077	307.5253
1847	1.2	2.7	1.5	20	15	0.000524	0.0216	171.9516
1849	1.2	2.7	4.5	30	15	0.000604	0.3459	315.3373
1857	1.2	2.7	1	20	15	0.000524	0.0080	136.404
1859	1.2	2.7	1	30	10	0.000459	0.0075	128.85
1860	1.2	2.6	2	20	30	0.000689	0.0620	215.6824
1864	1.2	2.7	5.5	35	10	0.000474	0.5310	356.8284
1869	1.2	2.3	6	20	10	0.00035	0.7397	382.3757
1873	1.2	2.8	1	35	10	0.000491	0.0072	128.6701
1879	1.2	2.7	2	20	15	0.000524	0.0436	201.721
1884	1.2	2.6	6	20	10	0.000396	0.6188	372.823
1886	1.2	2.1	6	50	10	0.00039	1.0573	406.9878
1893	1.2	2.6	4	40	10	0.000467	0.2568	289.3232
1894	1.2	2.7	1	35	10	0.000474	0.0076	129.0437
1903	1.2	2.6	2	35	35	0.000953	0.0821	228.75
1906	1.2	2.7	5	10	15	0.000372	0.3812	327.5282
1914	1.2	1.9	6	60	15	0.000491	1.5776	439.0405
1927	1.2	2	6	60	15	0.000517	1.4353	433.2456
1935	1.2	3	1	25	10	0.000487	0.0067	128.3398
1947	1.2	2.7	5.5	10	10	0.000311	0.4462	336.8424

Design ID	S_L^*	S_T^*	V_{in} [m/s]	θ_1 [°]	θ_2 [°]	Volume [m^3]	$\dot{W}_{pump}$ [W]	$\dot{Q}_{total}$ [W]
1969	1.2	2	6	85	15	0.000533	1.5709	438.5946
1971	1.2	2.7	2	30	30	0.000871	0.0661	216.4356
1977	1.2	2.9	4	20	30	0.000768	0.3073	302.8213
1982	1.2	2.6	1.5	30	15	0.000581	0.0233	172.4776
1991	1.2	2.6	1.5	40	50	0.001137	0.0540	207.9792
1995	1.2	2.2	1	40	55	0.000987	0.0247	173.7592
1996	1.2	2.7	1.5	30	25	0.000802	0.0282	176.3789
1998	1.2	2.4	1.5	35	45	0.000962	0.0516	206.037
2010	1.2	2.7	1	20	20	0.000606	0.0087	137.0936
2023	1.2	2.7	6	65	10	0.000515	0.7923	390.5808
2024	1.2	2.8	3.5	15	10	0.000386	0.1453	262.841
2027	1.2	2.9	1.5	35	35	0.001063	0.0354	191.6486
2039	1.2	2.9	1.5	20	35	0.000808	0.0291	184.6405
2062	1.2	2.6	4.5	30	10	0.000442	0.3224	308.9704
2076	1.2	2.6	4	35	10	0.000456	0.2504	289.2068
2090	1.2	2.6	1.5	30	90	0.001095	0.0590	209.2156
2095	1.2	2.5	1.5	30	40	0.000899	0.0429	198.2391
2103	1.2	2.7	1.5	20	40	0.000781	0.0335	189.3409
2143	1.3	3	1.5	35	60	0.001403	0.0492	205.097
2147	1.3	2.3	2.5	15	45	0.000615	0.1390	256.131
2152	1.2	2.5	1.5	20	80	0.000814	0.0481	202.8839
2183	1.2	2.5	1	20	40	0.000723	0.0128	151.0833
2198	1.3	2.5	3	15	35	0.000632	0.1799	274.4454
2205	1.2	2.8	2	35	35	0.001026	0.0756	225.3796
2209	1.2	2.4	1.5	15	45	0.000592	0.0356	194.0513
2244	1.3	2.6	3	15	35	0.000657	0.1687	272.2423
2246	1.2	2.6	1.5	35	40	0.001002	0.0434	199.4736
2253	1.3	2.7	3	15	35	0.000682	0.1656	272.0909
2260	1.2	2.2	6	50	20	0.000671	1.2711	415.5205
2274	1.2	2.6	1	30	35	0.000892	0.0132	152.4581
2290	1.2	3	1.5	40	50	0.001312	0.0470	202.2052
2295	1.2	2.2	6	75	15	0.000582	1.2760	424.6252
2300	1.5	2.7	4	15	35	0.000787	0.3400	314.6228
2304	1.3	2.8	2	30	40	0.001091	0.0791	226.7998
2317	1.3	2.8	2	30	35	0.001041	0.0726	223.3108
2333	1.2	2.6	2	10	30	0.000442	0.0518	206.4249
2358	1.3	2.8	2	20	45	0.000904	0.0716	223.1266
2363	1.2	2.8	2	30	35	0.000961	0.0719	223.1481
2372	1.2	2.8	2	20	40	0.00081	0.0674	221.3317
2402	1.3	2.8	2	30	45	0.001132	0.0854	229.9542
2419	1.2	2.9	2	35	40	0.001118	0.0799	227.8504
2425	1.3	2.8	3	30	50	0.001165	0.2629	289.5025
2433	1.2	2.4	4	15	20	0.000466	0.2915	300.1809

Design ID	S_L^*	S_T^*	V_{in} [m/s]	θ_1 [°]	θ_2 [°]	Volume [m^3]	$\dot{W}_{pump}$ [W]	$\dot{Q}_{total}$ [W]
2453	1.3	2.8	2.5	20	45	0.000904	0.1267	251.8655
2457	1.2	2.5	2.5	20	40	0.000723	0.1344	254.5617
2467	1.3	2.7	2.5	15	40	0.000704	0.1097	249.5271
2470	1.2	2.5	3	20	50	0.000762	0.2470	288.2369
2473	1.3	2.9	2	35	40	0.001211	0.0811	228.1905
2481	1.3	2.4	2.5	20	50	0.000793	0.1635	263.1903
2483	1.3	2.8	3	15	50	0.000763	0.1940	281.5589
2486	1.3	2.4	3	15	50	0.000654	0.2280	286.6526
2487	1.2	3	1.5	30	50	0.001152	0.0405	196.7962
2498	1.3	2.6	3	15	55	0.000719	0.2142	285.8886
2502	1.2	2.7	1	35	50	0.001116	0.0167	161.255
2504	1.3	2.8	2.5	15	45	0.000748	0.1109	250.6245
2510	1.2	2.5	3	20	55	0.000776	0.2633	291.7188
2513	1.2	2.7	1	15	45	0.000666	0.0108	150.0018
2515	1.3	2.8	2.5	15	35	0.000708	0.1003	246.2256
2521	1.2	2.5	2	15	80	0.000664	0.0885	237.7389
2525	1.3	2.7	3	15	55	0.000747	0.2053	284.4467
2526	1.3	2.6	3.5	15	65	0.000735	0.3391	311.6055

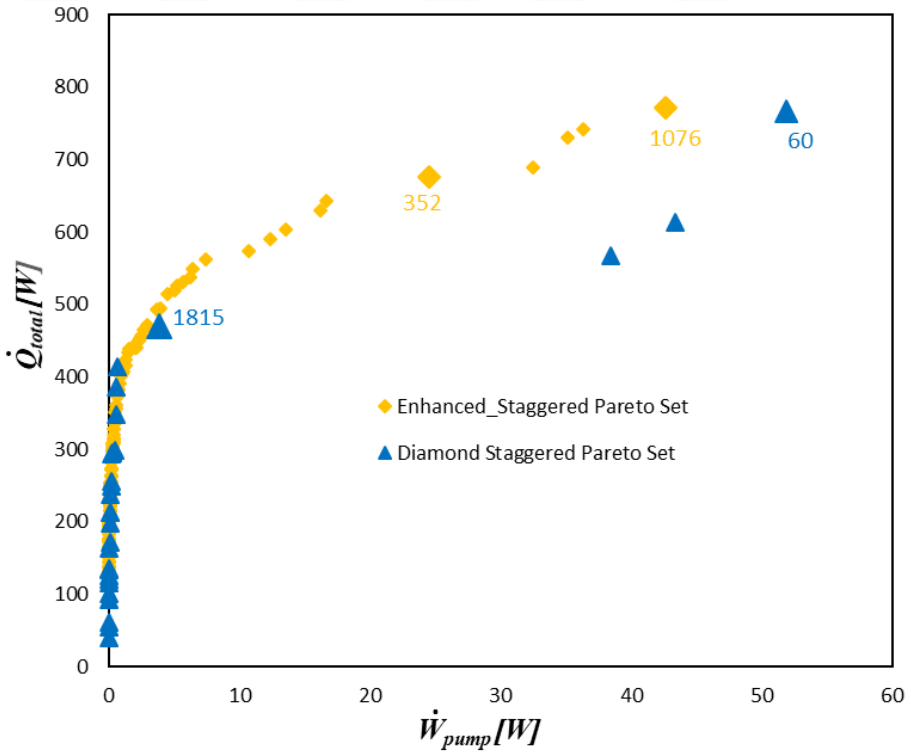


Figure 4.33. Scatter of $\dot{Q}_{total}$ vs $\dot{W}_{pump}$

Figure 4.33 shows the scatter of $\dot{Q}_{total}$ as a function of for Pareto designs of diamond and enhanced staggered tube bank. It is observed that $\dot{Q}_{total}$ value tend to increase with increasing $\dot{W}_{pump}$. Additionally, in Pareto designs, maximizing $\dot{Q}_{total}$ is improved while minimizing $\dot{W}_{pump}$ is worsened. It is observed that, beyond $\dot{Q}_{total}$=500 W there are only 3 designs for diamond geometry however, there are 17 designs for enhanced geometry. Among the Pareto diamond results, design with ID 60 has the max $\dot{Q}_{total}$ value of 766.8 where $\dot{W}_{pump}$ is 51.92. Whereas, among the enhanced Pareto results design ID 1076 $\dot{Q}_{total}$ value of 771.3 where $\dot{W}_{pump}$=42.65 which is the optimum design is. Moreover, this thermal performance is obtained in a smaller total tube bank volume which is 0.000684 m^3, while volume of the optimum designs of diamond geometries are set as 0.00075 m^3. Alternatively, ID 352 can be chosen as an optimum design for enhanced geometry with $\dot{W}_{pump}$value of 24.54 W (42.46 % lower than ID 1076) and $\dot{Q}_{total}$ value of 675.94 W (only 12.36 % lower than ID 1076) and ID 1815 can be considered as optimum for diamond geometry with $\dot{W}_{pump}$value of 3.86 W (92.57 % lower than ID 60) and $\dot{Q}_{total}$ value of 469.38 W (only 38.78 % lower than ID 60). These selected designs are given in Table 4.20.

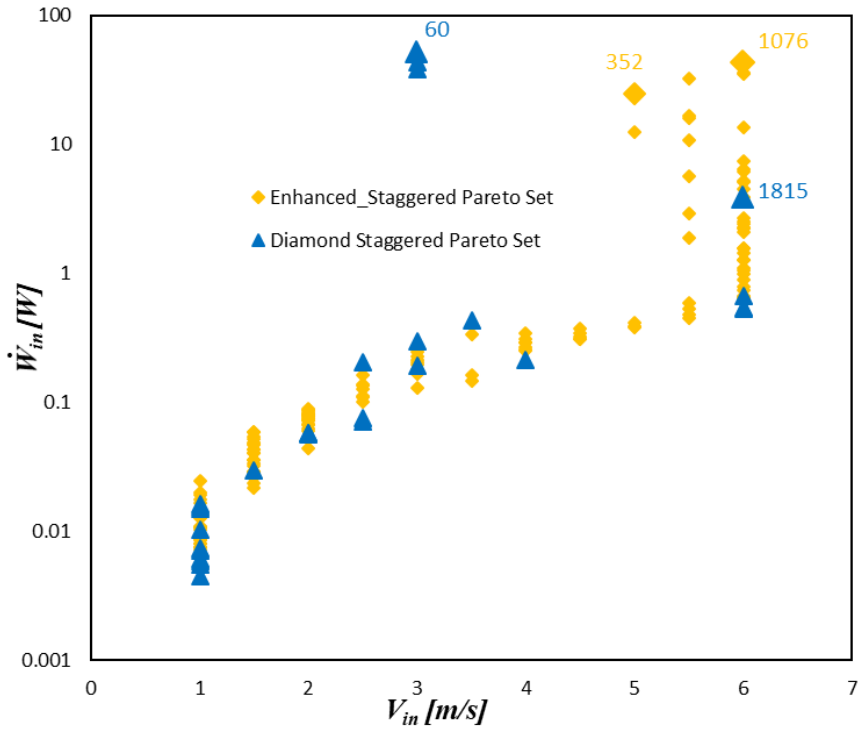


Figure 4.34. Scatter of $\dot{W}_{pump}$ vs V_{in}

Figure 4.34 displays the scatter of $\dot{W}_{pump}$ with varying V_{in} for Pareto designs of staggered diamond and enhanced shaped tube banks. Generally, increment in V_{in} results in rise in required $\dot{W}_{pump}$ value for both tube bank geometries. For enhanced geometry, designs with high $\dot{W}_{pump}$ values are combined in the zone where V_{in} is 3 m/s. However, for diamond staggered tubes. high $\dot{W}_{pump}$values are accumulated where V_{in} is between 5 to 6 m/s. Optimum values are obtained where 3 and 6 m/s (ID 60 and ID 1076) for diamond and enhanced geometries. On the other hand, alternative optimum values ID 1815 and ID 352 of diamond and enhanced geometry are obtained for V_{in} value of 6 and 5 m/s.

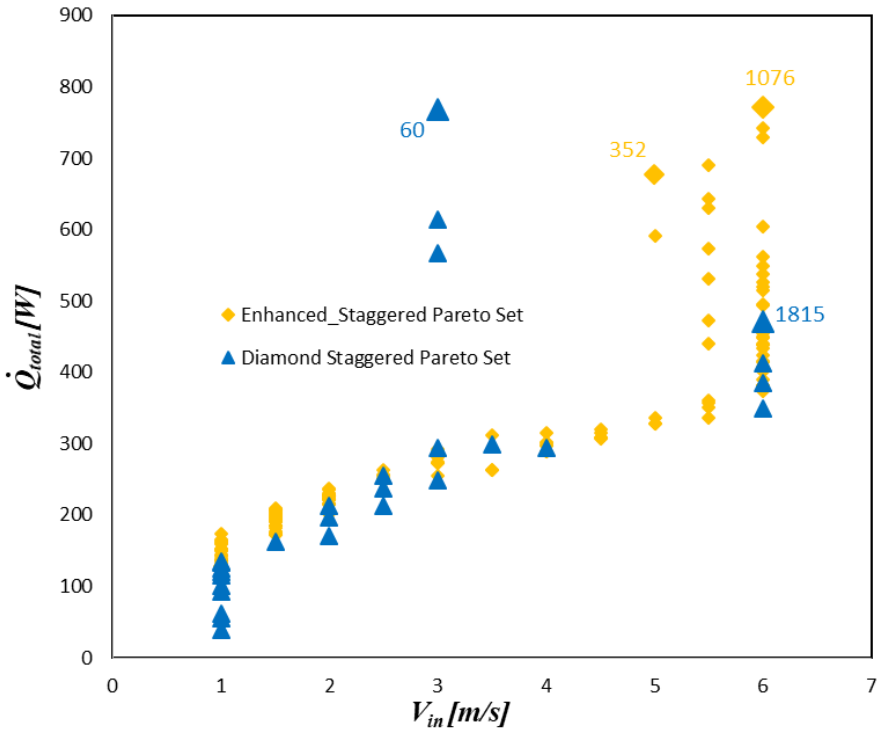
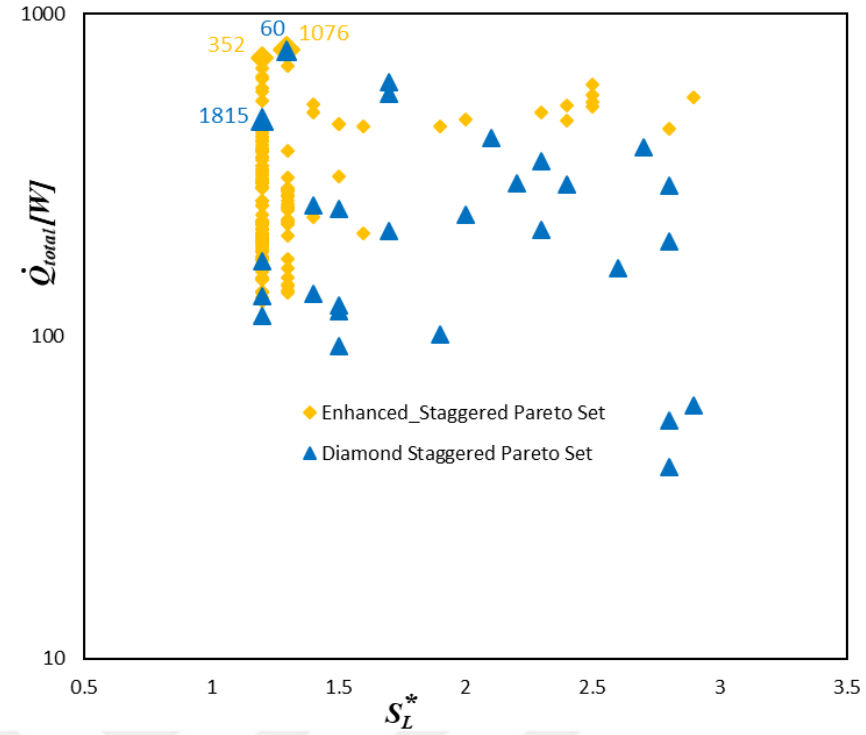
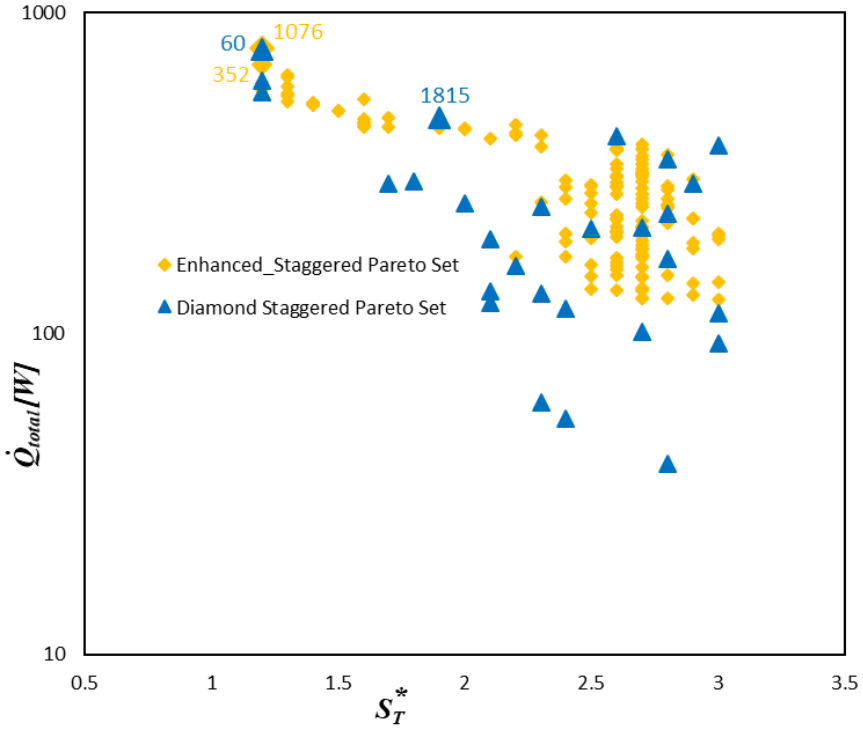


Figure 4.35. Scatter of $\dot{Q}_{total}$ vs V_{in}

Figure 4.35 shows the scatter of $\dot{Q}_{total}$ as a function of V_{in} for Pareto designs of staggered diamond and enhanced tube bank. Mostly, increase in V_{in} results in rise in $\dot{Q}_{total}$ value for both tube bank geometries. For enhanced geometry, designs with high $\dot{Q}_{total}$ values are combined where V_{in} is 3 m/s. On the other hand, for diamond staggered tubes high $\dot{Q}_{total}$ values are accumulated where V_{in} is between 5 to 6 m/s.



(a)

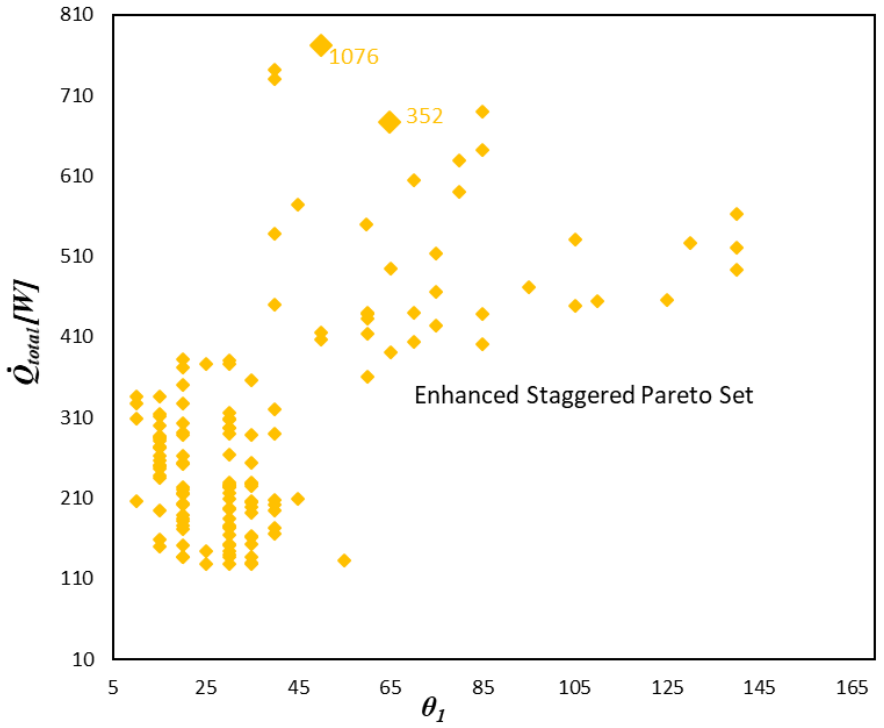


(b)

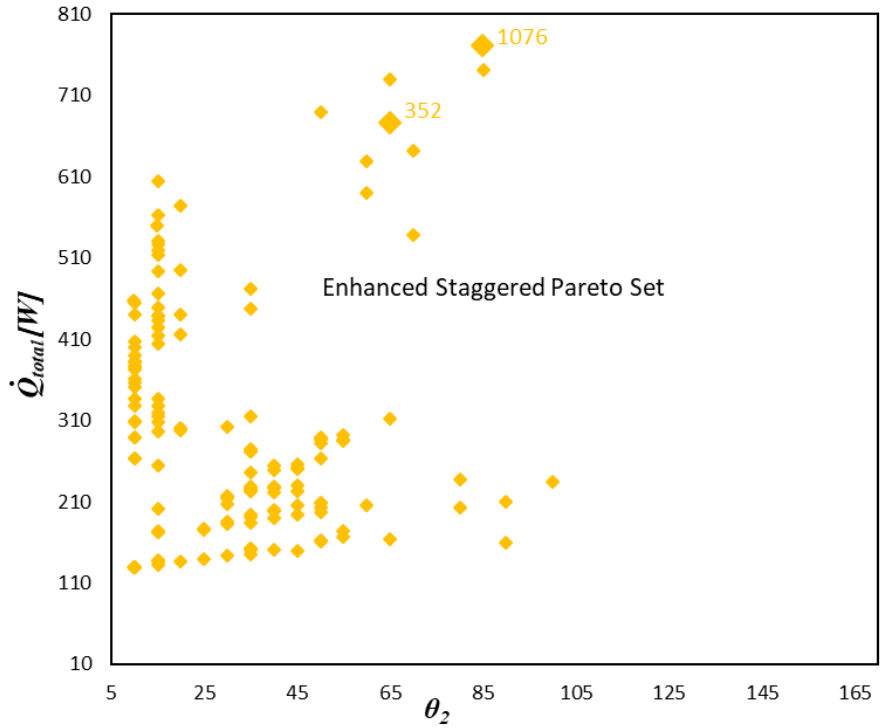
Figure 4.36. (a) Scatter of $\dot{Q}_{total}$ vs S_L^* (b) Scatter of $\dot{Q}_{total}$ vs S_T^*

Figure 4.36 (a) and (b) show scatter of $\dot{Q}_{total}$ as a function of S_L^* and S_T^*, respectively. It can be observed that, generally for diamond design $\dot{Q}_{total}$ has a decreasing trend with increasing S_L^*. Contrary to this, it tends to decrease with increasing S_L^* for enhanced staggered tube bank. However, both geometries show an increasing trend with increasing S_T^*. Most of the designs are gathered in the

high S_T^* region. Optimum values are (ID 60 and ID 1076) obtained for both geometries where S_L^*=1.3 and S_T^*=1.2. Whereas, alternative optimum values for diamond geometry with is determined where S_L^*=1.2 and S_T^*=1.9 and for enhanced geometry it is obtained where S_L^*=S_T^*=1.2.



(a)



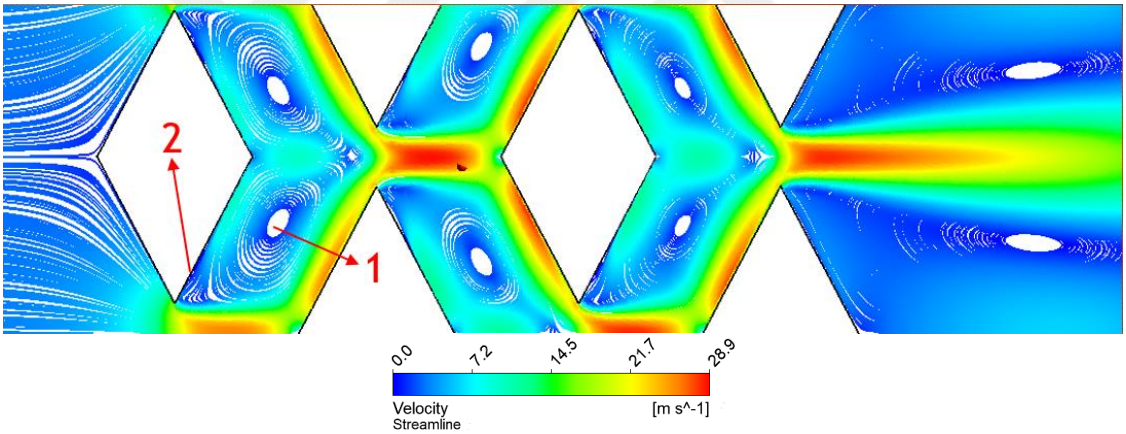
(b)

Figure 4.37. (a) Scatter of $\dot{Q}_{total}$ vs θ_1 (b) Scatter of $\dot{Q}_{total}$ vs θ_2

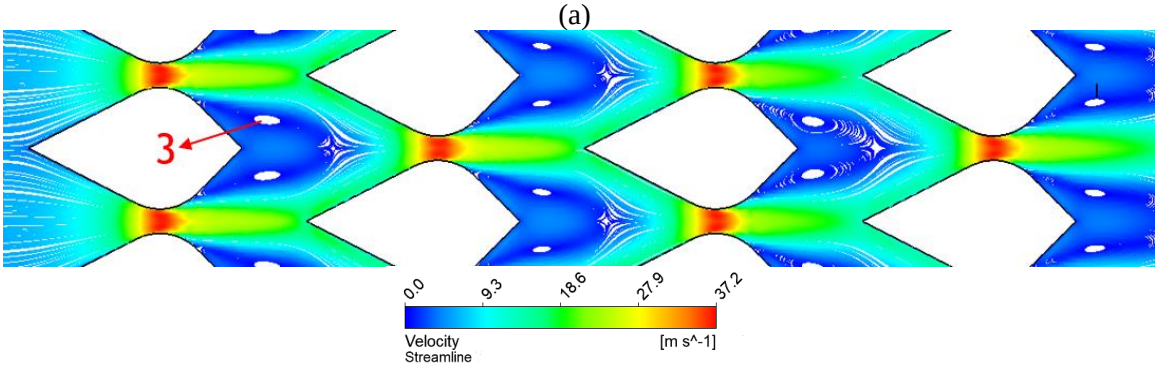
Figure 4.37 (a) and (b) show scatter of $\dot{Q}_{total}$ as a function of θ_1 and θ_2 for enhanced staggered tube bank, respectively. It can be seen that Pareto designs are obtained for θ_1 and θ_2 in the range of 10-140˚ and 10-100˚, respectively. For θ_1, most of the designs are gathered in the low angle region. However, these are located in a more homogeneous way for θ_2. Optimum design is obtained where θ_1 and θ_2 are 50˚ and 85˚. On the other hand, an alternative optimum point is obtained where $\theta_1 = \theta_2$ is 65˚.

Table 4.20. Selected designs of diamond and enhanced shaped staggered tube bank from the second step optimization study.

Design ID	Pareto Design	$\dot{Q}_{total}$ [W]	$\dot{W}_{pump}$ [W]	V_{in} [m/s]	S_L^*	S_T^*	θ_1 [°]	θ_2 [°]	L_D [m]	Volume [m^3]
60	Dia.	766.77	51.92	3	1.3	1.2	120	120	1	0.00075
1815	Dia.	469.38	3.86	6	1.2	1.9	40	40	0.92	0.00075
1076	Enh.	771.31	42.65	6	1.3	1.2	50	85	1	0.000684
352	Enh.	675.94	24.54	5	1.2	1.2	65	65	1	0.000652



(a)



(b)

Figure 4.38. Streamlines of optimum a) diamond b) enhanced shaped staggered tube banks

Figure 4.38 demonstrates streamlines of the optimum shaped diamond (ID 60) and enhanced (ID 1076) staggered tube bank. Flow separation is observed at rear side of the tubes where fluid momentum cannot overcome the adverse pressure gradient. In the wake zone of both optimum tubes, a couple of large recirculation zones are observed (see Figure 4.39 (a) and (b)). However, there is a second small vortex in the rear border of the diamond tubes. Figure 4.40 shows the temperature distribution of optimum diamond and enhanced shaped staggered tube bank. Since, the tube temperature is higher than that of the inlet fluid, temperature value increases in the flow direction. Due to the thin boundary layer, higher temperature gradient is observed near the upstream of the tubes. However, temperature gradient becomes lower since the vortex formed as a result of flow separation. Figure 4.41 demonstrates the pressure contours optimum diamond and enhanced shapes tube banks. Lowest local static pressure is observed at the back side of each tube which is the indication of flow separation. At the front tip of the tubes maximum local static pressure is detected as a proof of stagnation point.

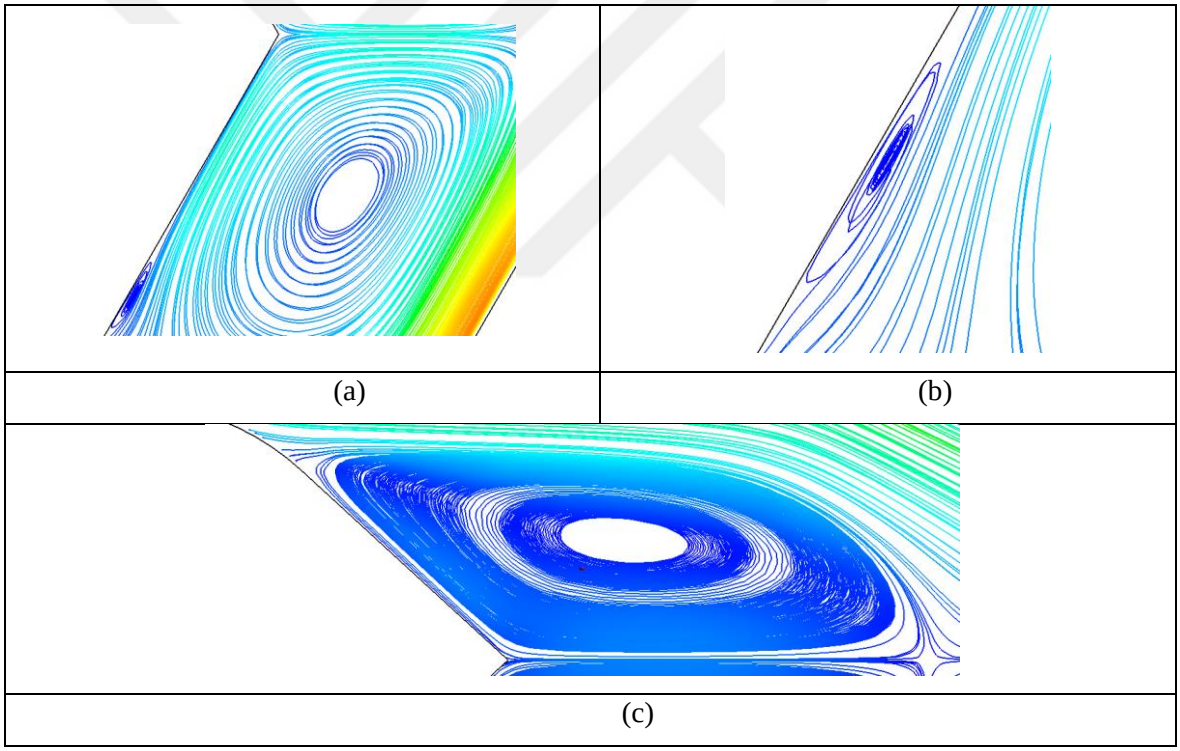


Figure 4.39. Enlarge view of optimum diamond a. b (1.2) and enhanced c (3) shaped geometry streamlines

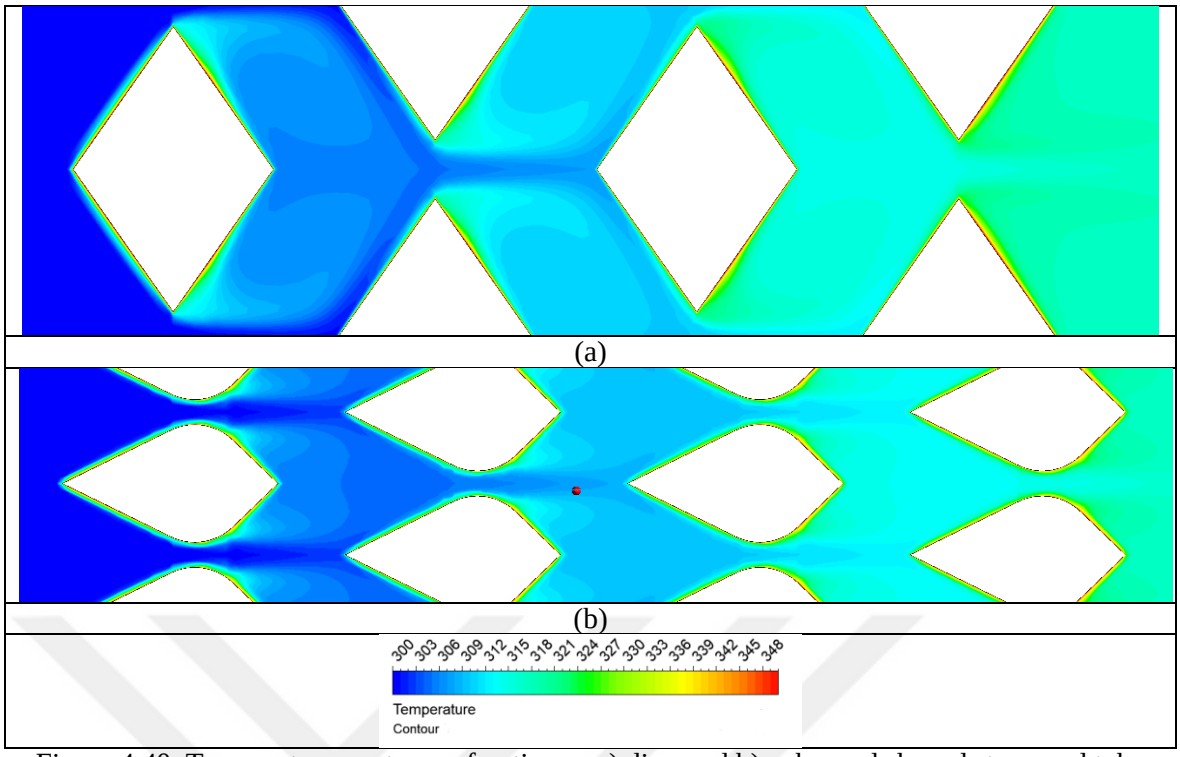


Figure 4.40. Temperature contours of optimum a) diamond b) enhanced shaped staggered tube banks

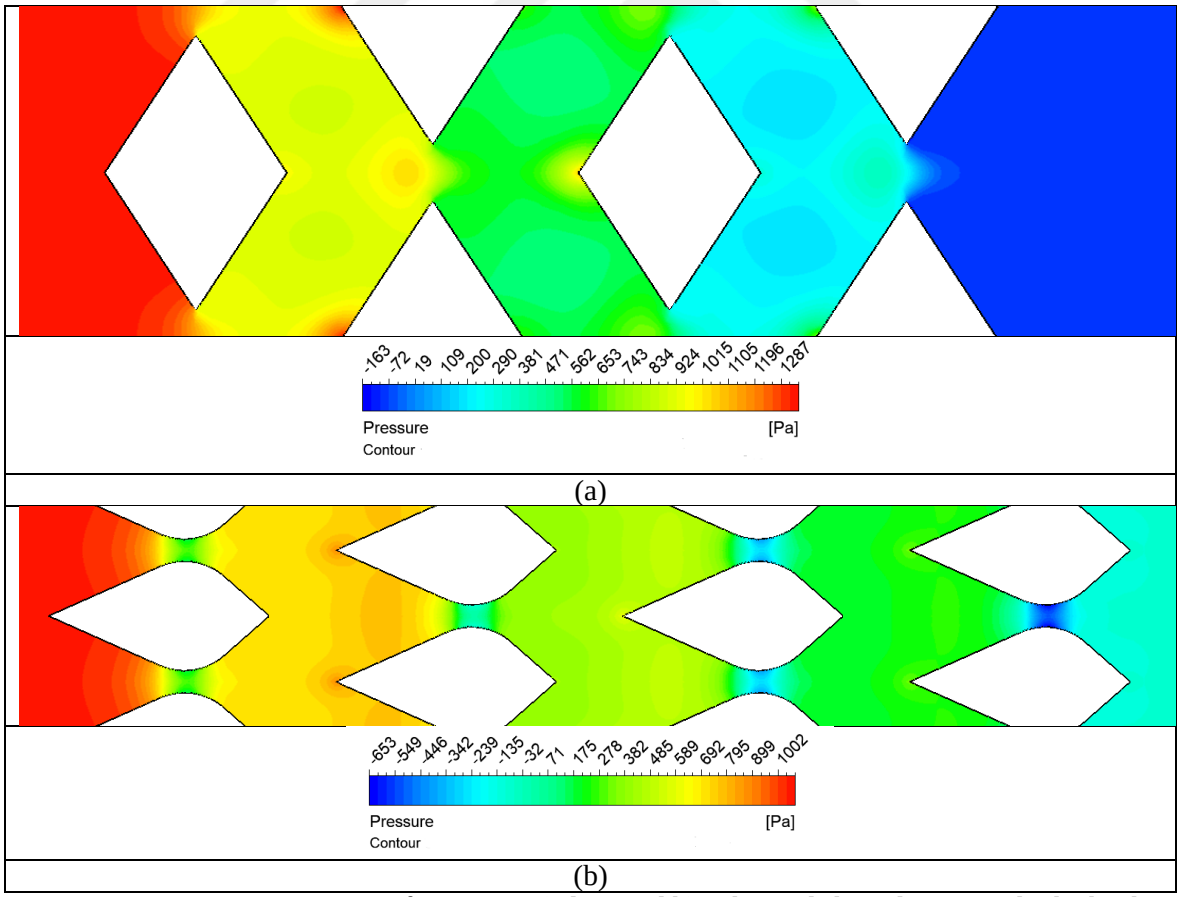


Figure 4.41. Pressure contours of optimum a) diamond b) enhanced shaped staggered tube banks

5. CONCLUSIONS

In this study, a novel tube bank geometry which is called enhanced is introduced mathematically and geometrically. Optimum design parameters of circular, diamond and enhanced shaped tube banks for inline and staggered arrangements are obtained using MOGA-II.

For inline arrangement, optimization is done in two steps. In first step. Pareto designs are determined for circular and diamond shaped tube banks using the objective functions of maximization of heat transfer and minimization of pump power. In the second step, diamond shaped and enhanced shaped tube banks with tube length constraint compared with enhanced geometry to reach optimum designs. The following results can be made from the first section:

- In the first optimization study, a total of 483 designs are obtained for circular tube bank. Among these, 87 designs are identified as Pareto. For diamond inline arrangement, 647 of total designs are determined and 84 of these are identified as Pareto.
- Generally $\dot{Q}_{total}$ values are increased with increasing $\dot{W}_{pump}$. For the same $\dot{W}_{pump}$=4.9 W value ID 482 within the circular Pareto set has a $\dot{Q}_{total}$=491W and ID 1940 within the diamond Pareto set has a $\dot{Q}_{total}$=1601W which is 3 times higher.
- $\dot{Q}_{total}$ values are increased with increasing V_{in} for both geometries. Maximum $\dot{Q}_{total}$ value is achieved at 6 m/s for circular (ID 1512) and diamond shaped (ID 354) inline arrangement.
- Pareto $\dot{Q}_{total}$ values of circular inline tube bank is distributed in the S_L^* range of 1.2 to 1.5. However, these values are mostly obtained when S_L^*=1.2 for diamond shaped inline tube bank.
- $\dot{Q}_{total}$ values gradually decreases with increasing S_T^* for both geometries. Pareto designs are obtained for all S_T^* range (1.2-3.0). Maximum $\dot{Q}_{total}$ values are achieved where S_L^*=S_T^*=1.2 for both circular and diamond shaped geometry.
- All Pareto designs are achieved for attack angle θ between 10 to 25˚. Maximum value is obtained where θ is 10˚.
- In the second optimization study, a total of 422 designs are obtained for diamond tube bank. Among these, 55 designs are identified as Pareto. For enhanced shaped inline arrangement, 1757 of total designs are determined and 117 of these are identified as Pareto.
- In the zone $\dot{W}_{pump} < 0.7\ W$ diamond geometries show higher $\dot{Q}_{total}$ values than enhanced geometry for the same $\dot{W}_{pump}$. However, in the zone $\dot{W}_{pump} > 0.7\ W$ opposite is true. There are 12 Pareto designs for enhanced and only two Pareto designs for diamond geometry in this zone.

- Maximum $\dot{Q}_{total}$ is found to be 442.87 W at $\dot{W}_{pump}$=10.05 W among diamond Pareto set with ID 31. However, Maximum among enhanced Pareto set $\dot{Q}_{total}$ is obtained as 623.34 W (41% higher than that of diamond one with ID 31) at $\dot{W}_{pump}$=19.147 W 41% higher than that of diamond one with ID 31) with ID 1402.
- Maximum $\dot{Q}_{total}$ value is achieved at 5 m/s and 6 m/s for diamond (ID 31) and enhanced shaped (ID 1402) inline arrangement, respectively.
- Maximum $\dot{W}_{pump}$ value is achieved at 6 m/s and 5 m/s for diamond (ID 31) and enhanced shaped (ID 1402) inline arrangement, respectively.
- For diamond tube bank, all Pareto designs are obtained within the range of S_L^* =1.8-3. Whereas, enhanced geometries are obtained within the range of S_L^* =1.6-3.
- Maximum $\dot{Q}_{total}$ value is achieved at $S_L^* = 2.7$ and $S_L^* = 1.2$ for diamond (ID 31) and S_L^* =2 and $S_L^* = 1.2$ for enhanced shaped (ID 1402) inline arrangement.
- Pareto designs are obtained θ_1 =10-85˚ and θ_2 =10-45˚ (only one exceptional design at θ_2 =160˚) for enhanced inline tube bank. Maximum $\dot{Q}_{total}$ value of inline arranged enhanced tube bank (ID 1076) is achieved at θ_1 =80˚ and θ_2 = 25˚, respectively.

For staggered arrangement, optimization study is carried out in two steps. In first step Pareto designs are generated for circular and diamond shaped tube banks using the objective functions maximization of heat transfer and minimization of pump power. Using the same objectives in the second step Pareto designs of diamond shaped are determined with tube length constraints. Whereas, Pareto designs of enhanced shaped tube banks are generated for constant tube length constraint.

- At the first step optimization study, a total of 477 designs are obtained for circular tube bank. Among these, 108 designs are identified as Pareto. For diamond inline arrangement, 736 of total designs are determined and 99 of these are identified as Pareto.
- For the first step optimization study, Pareto designs of diamond shaped staggered tube bank gathered in the attack angle range 10–40 and 170◦.
- Increment in S_L^* results in lower heat transfer for circular and diamond geometries whereas opposite is true for enhanced geometry. Besides, heat transfer value tends to decrease with the increment in S_T^* for all three geometries.
- Pareto designs of diamond shaped staggered tube banks shows higher heat transfer performance than circular staggered tube banks. For example, design with ID 1020 of diamond design exhibits 156% higher heat transfer rate than circular design with ID 1832.
- Most of the Pareto diamond designs are located in the zone where $\dot{Q}_{total}$ < 500 W and $\dot{W}_{pump}$ < 10 W. However, Pareto designs of enhanced geometry are dissipated in a larger range.

- As a result of optimization study, ID 60 of diamond staggered tube bank with V_{in}= 3. S_L^*= 1.3. S_T^*= 1.2 and θ = 120◦ besides ID 1070 of enhanced staggered tube bank with V_{in}= 6. S_L^*= 1.3. S_T^* = 1.2 θ_1= 50◦ and θ_2 = 85◦ are selected as optimum designs.
- For the second step optimization study optimal design of enhanced geometry with ID 1076 has 0.59% higher heat transfer rate, 21.73% lower pump power requirement and 9.65% lower total tube bank volume than diamond design with ID 60.

REFERENCES

Ahmed, S.A., Ibrahiem, E., Mesalhy, O., and Abdelatief, M.A., 2013. Study of Cross Flow Air-Cooling Process via Water-Cooled Wing-Shaped Tubes in Staggered Arrangement at Different Angles of Attack, Part 2: Heat Transfer Characteristics and Thermal Performance Criteria. undefined.

Aiba, S., Ota, T., and Tsuchida, H., 1980. Heat transfer of tubes closely spaced in an in-line bank. International Journal of Heat and Mass Transfer, 23(3), 311–319. doi:10.1016/0017-9310(80)90119-2

Aiba, S., Tsuchida, H., and Ota, T., 1982. Heat Transfer Around Tubes in In-line Tube Banks. Bulletin of JSME, 25(204), 919–926. doi:https://doi.org/10.1299/jsme1958.25.919

Aktas, A.E., Kuru, N., Tahir Erdinc, M., Aydin, O., and Bilgili, M., 2023. Optimizing the tube geometry to enhance thermohydraulic performance of tube bank heat exchanger. International Journal of Thermal Sciences, 193, 108460. doi:10.1016/j.ijthermalsci.2023.108460

Alavi, M., and Goshayeshi, H., 2009. Analysis of non-isothermal fluid flow past an in-line tube bank. WIT Transactions on Modelling and Simulation, 48, 425–435. doi:10.2495/CMEM090391

Ansys Fluent User's Guide 2013. Canonsburg.

Baghban, H.N., 1987. Transfer Coefficient over Inclined Tube Banks. The University of Aston.

Bayat, H., Lavasani, A.M., and Maarefdoost, T., 2014. Experimental study of thermal-hydraulic performance of cam-shaped tube bundle with staggered arrangement. Energy Conversion and Management, 85, 470–476. doi:10.1016/j.enconman.2014.06.009

Beale, S.B., and Spalding, D.B., 1998. Numerical study of fluid flow and heat transfer in tube banks with stream-wise periodic boundary conditions. Transactions of the Canadian Society for Mechanical Engineering, 22(4 A), 397–416. doi:10.1139/tcsme-1998-0022

Beziel, M., and Stephan, K., 1992. Heat transfer and pressure drop in single rows of tubes in cross-flow. Chemical Engineering & Technology, 15(4), 219–223. doi:10.1002/ceat.270150402

Buzatu, R., Ungureanu, V., Ciutina, A., Gireadă, M., Vitan, D., and Petran, I., 2021. Experimental evaluation of energy-efficiency in a holistically designed building. Energies, 14(16). doi:10.3390/en14165061

Castiglia, D., Balabani, S., Papadakis, G., and Yianneskis, M., 2001. An experimental and numerical study of the flow past elliptic cylinder arrays. Proceedings of the Institution of Mechanical Engineers, Part C: Journal of Mechanical Engineering Science, 215(11), 1287–1302. doi:10.1243/0954406011524658

Cengel, Yunus, Ghajar, A., 2014. Heat and Mass Transfer (in SI Units) (4th Revise.). London, United States: Mcgraw-Hill Education-Europe. https://www.amazon.com.tr/Heat-Mass-Transfer-SI-Units/dp/9814595276 from retrieved.

Chen, C.K., Wong, K.L., and Cleavert, J.W., 1988. The finite element solutions of laminar flow and combined convection of air in a staggered or an in-line tube-bank. Wärme- und Stoffübertragung, 23(2), 93–101. doi:10.1007/BF01637131

Churchill, S.W., and Bernstein, M., 1977. A correlating equation for forced convection from gases and liquids to a circular cylinder in crossflow. Journal of Heat Transfer, 99(2), 300–306. doi:10.1115/1.3450685

Erdinc, M.T., Aktas, A.E., Kuru, M.N., Bilgili, M., and Aydin, O., 2021. An optimization study on thermo-hydraulic performance arrays of circular and diamond shaped cross-sections in periodic flow. International Communications in Heat and Mass Transfer, 129, 105706. doi:10.1016/j.icheatmasstransfer.2021.105706

Erguvan, M., 2018. Numerical and Thermodynamic Analysis of External Flow over Tube Banks for Waste Heat Recovery. University of Alabama.

Erguvan, M., and MacPhee, D.W., 2018. Energy and exergy analyses of tube banks in waste heat recovery applications. Energies, 11(8). doi:10.3390/en11082094

Erguvan, M., and MacPhee, D.W., 2019. Second law optimization of heat exchangers in waste heat recovery. International Journal of Energy Research, 43(11), 5714–5734. doi:10.1002/er.4664

Fand, R.M., 1965. Heat transfer by forced convection from a cylinder to water in crossflow. International Journal of Heat and Mass Transfer, 8(7), 995–1010. doi:10.1016/0017-9310(65)90084-0

Fujii, M., Fujii, T., and Nagata, T., 1984. A Numerıcal Analysıs Of Lamınar Flow And Heat Transfer Of Aır In An In-Lıne Tube Bank. Numerical Heat Transfer, 7(1), 89–102. doi:10.1080/01495728408961813

Fullerton, T.L., and Anand, N.K., 2010. Periodically fully-developed flow and heat transfer over flat and oval tubes using a control volume finite-element method. Numerical Heat Transfer; Part A: Applications, 57(9), 642–665. doi:10.1080/10407781003744888

Ge, Y., Lin, Y., Tao, S., He, Q., Chen, B., and Huang, S.M., 2021. Shape optimization for a tube bank based on the numerical simulation and multi-objective genetic algorithm. International Journal of Thermal Sciences, 161. doi:10.1016/J.IJTHERMALSCI.2020.106787

Gharbi, N. El, Kheiri, A., Ganaoui, M. El, and Blanchard, R., 2015. Numerical optimization of heat exchangers with circular and non-circular shapes. Case Studies in Thermal Engineering, 6, 194–203. doi:10.1016/j.csite.2015.09.006

Grannis, V.B., and Sparrow, E.M., 1991. Numerical Simulatıon Of Fluid Flow Through An Array Of Diamond-Shaped Pin Fins. http://dx.doi.org/10.1080/10407789108944856, 19(4), 381–403. doi:10.1080/10407789108944856

Griffiths, E., and Awbery, J.H., 1933. Heat Transfer between Metal Pipes and a Stream of Air. Proceedings of the Institution of Mechanical Engineers, 125(1), 319–382. doi:10.1243/pime_proc_1933_125_020_02

Heat Exchanger Market Size, Share Analysis - 2030 | Industry Forecast 2020. 26 September 2022 tarihinde https://www.alliedmarketresearch.com/heat-exchanger-market from retrieved.

Hilpert, R., 1933. Wärmeabgabe von geheizten Drähten und Rohren im Luftstrom. Forschung auf dem Gebiet des Ingenieurwesens A 1932 4:5, 4(5), 215–224. doi:10.1007/BF02719754

Ibrahim, T.A., and Gomaa, A., 2009. Thermal performance criteria of elliptic tube bundle in crossflow. International Journal of Thermal Sciences, 48(11), 2148–2158. doi:10.1016/j.ijthermalsci.2009.03.011

Ikpotokin, I., and Osueke, C.O., 2014. Heat transfer and fluid flow characteristics study for in-line tube bank in cross-flow. International Journal of Mechanical and Mechatronics Engineering, 14(3), 93–105.

Ishigai, S., and Nishikawa, E., 1975. Experimental Study of Structure of Gas Flow in Tube Banks with Tube Axes Normal to Flow Part II ; On the Structure of Gas Flow in Single-Column, Single-Row, and Double-Rows Tube Banks. Bulletin of JSME, 18(119), 528–535. doi:10.1299/JSME1958.18.528

Ishigai, S., Nishikawa, E., Nishimura, K., and Cho, K., 1972. Experimental Study on Structure of Gas Flow in Tube Banks with Tube Axes Normal to Flow : Part 1, Karman Vortex Flow from Two Tubes at Various Spacings. Bulletin of JSME, 15(86), 949–956. doi:10.1299/JSME1958.15.949

Jeng, T.M., 2006. Thermal performance of in-line diamond-shaped pin fins in a rectangular duct. International Communications in Heat and Mass Transfer, 33(9), 1139–1146. doi:10.1016/j.icheatmasstransfer.2006.06.001

Khan, W.A., Culham, J.R., and Yovanovich, M.M., 2006a. Convection heat transfer from tube banks in crossflow: Analytical approach. International Journal of Heat and Mass Transfer, 49(25–26), 4831–4838. doi:10.1016/j.ijheatmasstransfer.2006.05.042

Khan, W.A., Culham, J.R., and Yovanovich, M.M., 2006b. Analytical model for convection heat transfer from tube banks. Journal of Thermophysics and Heat Transfer, 20(4), 720–727. doi:10.2514/1.15453

Khan, W.A., Culham, J.R., and Yovanovich, M.M., 2007. Optimal design of tube banks in crossflow using entropy generation minimization method. Journal of Thermophysics and Heat Transfer, 21(2), 372–378. doi:10.2514/1.26824

Launder, B.E., and Massey, T.H., 1978. The numerical prediction of viscous flow and heat transfer in tube banks. Journal of Heat Transfer, 100(4), 565–571. doi:10.1115/1.3450858

Lee, D., Ahn, J., and Shin, S., 2013. Uneven longitudinal pitch effect on tube bank heat transfer in cross flow. Applied Thermal Engineering, 51(1–2), 937–947. doi:10.1016/j.applthermaleng.2012.10.031

Mandhani, V.K., Chhabra, R.P., and Eswaran, V., 2002. Forced convection heat transfer in tube banks in cross flow. Chemical Engineering Science, 57(3), 379–391. doi:10.1016/S0009-2509(01)00390-6

Matos, R.S., Laursen, T.A., Vargas, J.V.C., and Bejan, A., 2004. Three-dimensional optimization of staggered finned circular and elliptic tubes in forced convection. International Journal of Thermal Sciences, 43(5), 477–487. doi:10.1016/j.ijthermalsci.2003.10.003

Matos, R.S., Vargas, J.V.C., Laursen, T.A., and Saboya, F.E.M., 2001. Optimization study and heat transfer comparison of staggered circular and elliptic tubes in forced convection. International Journal of Heat and Mass Transfer 44, 44, 3953±3961. www.elsevier.com/locate/ijhmt from retrieved.

Mehrabian, M.A., 2006. Heat Transfer And Pressure Drop Characterıstıcs Of Cross Flow Of Aır Over A Cırcular Tube In Isolatıon And/Or In A Tube Bank. The Arabian Journal for Science and Engineering, 32(2B), 12. https://www.semanticscholar.org/paper/HEAT-TRANSFER-AND-PRESSURE-DROP-CHARACTERISTICS-OF-Mehrabian/1cfdfb23b35833189472ddd33cabc84f286032e6 from retrieved.

Molki, M., and Bhamidipati, K.L., 2004. Enhancement of convective heat transfer in the developing region of circular tubes using corona wind. International Journal of Heat and Mass Transfer, 47(19–20), 4301–4314. doi:10.1016/j.ijheatmasstransfer.2004.04.014

Mustafa, A.W., 2019. Maximization of heat transfer density rate from a single row of rhombic tubes cooleAd by forced convection based on constructal design. Heat Transfer - Asian Research, 48(2), 624–643. doi:10.1002/htj.21398

Park, J.M., Kim, O.J., Kim, S.J., and Shin, Y.C., 2015. Heat transfer characteristics of circular and elliptic cylinders in cross flow. Advances in Mechanical Engineering, 7(11), 1–8. doi:10.1177/1687814015619553

Patankar, S. V., Liu, C.H., and Sparrow, E.M., 1977. Fully developed flow and heat transfer in ducts having streamwise-periodic variations of cross-sectional area. Journal of Heat Transfer, 99(2), 180–186. doi:10.1115/1.3450666

Rahmani, R., Mirzaee, I., and Shirvani, H., 2005. Computation of a laminar flow and heat transfer of air for staggered tube arrays in cross-flow. Iranian Journal of Mechanical Engineering, 6(2), 19–33. http://www.sid.ir/en/VEWSSID/J_pdf/102720050203.pdf from retrieved.

Ram, R.P., Bharti, R.P., and Dhiman, A.K., 2016. Forced convection flow and heat transfer across an in-line bank of circular cylinders. Canadian Journal of Chemical Engineering, 94(7), 1381–1395. doi:10.1002/cjce.22483

Ranut, P., Janiga, G., Nobile, E., and Thévenin, D., 2014. Multi-objective shape optimization of a tube bundle in cross-flow. International Journal of Heat and Mass Transfer, 68, 585–598. doi:10.1016/j.ijheatmasstransfer.2013.09.062

Reiher, H., 1925. Warmeubergang von stromender Luft an Rohre und rohrbundel im Kreuzstrom. VDI-Verlag, 269.

Rocha, L.A.O., and Bejan, A., 2001. Geometric optimization of periodic flow and heat transfer in a volume cooled by parallel tubes. Journal of Heat Transfer, 123(2), 233–239. doi:10.1115/1.1337654

Sahamifar, S., Kowsary, F., and Mazlaghani, M.H., 2019. Generalized optimization of cross-flow staggered tube banks using a subscale model. International Communications in Heat and Mass Transfer, 105, 46–57. doi:10.1016/j.icheatmasstransfer.2019.03.004

Saraireh, M.A., Alsaraireh, F.M., and Alrwashdeh, S.S., 2017. Investigation of heat transfer for staggered and in-line tubes. International Journal of Mechanical Engineering and Technology, 8(11), 476–483.

Sayed Ahmed, S.A.E., Ibrahiem, E.Z., Mesalhy, O.M., and Abdelatief, M.A., 2014a. Heat transfer characteristics of staggered wing-shaped tubes bundle at different angles of attack. Heat and Mass Transfer, 50(8), 1091–1102. doi:10.1007/s00231-014-1323-3

Sayed Ahmed, S.A.E., Ibrahiem, E.Z., Mesalhy, O.M., and Abdelatief, M.A., 2014b. Heat transfer characteristics of staggered wing-shaped tubes bundle at different angles of attack. Heat and Mass Transfer/Waerme- und Stoffuebertragung, 50(8), 1091–1102. doi:10.1007/s00231-014-1323-3

Sayed Ahmed, S.A.E., Mesalhy, O.M., and Abdelatief, M.A., 2016a. Heat transfer characteristics and entropy generation for wing-shaped-tubes with longitudinal external fins in cross-flow. Journal of Mechanical Science and Technology, 30(6), 2849–2863. doi:10.1007/s12206-016-0544-4

Sayed Ahmed, S.A.E., Mesalhy, O.M., and Abdelatief, M.A., 2016b. Heat transfer characteristics and entropy generation for wing-shaped-tubes with longitudinal external fins in cross-flow. Journal of Mechanical Science and Technology, 30(6), 2849–2863. doi:10.1007/s12206-016-0544-4

Shah, K.N., Mahant, K. V., Patel, P.D., and Yadav, C.O., 2013. Cfd Analysis Of Heat Exchanger Over A Staggered Tube Bank For Different Angle Arrangement Of Tube Bundles. International Journal of Engineering Research & Technology, 2(1). www.ijert.org from retrieved.

Shah, R.K., and Sekuli, D.P., 2003. Fundamentals of Heat Exchanger Design. Fundamentals of Heat Exchanger Design. doi:10.1002/9780470172605

Sparrow, E.M., and Grannis, V.B., 1990. Pressure drop characteristics of heat exchangers consisting of arrays of diamond-shaped pin fins. International Journal of Heat and Mass Transfer, 34(3), 589–600. doi:10.1016/0017-9310(91)90108-Q

Sparrow, E.M., and Prata, A.T., 1983. Numerical solutions for laminar flow and heat transfer in a periodically converging-diverging tube, with experimental confirmation. Numerical Heat Transfer, 6(4), 441–461. doi:10.1080/01495728308963099

Tanda, G., 2001. Heat transfer and pressure drop in a rectangular channel with diamond-shaped elements. International Journal of Heat and Mass Transfer, 44(18), 3529–3541. doi:10.1016/S0017-9310(01)00018-7

Vessakosol, P., and Charoensuk, J., 2010. Numerical analysis of heat transfer and flow field around cross-flow heat exchanger tube with fouling. Applied Thermal Engineering, 30(10), 1170–1178. doi:10.1016/j.applthermaleng.2010.01.034

Waheed, A., Adil, A., and Razzaq, A., 2018. The Optimal Spacing Between Diamond-Shaped Tubes Cooled By Free Convection Using Constructal Theory. Proceedings Of The Romanian Academy, Series A in (pp. 129–134). The Publishing House Of The Romanian Academy.

Wahid, M.A., Gholami, A.A., and Mohammed, H.A., 2013. Numerical study of fluid flow and heat transfer enhancement of nanofluids over tube bank. Applied Mechanics and Materials, 388, 149–155. doi:10.4028/www.scientific.net/AMM.388.149

Widodo, B.U.K., and Hanifah, S.D., 2016. Numerical analysis on the effect of longitudinal and transversal pitch ratio to the flow and heat transfer characteristic of staggered elliptical tubes-bank. AIP Conference Proceedings, 1778. doi:10.1063/1.4965754

Wilson, S.A., and Bassiouny, M.K., 2000. Modeling of heat transfer for flow across tube banks. Chemical Engineering and Processing: Process Intensification, 39(1), 1–14. doi:10.1016/S0255-2701(99)00069-0

Yilmaz, A., and Yilmaz, T., 2016. Optimum Design of Cross-Flow In-Line Tube Banks at Constant Wall Temperature. Heat Transfer Engineering, 37(6), 523–534. doi:10.1080/01457632.2015.1060753

Yoo, S.Y., Kwon, H.K., and Kim, J.H., 2007. A study on heat transfer characteristics for staggered tube banks in cross-flow. Journal of Mechanical Science and Technology, 21(3), 505–512. doi:10.1007/BF02916312

Zdravistch, F., Fletcher, C.A., and Behnia, M., 1995. Numerical laminar and turbulent fluid flow and heat transfer predictions in tube banks. International Journal of Numerical Methods for Heat & Fluid Flow, 5(8), 717–733. doi:10.1108/EUM0000000004086

Zeeshan, M., Nath, S., and Bhanja, D., 2017. Numerical study to predict optimal configuration of fin and tube compact heat exchanger with various tube shapes and spatial arrangements. Energy Conversion and Management, 148, 737–752. doi:10.1016/j.enconman.2017.06.011

Zukauskas, A., 1972. Heat Transfer from tubes in Crossflow. Advances in Heat Transfer, 8, 93–160.

Zukauskas, A., and Ulinskas, R., 1985. Efficiency parameters for heat transfer in tube banks. Heat Transfer Engineering, 6(1), 19–25. doi:10.1080/01457638508939614

Zukauskas, A., and Ziugzda, J., 1985. Heat transfer of a cylinder in crossflow. wdch. https://ui.adsabs.harvard.edu/abs/1985wdch.book.....Z/abstract from retrieved.

Zukauskas, A., 1987. Heat Transfer from Tubes in Crossflow. Advances in Heat Transfer, 18(C), 87–159. doi:10.1016/S0065-2717(08)70118-7

CURRICULUM VITAE

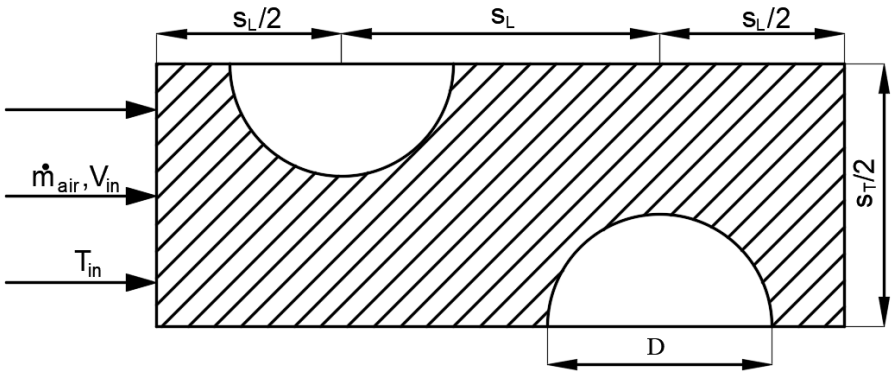
Arif Emre AKTAŞ, completed his education in Kemalpaşa Primary & Secondary School in GHK. and Merzifon Anatolia High School in Merzifon. He enrolled in Çukurova University Automotive Engineering Department in 2009. He had graduated in 2014. In the same year, he had started to Master of Science education in Automotive Engineering Department. In 2017 he started PhD education. Currently, he is a research assistant in the same department.

APPENDICES

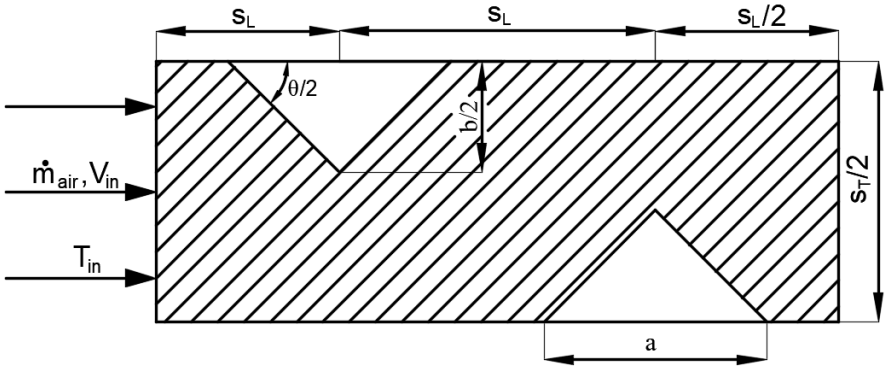
A.1. COMPUTATIONAL MODELING (Erdinc et al., 2021)

Solution domains of circular and diamond-shaped geometries are depicted in Figure A.1. Air with constant inlet temperature T_i flows over the geometries with a fixed mass flow rate $\dot{m}_{air}$ and leaves with exit temperature T_o. Wall temperature value T_w is also assigned as constant. For circular geometry, dimensionless longitudinal s_L^* and transverse s_T^* pitches are defined as parameters. However, in addition to s_L^* and s_T^* values; vertex angle θ value is also specified as parameter for diamond shaped geometry.

Due to the symmetric arrangement of the geometries, a repeated portion of the whole fluid domain can be taken as computational domain. Hence, computational time can be diminished to solve governing equations. Since the tube length is much higher than equivalent diameter, fluid domain is considered as two-dimensional. In addition, since the tubes along the fluid flow have a periodically repeated form. the theory of periodically fully developed regime (Patankar et al.. 1977; Sparrow and Prata. 1983) can be applied to the selected fluid domain.



(a)



(b)

Figure A.1. Computational domain for (a) circular (b) diamond shaped geometries with staggered arrangements

Two optimization case studies are performed for circular and diamond shaped geometries. For the optimization of both cases fluid properties are taken for Pr=0.707. Constant mass flow rate $\dot{m}_a = 0.025\ \mathrm{kg/s}$ is set for both optimization studies for circular and diamond shaped geometries. Moreover, inlet and wall temperatures are $T_i = 298.15\ \mathrm{K}$ and $T_w = 328.15\ \mathrm{K}$, respectively. In order to keep equal comparison conditions, same circumference is used for both circular and diamond shaped geometries, and equivalent diameter is taken as $D_e = 10\ \mathrm{mm}$.

Solution Methods for Conservation Equations

In the numerical simulation, heated fluid provide thermal energy to staggered arranged circular and diamond shaped geometries. Numerical analysis is carried out assuming two-dimensional, steady state and incompressible turbulent flow. Over the computation domain, implemented turbulence equations, as well as conservation equations are given below (Ansys Fluent User's Guide. 2013):

Mass Conservation

$$\frac{\partial}{\partial x_i}\left(\rho u_j\right) = 0 \tag{A.1}$$

Momentum Conservation

$$\frac{\partial}{\partial x_j}\left(\rho u_i u_j\right) = -\frac{\partial p}{\partial x_i} + \frac{\partial}{\partial x_j}\left[\mu\left(\frac{\partial u_i}{\partial x_j} + \frac{\partial u_j}{\partial x_i}\right)\right] + \frac{\partial}{\partial x_j}(\mu\left(\frac{\partial u_i}{\partial x_j} + \frac{\partial u_j}{\partial x_i}\right)) \tag{A.2}$$

Energy Conservation

$$\frac{\partial}{\partial x_j}(\rho u_i T) = \frac{\partial}{\partial x_j}\left(\frac{\mu}{Pr}\frac{\partial T}{\partial x_j} + \frac{\mu}{Pr_t}\left(\frac{\partial T}{\partial x_j}\right)\right) \tag{A.3}$$

In order to simulate turbulence flow, k-ε model which involves two equations is applied to predict the flow behavior. Realizable k-ε model with enhanced wall treatment is preferred in the current heat transfer and fluid flow analysis due to the well compatibility with experimental results. It includes a novel formulation for viscosity of turbulent. It precisely estimates the characteristic the flow involving boundary layers under strong adverse pressure gradients. recirculation and separation ("Ansys Fluent User's Guide". 2013). Equations for turbulence kinetic energy (k) and energy dissipation rate (ε) are given as follows:

$$\frac{\partial}{\partial x_j}(\rho k u_j) = \frac{\partial}{\partial x_j}\left[(\mu + \frac{\mu_t}{\sigma_k})\frac{\partial k}{\partial x_j}\right] + G_k - \rho\varepsilon \quad (A.4)$$

and

$$\frac{\partial}{\partial x_j}(\rho \epsilon u_j) = \frac{\partial}{\partial x_j}\left[(\mu + \frac{\mu_t}{\sigma_\epsilon})\frac{\partial_\epsilon}{\partial x_j}\right] - \rho C_2 \frac{\epsilon^2}{k + \sqrt{\nu\epsilon}} \quad (A.5)$$

Where the turbulent Prandtl numbers of k and ε are denoted as σ_k and σ_ε. $G_k = \mu_t S^2$ indicates turbulence kinetic energy generation. Here, S represents mean rate-of-strain tensor modulus. Also, $C_1 = max\left[0.43.\frac{\eta}{\eta+5}\right]. \eta = S\frac{k}{\epsilon}$ and $S = \sqrt{2S_{ij}S_{ij}}$ μ_t indicates the turbulent viscosity.

$$\mu_t = \rho C_\mu \frac{k^2}{\varepsilon} \quad (A.6)$$

$$C_\mu = \frac{1}{A_0 + A_s\frac{kU^*}{\epsilon}} \quad (A.7)$$

Where $A_0 = 4.04$ and $A_s = \sqrt{6}\cos\Phi$ are model constants where $\Phi = \frac{1}{3}\cos^{-1}(\sqrt{6}W). W = \frac{S_{ij}S_{jk}S_{ki}}{\tilde{S}^3}. \tilde{S} = \sqrt{S_{ij}S_{ij}}. S_{ij} = \frac{1}{2}(\frac{\partial u_j}{\partial x_i} + \frac{\partial u_i}{\partial x_j})$. U^* can be calculated from

$$U^* = S_{ij}S_{ij} + \tilde{\Omega}_{ij}\tilde{\Omega}_{ij} \quad (A.8)$$

Where

$$\tilde{\Omega}_{ij} = \Omega_{ij} - 2\epsilon_{ijk}\omega_k \quad (A.9)$$

$$\Omega_{ij} = \bar{\Omega}_{ij} - \epsilon_{ijk}\omega_k \quad (A.10)$$

Here, $\bar{\Omega}_{ij}$ is mean rate of rotation tensor with angular velocity of ω_k.

A.2. DATA ANALYSIS

In order to compare the heat transfer and pressure drop results of circular and diamond shaped geometries, following definitions are given below:

Geometrical parameters

For circular geometry, dimensionless longitudinal and transversal pitches are defined as

$$s_L^* = \frac{s_L}{\mathrm{D_e}} \tag{A.11}$$

$$s_T^* = \frac{s_T}{\mathrm{D_e}} \tag{A.12}$$

Where s_L and s_T are longitudinal and transversal pitches, respectively. Unlike circular geometries, s_L^* and s_T^* are defined in a different way for diamond shaped geometries. The formulations of θ, s_L^* and s_T^* are given below:

$$\frac{\theta}{2} = arctan\left(\frac{b}{a}\right) \tag{A.13}$$

$$\pi \,.\, D = 4 \,.\, \sqrt{\left(\frac{a}{2}\right)^2 + \left(\frac{b}{2}\right)^2} \tag{A.14}$$

$$s_L^* = \frac{s_L}{a} \tag{A.15}$$

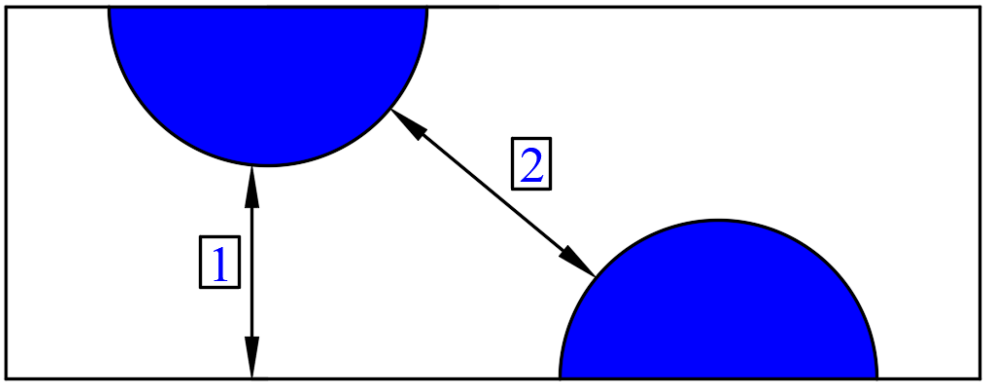
$$s_T^* = \frac{s_T}{b} \tag{A.16}$$

Where a is the length in longitudinal direction and b is the width in transversal direction of the diamond shaped geometry. Thus, it is possible to obtain a smaller volume than a circular has.

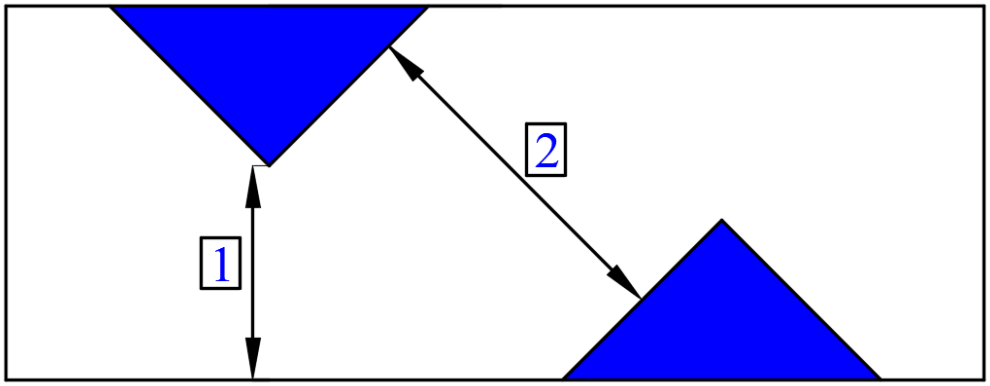
Maximum Reynolds number and minimum flow cross-sectional area definition

In order to define the maximum Reynolds number minimum cross-sectional area should be formulated for circular and diamond shaped geometries where maximum velocity occurs. Also, equivalent diameter is used in this formula. Re_{max} based on equivalent diameter D_e is given below.

$$R_{e_{max}} = \frac{D_e\, V_{max}}{\nu} \tag{A.17}$$



(a)



(b)

Figure A.2. Possible flow areas for minimum cross-section of (a) circular (b) diamond shaped geometries

For circular geometry, there are two possible flow areas ($A_{min.circular.1}$. $A_{min.circular.2}$) for minimum cross-section area which are shown in Figure A.2 (a).

$$A_{min.circular.1} = D_e(s_T^* - 1) \tag{A.18}$$

$$A_{min.circular.2} = D(s_D - D) \tag{A.19}$$

Here, s_D is diagonal pitch and given as;

$$s_D = \sqrt{(s_L^2) + \left(\frac{s_T}{2}\right)^2} \tag{A.20}$$

Smaller one from these obtained possible two minimum flow cross-sectional area is taken into consideration as minimum cross-section area of circular geometry. $A_{min.circular}$.

$$A_{min.circular} = \min(A_{min.circular.1}. A_{min.circular.2}) \tag{A.21}$$

For diamond shaped geometry, there are two passages where can be obtained the minimum cross-section area. These are demonstrated in Figure A.2 (b). One can easily find the $A_{min.diamond.1}$ which is denoted as (1) in Figure A.2.

$$A_{min.diamond.1} = \frac{s_T - b}{2} \tag{A.22}$$

Since there is no formula provided in the literature for section denoted as (2) in Figure A.2, it is required to derive a formula for $A_{min.diamond.2}$ which is given below.

$$A_{min.diamond.2} = \cos\left[\frac{\theta}{2} - \arctan\left(\frac{s_L - \frac{x}{2}}{\frac{s_T - y}{2}}\right)\right] \cdot \sqrt{\left(s_L - \frac{x}{2}\right)^2 + \left(\frac{s_T - y}{2}\right)^2} \tag{A.23}$$

$$A_{min.diamond} = \min(A_{min.diamond.1}. A_{min.diamond.2}) \tag{A.24}$$

As maximum velocity occurs in the minimum flow cross-sectional area, this definition enables us to calculate maximum Reynolds number. Hence, the maximum average velocity $\mathrm{V_{max}}$ is defined as:

$$\mathrm{V_{max}} = \frac{\mathrm{A}_{inlet}}{\mathrm{A}_{min}} \mathrm{V_{in}} \tag{A.25}$$

Where $\mathrm{V_{in}}$ is the average velocity in the inlet section of circular and diamond shaped geometries.

Convective heat transfer coefficient and average Nusselt number

Based on the assumption of fully developed flow, heat flux from geometries. $\dot{q}_s$ is evaluated utilizing Ansys Fluent package (Ansys Fluent User's Guide. 2013). Therefore, average heat transfer coefficient is calculated as follows:

$$\mathrm{h_{ave}} = \frac{\dot{q}}{\Delta \mathrm{T_{lm}}} \tag{A.26}$$

Where $\dot{q}$ is heat flux from wall to fluid medium. Logarithmic average temperature difference ΔT_{lm} is given as:

$$\Delta T_{lm} = \frac{(T_w - T_i) - (T_w - T_o))}{\ln \frac{T_w - T_i}{T_w - T_o}} \quad (A.27)$$

Average Nusselt number Nu_{ave} is defined as;

$$Nu_{ave} = \frac{h_{ave}\, D_e}{k} \quad (A.28)$$

Where k is the thermal conductivity of the working fluid.

Pressure drop and friction factor

Pressure drop ΔP is calculated as a function of friction factor f in the fluid zone and given below:

$$\Delta p = f\, N_L \frac{\rho\, V_{max}^2}{2} \quad (A.29)$$

Where N_L is number of longitudinal geometries within the fluid zone.

Limiting Conditions for Optimization Studies

Minimum cross-sectional flow area of diamond shaped geometry is limited by the minimum possible cross-section area of circular geometry therefore the designs of diamond shaped geometries do not exceed the maximum Reynolds number of circular geometry. For the limiting condition of maximum Reynolds number s_T^* and s_L^* is taken as 1.05 which are selected as the lower bounds of for this optimization study. Thus, minimum flow cross section area for circular geometry is obtained as 0.5 mm^2 using the equations (21).

Periodic Flow

Along the flow field, periodically repeated arrangement of geometries is the fundamental feature of the periodically fully developed flow assumption. Therefore, periodic boundary conditions applied for the velocity, pressure drop and dimensionless temperatures in the present numerical optimization study. Solution domain for each geometry is shown in Figure A.2. in which periodic lengths is $2\, s_L$. Velocity components in x and y directions are equal to each other at the inlet and outlet sections. In terms of Cartesian coordinates following definitions are made for x and y velocities.

$$u(x.y) = u(x + 2\, s_L.y) \quad (A.30)$$

$$v(x.y) = v(x + 2\,s_L.y) \tag{A.31}$$

Periodic characteristic of Δp_N is defined as follows:

$$\Delta p_N = p(x.y) - p(x + 2\,s_L.y) = p(x + 2\,s_L.y) - p(x + 4\,s_L.y) = \cdots \tag{A.32}$$

Pressure gradient β is constant and can be obtained by dividing pressure drop of the solution domain to the periodic length:

$$\beta = \frac{p(x.y) - p(x + 2\,s_L.y)}{2\,s_L} = \frac{\Delta p_N}{2\,s_L} \tag{A.33}$$

In the periodic flow assumption, two different boundary conditions can be applied which are constant heat flux and constant wall temperature (Ansys Fluent User's Guide. 2013). In this study, constant wall temperature is preferred. Thus, temperature values change along the flow direction in the solution domain. To construct the periodicity, temperature values must be scaled as follows (Patankar et al.. 1977; Sparrow and Prata. 1983):

$$\theta(x.y) = \frac{T(x.y) - T_w}{T_x^* - T_w} \tag{A.34}$$

T_x^* is defined as local reference temperature and given as

$$T_x^* - T_w = \left[\int_{Y_1}^{Y_2} (T - T_w)|u|\,dy\right] / \left[\int_{Y_1}^{Y_2} |u|dy\right] \tag{A.35}$$

Y_1 and Y_2 values express wall or symmetry coordinates for the given x coordinate where there is not fluid flow.

Optimization Problem

In order to execute the optimization problem two objective functions are specified (1) minimization of volume. V_N (2) maximization of total heat transfer. $\dot{Q}_N$. To get better design for diamond shaped geometry, heat transfer and pressure drop values which are obtained from optimum circular geometry study are given as constraints. For diamond shaped geometry, two constraints must be satisfied: heat transfer from diamond shaped geometry $\dot{Q}_{diamond}$ is higher than optimum heat transfer value of circular geometry $\dot{Q}_{circular.optimum}$ and pressure drop value of diamond shaped geometry $\Delta p_{diamond}$

is lower than circular geometry's pressure drop value $\Delta p_{circular.optimum}$. Multi-objective design optimization formulation can be written as follows:

Objective Functions	Maximize $\dot{Q}_{total}$, Minimize $Volume$
Constraints	$\dot{Q}_{circular.optimum} \leq \dot{Q}_{diamond}$
	$\Delta p_{circular.optimum} \geq \Delta p_{diamond}$
Optimization Variables	$s_L^* \,.\, s_T^* \,.\, \theta$
Input Data	$\dot{m}$. T_i . T_w. D_e

For the periodic flow definition, there are two boundary condition choices which are pressure gradient (β) and mass flow rate ($\dot{m}$). Mass flow rate ($\dot{m}$) is preferred as constant input value in the current optimization work. Therefore, in addition to pressure gradient (β), $\dot{q}$ can be obtained as an output value. Other quantities are defined below:

Heat Transfer ($\dot{Q}_{total}$)

Transferred heat within the fluid zone can be calculated as:

$$\dot{Q}_{total} = \dot{q}. F_N \tag{A.36}$$

Where, F_N is the overall surface area of geometries for the fluid zone and it is calculated as:

$$F_N = N\, \pi\, D_e\, L \tag{A.37}$$

Here, number of tubes N is taken as 2 and L is taken as 1 m for the fluid zone.

Volume (V_{total})

Overall volume for the defined fluid zone is calculates as:

$$V_{total} = s_L\, s_T \tag{A.38}$$

Boundary Conditions

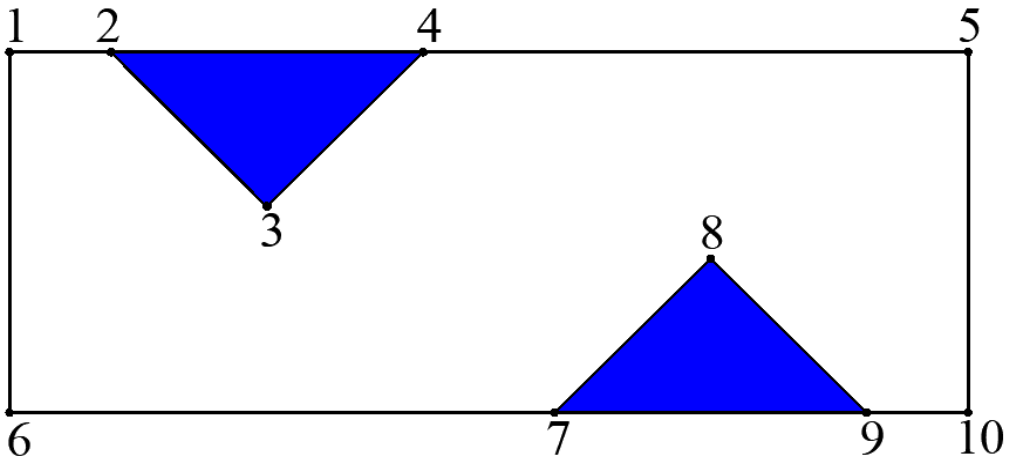


Figure A.3. Boundaries for diamond shaped geometry

Figure A.3 illustrates the solution domain for diamond shaped geometry and formulations of boundary conditions are tabulated in Table A.1. 1-2. 4-5. 6-7 and 9-10 are defined as symmetry lines where flow cannot cross. For the symmetry lines, temperature gradient ($\partial T(x.y)/\partial y$), velocity gradient in the x direction and velocity component in the y direction are fixed to zero. Inlet (1-6) and outlet (5-10) lines are the periodic boundaries. As well as dimensionless temperature $\theta(x.y)$, velocity components of $u(x.y)$ and $v(x.y)$ are as equivalent at the inlet and outlet lines. Constant temperature is assigned for inlet line and diamond-shaped tube wall which are different from each other. No-slip wall condition is assumed for diamond shaped geometry wall ensuring. $\theta(x.y)$. $u(x.y)$ and $v(x.y)$ are equal to zero.

Table A.1. Boundary conditions for computational domains

Type	u	v	T
Symmetry	$\frac{\partial u(x.y)}{\partial y} = 0$	$v(x.y) = 0$	$\frac{\partial T(x.y)}{\partial y} = 0$
Wall	$u(x.y) = 0$	$v(x.y) = 0$	$\theta(x.y) = 0$
Periodicity	$u(x.y) = u(x + 2\ s_L.y)$	$v(x.y) = v(x + 2\ s_L.y)$	$\theta(x.y) = \theta(x + 2\ s_L.y)$

A.3. COMPUTATIONAL DETAILS

Firstly, circular and diamond shaped geometries which are described in the previous section are created in the medium of Ansys Design Modeler. Triangular meshing scheme is generated for the computational domain using Ansys Mesher and quadrilateral elements are used for the inflation layers. Commercial CFD package Ansys Fluent is used to predict the fluid flow and heat transfer characteristics solving conservation equations. Second order upwind scheme is applied for the momentum, turbulent dissipation rate and turbulent kinetic energy equations. The COUPLED algorithm is implemented which enables to couple Navier-Stokes equations in an iterative manner.

The convergence is considered when the energy equation achieve 10^{-9} and the other equations achieve 10^{-6}. In order to reach the optimum design modeFRONTIER commercial software is coupled with Ansys Workbench and Ansys Fluent.

Figure A.4 demonstrates the flowchart of optimization workflow. In this figure, parametric model is incorporated into optimization algorithm to obtain the best designs which meet the requirements. The optimization algorithm used in this study is Multi-objective Genetic Algorithm (MOGA). Results are identified as feasible if the defined constraints are implemented, or else it is defined as unfeasible. Optimization algorithm calculates the objective functions. Subsequently, calculations are proceeds till convergence criteria is fulfilled.

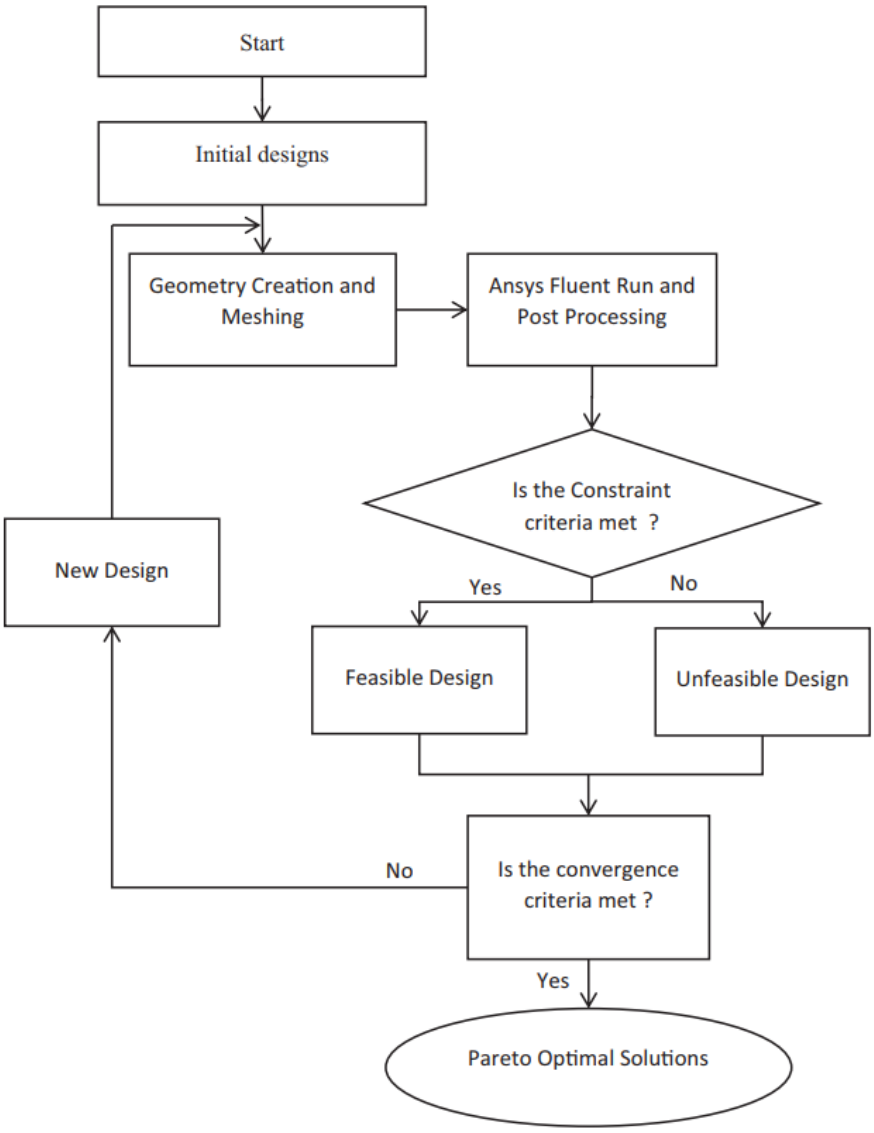


Figure A.4. Optimization algorithm flowchart

Definition of the optimization formulation which is made in the previous section involves two objective functions. If the problem has more than one objective function, it is entitled as a multi-objective optimization problem. At the end of multi-objective optimization study, the designs in which the objective functions do not prevail over each other are chosen as "Pareto Optimal Set" by modeFRONTIER optimization driver. Optimum designs can be selected from “Pareto Optimal Set” according to designer’s decision. At the beginning of the optimization study, preliminary designs “Design of Experiments (DOEs)” are assigned. DOE’s are used to create a starting population which enable the optimization algorithm to learn to design experiments. Definition of Input variables are made which are created by Ansys Workbench. A design is satisfied automatically by batch script for the specified geometrical configuration. After the calculation, outcomes of the CFD analysis used as output files for Optimization software.

Mesh Independence

In order to ensure the validity of the numerical results and save time, mesh independence study should be executed. Mesh are created in the medium of Ansys Mesher. Ansys Fluent was used to solve the governing equations. As demonstrated in Figure A.5, three different numbers of meshes are generated for an identical maximum Reynolds number of 1930. It shows variation of friction factor as a function of element number. It is seen that, difference of f in last two meshes are nearly 0.6%. Hence, computation time can be minimized without a penalty of poor accuracy if the third mesh with a nodes number of 51247 is agreed. As recommended by Ansys Fluent (Ansys Fluent User’s Guide. 2013). y+ values are kept between 1-5.

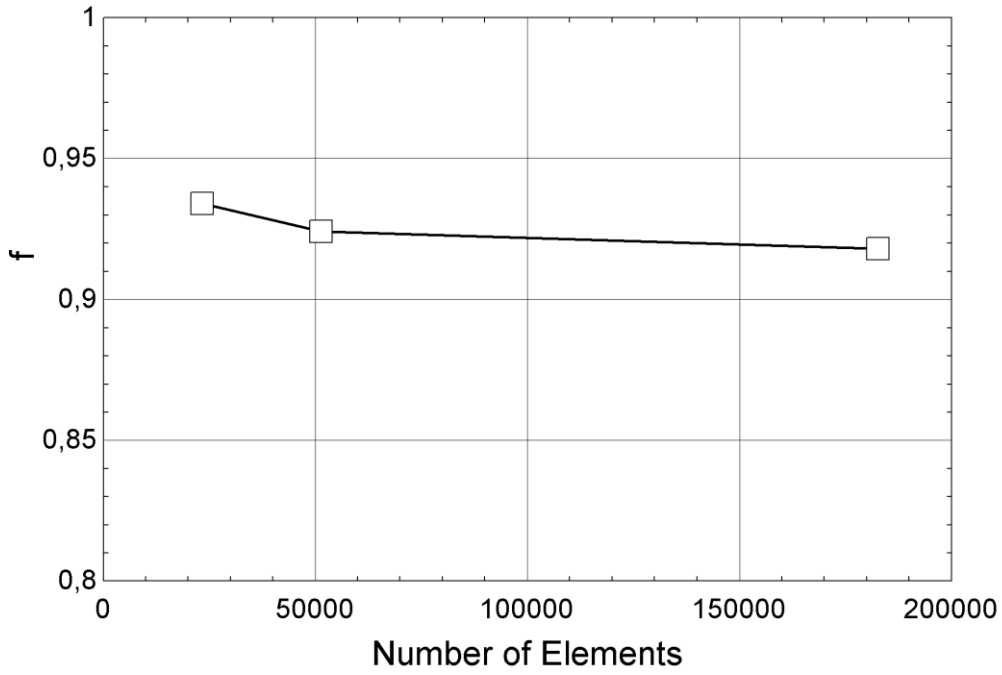


Figure A.5. Mesh independence study

A.4. VALIDATION STUDY

For validation study, experimental studies of Sparrow and Grannis (1990; 1991) and Jeng (Jeng. 2006) are utilized for comparison. Sparrow and Grannis presented their results for staggered arrangement of diamond shaped geometries in terms of flow behavior. Jeng [22], on the other hand, gave the results for both heat transfer and fluid flow of in-line arrangement of diamond-shaped fins in terms of average Nusselt number and friction factor, respectively. Data of the validation study is given in Table A.2.

Table A.2. Validation data from Sparrow and Grannis (1991) and Jeng (2006)

	Sparrow and Grannis (1991)	Jeng (2006)
Arrangement	Staggered	Inline
b (mm)	10	13.58
a (mm)	24.14	13.58
s_T / b	2	1.414
s_L / b	1.73	1.414
Vertex Angle	45	90
Fluid	Air	Air
Definition of Re	in the minimum cross-section area	in the inlet section
Re number Range	130-1930	1904-5409

Friction factor vs Re number comparison of the present study and Sparrow and Grannis's (1991) experimental data are given in Figure A.6. In addition, error of the numerical study with respect to experimental data is presented in Table A.3. The maximum difference of -9.78% is obtained for friction factor value and this is because of the experimental uncertainties and numerical errors that are within the acceptable range.

Table A.3. Comparison of numerical errors of present study vs. literature

Sparrow and Grannis (1991)		Jeng (2006)		
Re_{in}	f^+ (%)	Re_{max}	f^+ (%)	Nu_{ave}^+ (%)
130	-3.8	1904	-11.6	-12.8
910	-10.4	3025	-10.7	-10.8
1930	-7.9	4513	0.4	-8.5
		5409	-2.6	-10.1

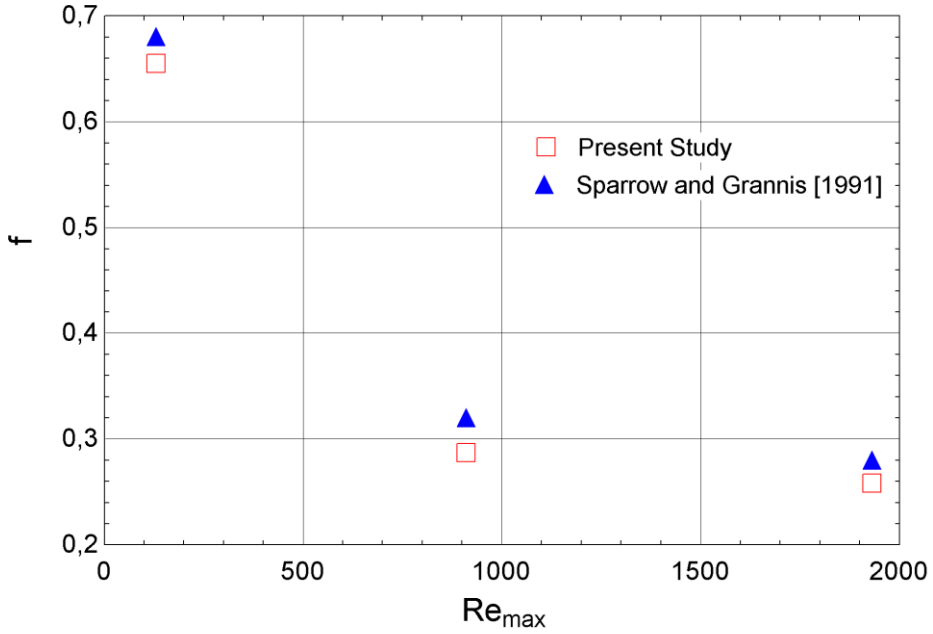


Figure A.6. Comparison of present study's friction factor values with Sparrow and Grannis (1991)

Friction factor vs Re number and Nu_{ave} vs Re are graphically presented in Figures A.7 and A.8, respectively. It is observed that maximum difference of 11.6% for friction factor and 12.8% for Nu_{ave} are obtained which are acceptable as well. Different turbulence models are examined and it is seen that realizable k-ε model is suitable for both in-line and staggered arrangement of diamond shaped geometries.

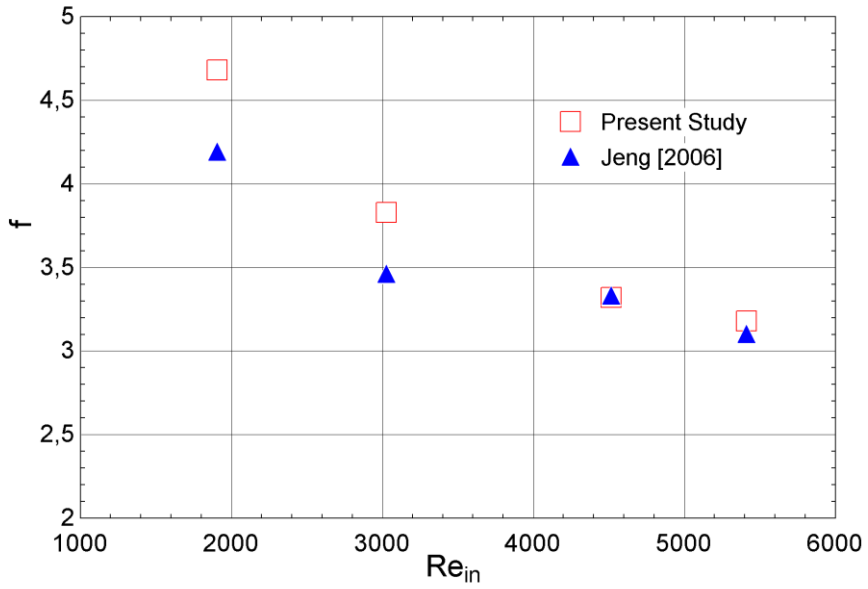


Figure A.7. Comparison of f and Re values for present study and Jeng [2006]

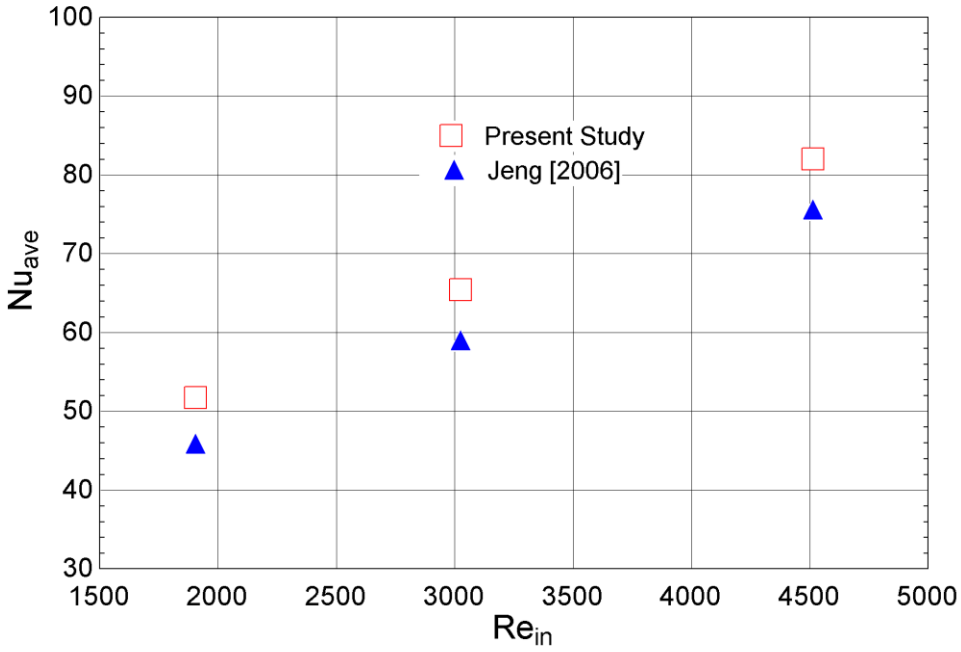


Figure A.8. Comparison of Nu and Re values for present study and Jeng [2006]

A.5. RESULTS AND DISCUSSIONS

In this section, optimization studies of circular and diamond shaped geometries are presented and discussed in detail. In the optimization problems, two objective functions which are conflictive each other are chosen. Namely, maximization of heat transfer and minimization of pressure drop. And the purpose of the study is to determine the optimum state for a given mass flow rate. Since the aim of this study is to obtain an optimal arrangement of diamond shaped geometries, firstly an optimization study is carried out for circular geometry. Then, the obtained optimal results are given as constraints for diamond shaped geometry optimization problem in order to find better design as compared to optimum circular geometry study. With the usage of optimization workflows, it is possible to achieve design points for optimal solutions with the same equivalent diameter, and mass flow rate which are given in Table A.4. Air with constant thermo-physical properties is used as the working fluid. These data were taken from (Cengel and Ghajar, 2014) for T=300 K as given in Table A.5.

Table A.4. Problem data for optimization studies of circular and diamond-shaped arrangements

T_{in} *[K]*	298.15
T_w *[K]*	328.15
$\dot{m}$ *[kg/s]*	0.025
D_{eq} *[mm]*	10

Table A.5. Thermo-physical properties of air at T=300 K (Cengel and Ghajar, 2014)

Property	*Value*
ρ *[kg/m^3]*	1.1614
Cp [kJ/kg.K]	1007
μ *[N.s/ m^2]*	1.846 X 10^{-5}
k [W/m.K]	0.0263
Pr	0.707

Case (a): Optimization of circular geometry results

The optimization problem is studied utilizing the modeFRONTIER commercial software. The workflow to be constructed and implemented in the modeFRONTIER interface is shown in Figure A.9.

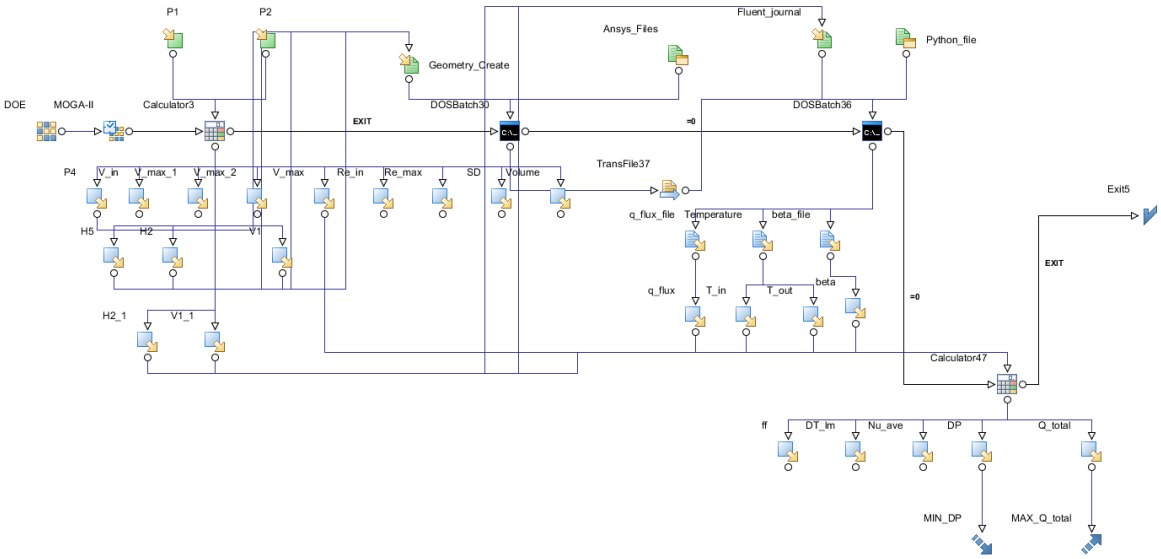


Figure A.9. Optimization workflow for circular geometry

Firstly, a parametric model is created, and grids are applied to the model in ANSYS Workbench Software. Then, the model is integrated into optimization program to obtain designs. As shown in Figure A.9, optimization algorithm, design of experiments, optimization variables, geometry/mesh creation journals with the usage of parametric model, transfer file, fluent journal file which controls numerical simulation, output files, variables, objective functions and constraints are described.

From Figure A.9, it is clear that optimization problem has two objectives: First one is to obtain total heat transfer ($\dot{Q}_{total}$) and the other one is to minimize pressure drop (ΔP). For this purpose, two non-dimensional optimization variables are chosen namely s_L^* and s_T^*. Identical lower and upper bounds are limited to be 1.05 and 2.0 for s_L^* and s_T^*, respectively with a step size of 0.05. Multi-objective design optimization problem is given in Table A.6, as follows:

Table A.6. Multi-objective design optimization problem for circular geometry

Objective Functions	(1)	Maximum $\dot{Q}_{total}$		
	(2)	Minimum ΔP		
Optimization Variables		***Lower Bound***	***Upper Bound***	***Step Size***
	s_L^*	1.05	2.0	0.05
	s_T^*	1.05	2.0	0.05

In this case study, heat flux $\dot{q}$. inlet T_{in} and outlet T_{out} temperatures and β values are written to output files using Ansys Fluent program's post-processor. ModeFRONTIER enables us to get values from output files and Python scripting language is used for file operations. Re_{max}. logarithmic-mean temperature difference, average Nusselt number, total heat transfer, friction factor, total pressure drop and volumes of parametric models are obtained for each design point using 'Calculator' of optimization software's scripts node for comparison.

Design of experiments (DOEs) method is used to generate initial designs in the design space of optimization problem, therefore it can be possible to obtain Pareto designs around DOEs. Sobol sequence method is chosen in this study for distribution of optimization variables to design space. 20 DOEs are generated to reach the optimum design. Total number of 269 designs are obtained at the end of the optimization run. 50 designs are marked as Pareto designs within those results. In Table A.7, three of the Pareto designs are tabulated and since design ID 0 is not a Pareto design, it is also given for the purpose of comparison.

Table A.7. Selected designs of circular geometry optimization study

Design ID	Pareto Design	Q_{total}	ΔP	Nu_{ave}	Re_{max}	s_L^*	s_T^*	Volume
382		292.30	3624.9	148.98	54171	1.1	1.05	1.1550E-4
160		77.07	9.903	32.8	2708.6	2.0	2.0	4.0E-4
0	X	292.20	3482.3	149.45	54171	1.05	1.05	1.1025E-4
408		158.0	133.09	71.43	10834	1.05	1.25	1.3125E-4

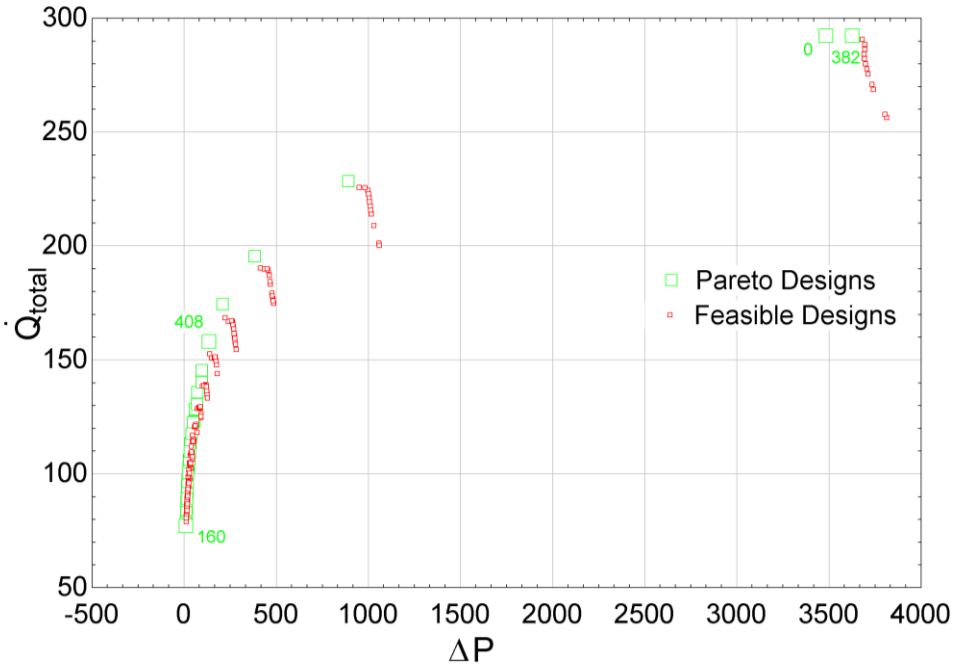


Figure A.10. Scatter of Q_{total} vs ΔP

Figure A.10 demonstrates the relationship between Q_{total} and ΔP where feasible designs are in red and Pareto designs are in green. Since, there is not any constraint, there is no unfeasible design in design space.

It is observed that Q_{total} increases with increasing ΔP in general. Moreover, for Pareto designs, maximization of Q_{total} is improved while minimization of ΔP is worsened. Within the Pareto designs with the ID of 382 has a pressure drop value of ΔP=3624.9 Pa and heat transfer value of Q_{total}=292.3 W. On the other hand, ID 160 has a pressure drop value of ΔP=9.903 Pa and heat transfer value of Q_{total}=77.065 W. Heat transfer value of ID 382 is improved by 279% as compared to ID 160, however ΔP value of these design is increased by 36505%. Since one can choose one of the Pareto designs as an optimum design due to purpose of usage. ID 408 where Q_{total}=158.00 W and ΔP=133.09 Pa is chosen as the optimum design.

Figure A.11 illustrates the variation of Nu_{ave} as a function of Re_{max}. It is seen that maximum Nu_{ave} is obtained at the Pareto design ID 0 which is 149.45 and corresponds to Re_{max} of 54171. Moreover, ID 382 with the maximum Q_{total} has the Nu_{ave} value of 148.98 which has a lower Nu_{ave} value than ID 0 at the same Re_{max}. It can be noticed that most design points accumulated at low Re_{max} below 10000. In addition, optimum Pareto design point with ID 408 has the Nu_{ave} value of 71.428 at Re_{max} 10834.

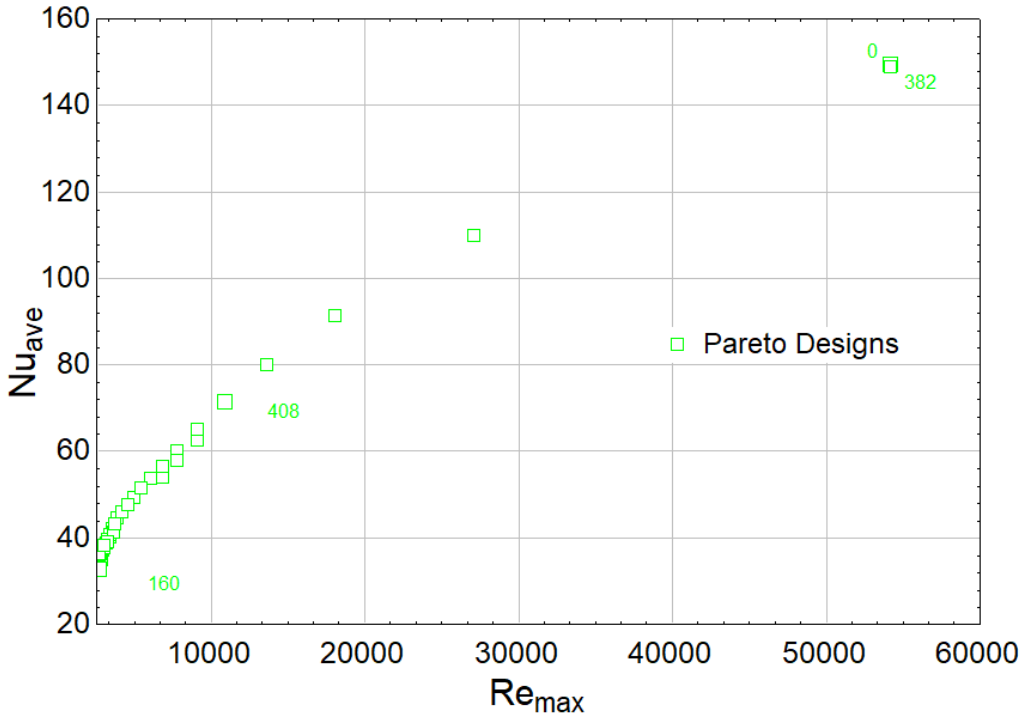


Figure A.11. Scatter of Nu_{ave} vs Re_{max}

Figures A.12 and A.13 shows the variations of Q_{total} and ΔP with Re_{max}, respectively. Since the optimization algorithm tends to find optimum designs in terms of maximum heat transfer and minimum pressure drop. Figures show that designs are denser in the lower pressure drop and lower heat transfer values, therefore it is concluded that much efforts are done to obtain minimum pressure drop as compared to get maximum heat transfer values corresponding low Re_{max}.

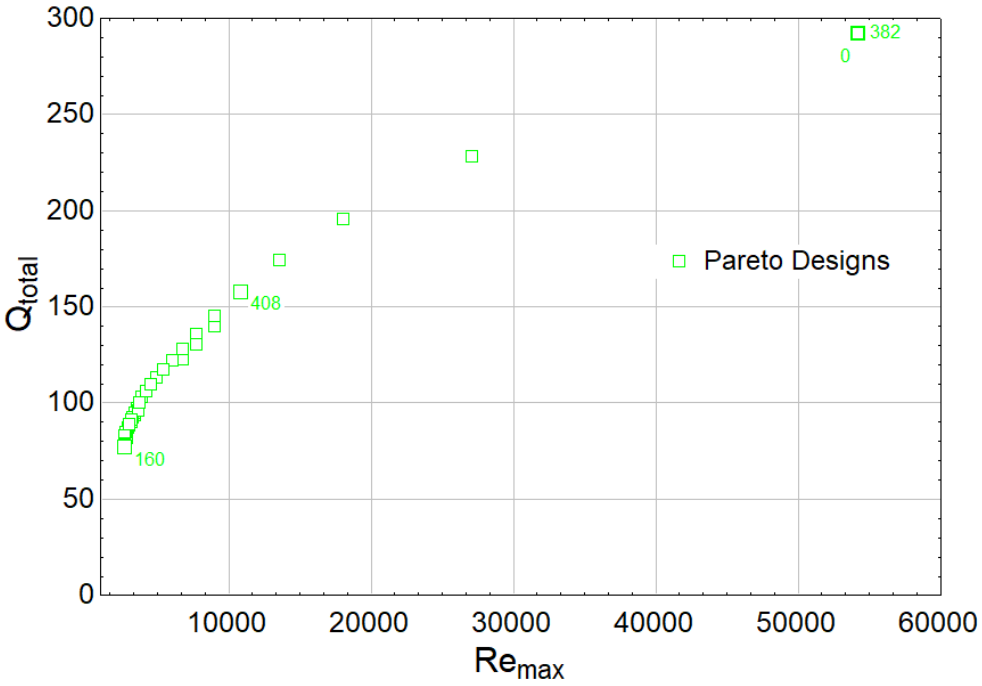


Figure A.12. Scatter of Q_{total} vs Re_{max}

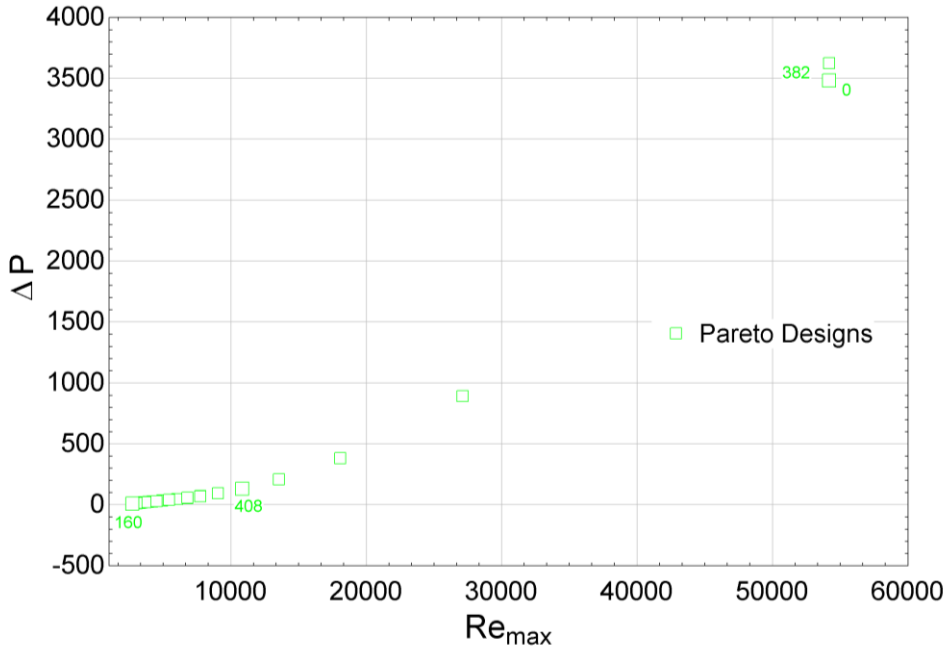
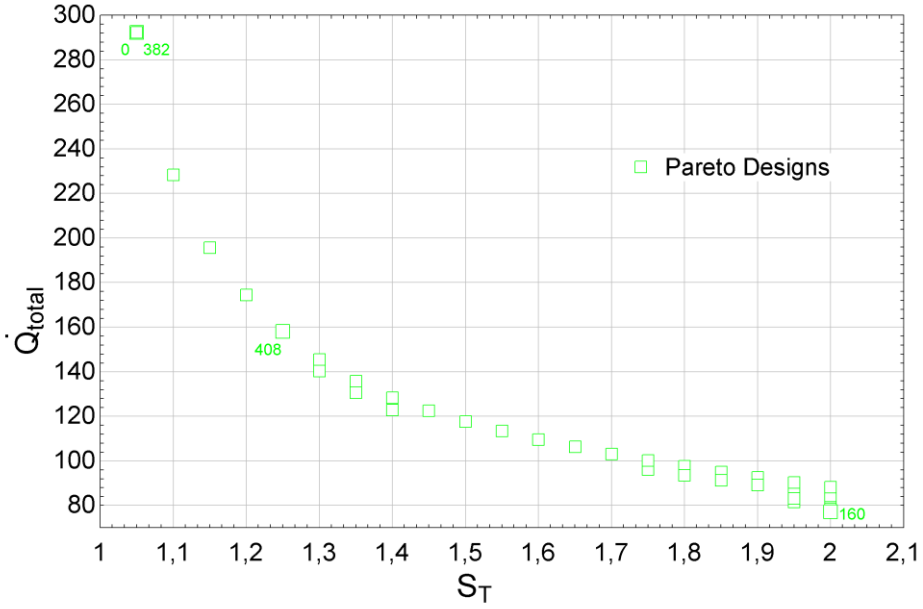


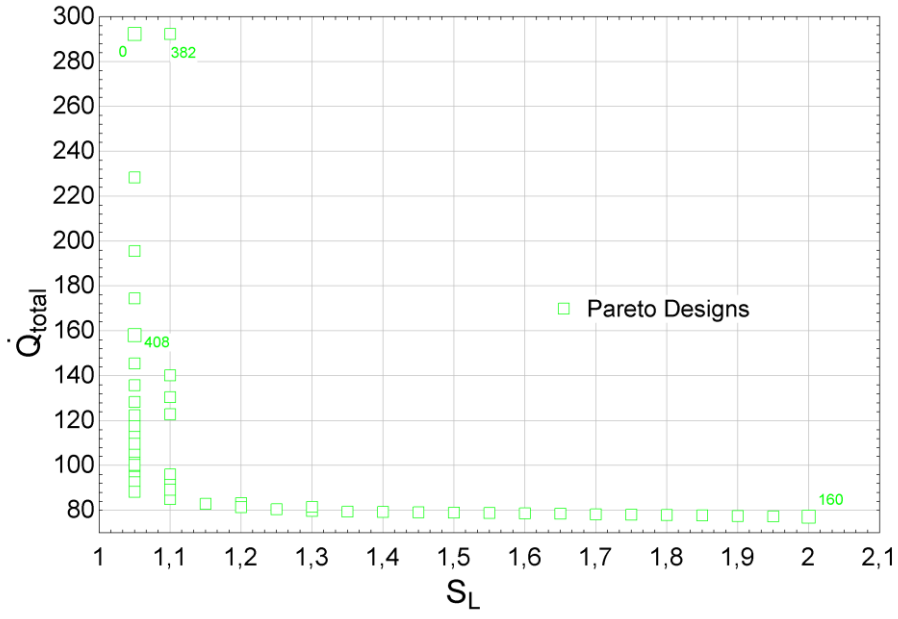
Figure A.13. Scatter of ΔP vs. Re_{max}

Figure A.14 (a) and Figure A.14 (b) depict effects of s_L^* and s_T^* values on Q_{total}. It is seen that Q_{total} shows a falling tendency with increasing s_L^* and s_T^* values. However, Q_{total} doesn't change too much for s_L^* above 1.2.

Generally, total heat transfer values increase with decreasing values of s_L^* and s_T^*. Maximum heat transfer value Q_{total} is obtained for s_L^*=1.1 and s_T^*=1.05. It can be inferred that there is an optimum point for s_L^* which has a value between the limits. However, optimum point for s_T^* is determined at the lower limit value. We limit the optimization problem with the lower value of s_T^*=1.05, because higher values of pressure drop is not desired.

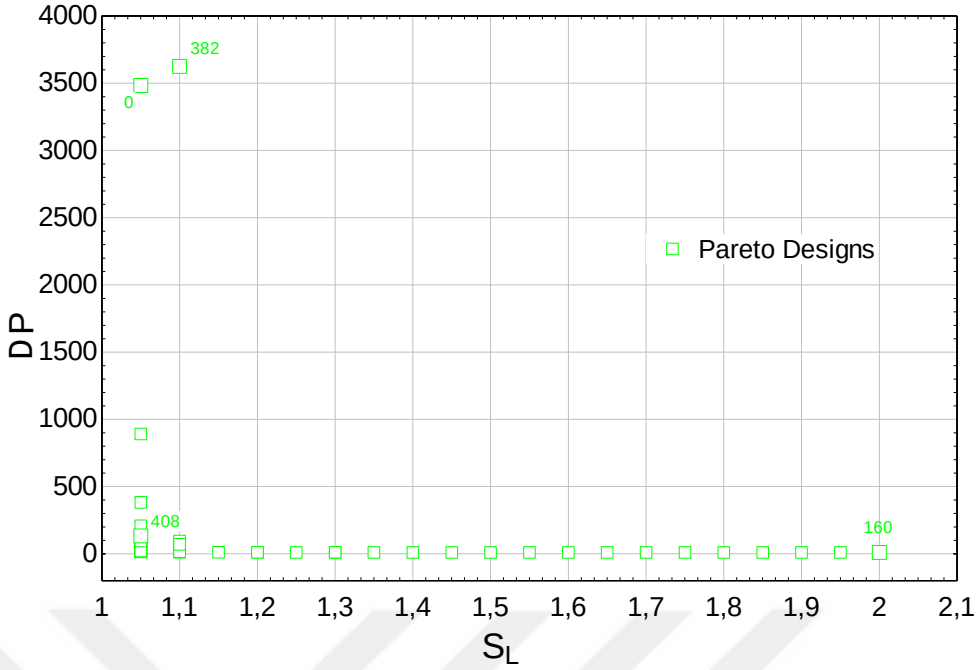


(a)

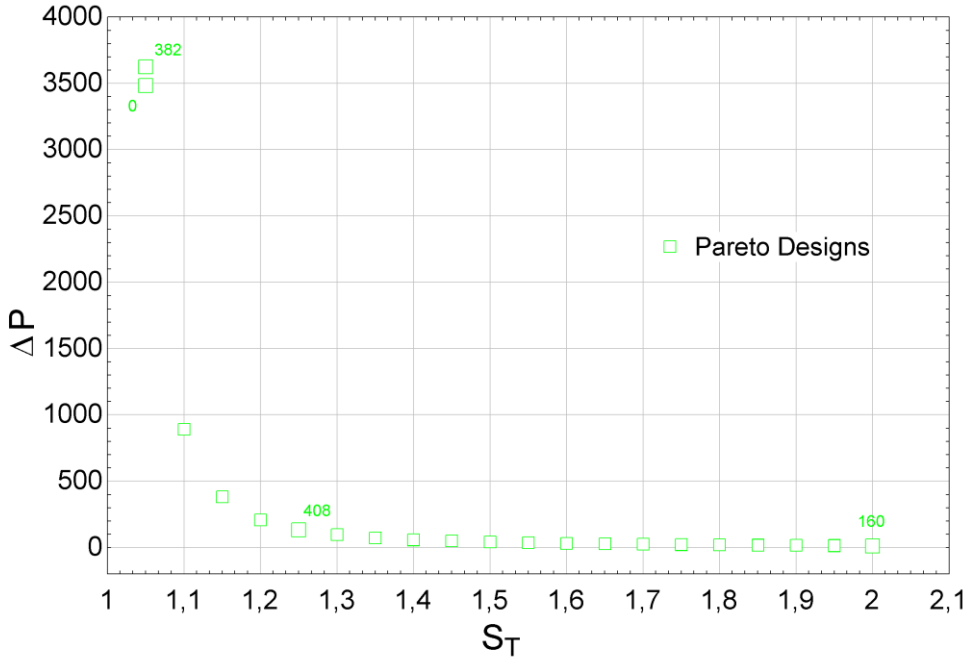


(b)

Figure A.14. (a) Scatter of s_L^* vs. Q_{total} (b) Scatter of s_T^* vs. Q_{total}



(a)



(b)

Figure A.15. (a.)Scatter of s_L^* vs. ΔP (b) Scatter of s_T^* vs. ΔP

Figure 15 (a) and Figure 15 (b) indicate the ΔP values as a function of s_L^* and s_T^*, respectively. Both figures show similar trends. The minimum pressure drop value is obtained as 9.9026 Pa at the design point ID 160 which has the maximum s_L^* and s_T^* values of 2. The increase in s_L^* and s_T^* results in lower ΔP, however this results in increment in volume of the parametric model. Furthermore, total heat transfer value is minimum for ID 160.

Case (b): Optimization of diamond shaped geometry results

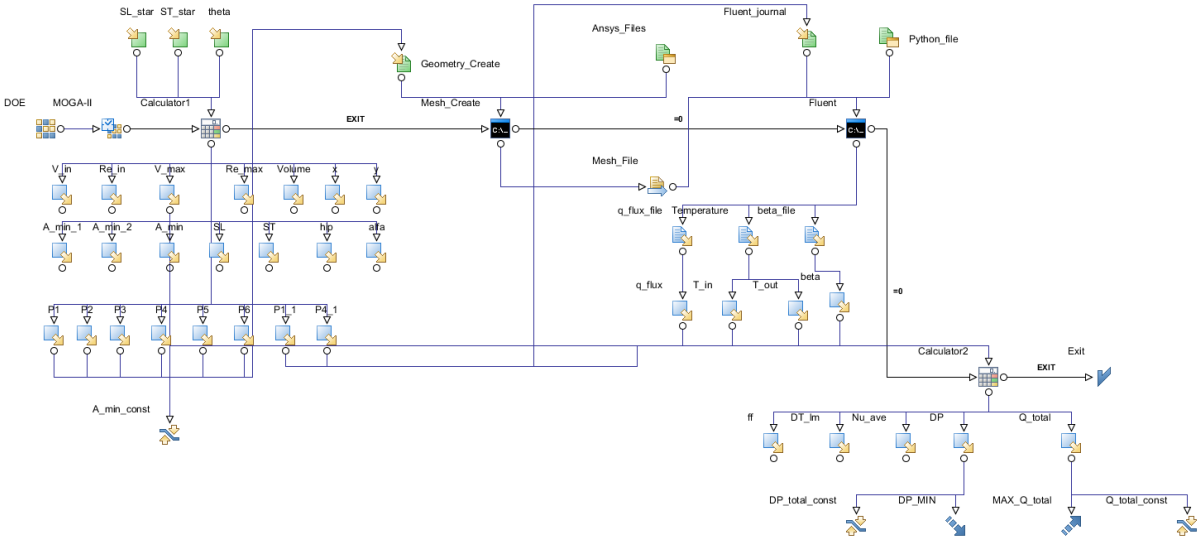


Figure A.16. Optimization workflow for diamond shaped geometry

Figure A.16 demonstrates the workflow employed for the optimization of the diamond shaped geometry. This workflow is constructed similar to Figure A.8. However, parametric model of diamond shaped geometries is created according to new optimization variable θ in addition to s_L^* and s_T^* .

Maximizing heat transfer and minimizing pressure drop are the objective functions of this case, apart from case 1, θ value is new optimization variable which ranges from 10 to 170 with a step size of 5. Multi-objective optimization of diamond shaped geometry is formulated in Table A.8.

Table A.8. Multi-objective design optimization problem for diamond shaped geometry

Objective Functions	(1)	Maximum Q_{total}		
	(2)	Minimum ΔP		
		Lower Bound	*Upper Bound*	*Step Size*
Optimization Variables	s_L^*	1.05	2.0	0.05
	s_T^*	1.05	2.0	0.05
	θ	10	170	5
Constraints	$\Delta P < 133.09$ Pa			
	$Q_{total} > 158$ W			
	$A_{min} \geq 0.5\ mm^2$			

Obtained optimum design values ΔP and Q_{total} in Case 1 corresponding to design number ID 408 are set as constraints in order to obtain better designs. Moreover, as mentioned earlier minimum flow cross section area should be equal or higher than 0.5 to provide maximum Reynolds number limitation.

20 DOEs created by Sobol sequence are configured in the optimization workflow. In order to obtain Pareto designs MOGA is utilized. After the optimization analysis, total number of 411 designs are determined. Within these designs, 389 designs of total designs are classified as unfeasible because the designs do not meet the optimization criteria. Remaining 22 designs are feasible and 4 design points are determined to be Pareto designs which are listed in Table A.9.

Table A.9. Selected designs of diamond shaped geometry optimization study

Design ID	Pareto Design	Q_{total} [W]	ΔP [Pa]	Nu_{ave}	Re_{max}	s_L^*	s_T^*	θ [°]	Volume $[m^3]$
482		167.46	103.09	76.32	14678	1.05	1.90	15	6.37E-05
519		163.27	91.213	74.16	13906	1.05	1.95	15	6.54E-05
544		171.94	117.25	78.65	15542	1.05	1.85	15	6.20E-05
639		159.32	81.164	72.12	13211	1.05	2.0	15	6.7E-05

Within the Pareto designs, Design ID 544 is selected as optimum design since it has the highest Q_{total} that satisfies the ΔP constraint. In Table A.10, optimum designs of circular and diamond shaped geometries are compared.

Table A.10. Comparison of optimum designs of circular and diamond shaped geometries

	Circular	Diamond-shaped	%
Pareto Design ID	408	544	-
Q_{total} [W]	158.0	171.94	8.82
ΔP [Pa]	133.09	117.25	-11.90
Nu_{ave}	71.43	78.65	10.11
s_L^*	1.05	1.05	-
s_T^*	1.25	1.85	-
Volume [m^3]	1.3125E-4	6.20E-05	-52.76

It is observed that, Q_{total} and Nu_{ave} are increased ΔP is reduced and more than %50 volume decrement is obtained with the usage of diamond shaped geometry.

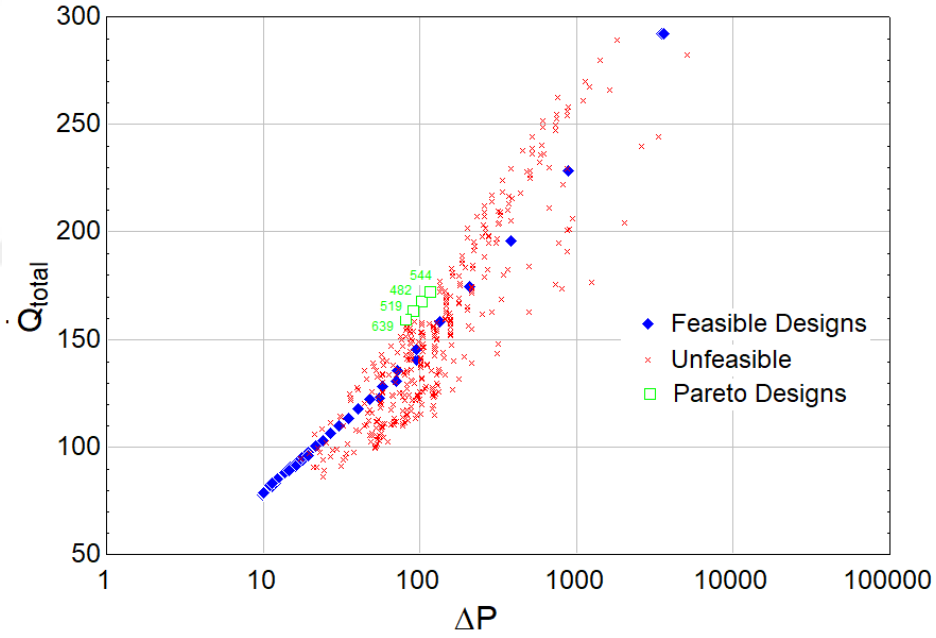


Figure A.17. Scatter of Q_{total} vs ΔP

Figure A.17 illustrates value of Q_{total} as a function of ΔP for diamond shaped geometry. There are numerous unfeasible designs which are marked in orange color. However, roughly 5% of total designs are determined as feasible designs. It can be observed that, Q_{total} tends to increase as ΔP increases. If Pareto design ID 639 was selected as an optimum design for this study, 39% pressure drop reduction would be achieved with the diamond shaped geometry while the heat transfer value obtained is almost the same as the optimum circular geometry. In addition, volume of the heat exchanger with diamond shaped geometry could be reduced by about 49%.

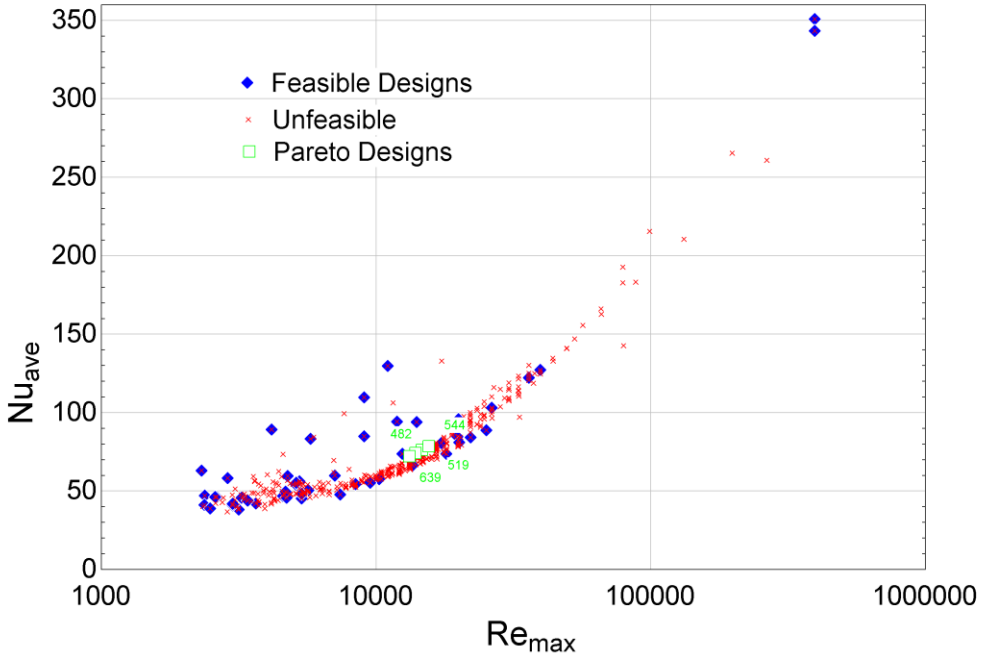
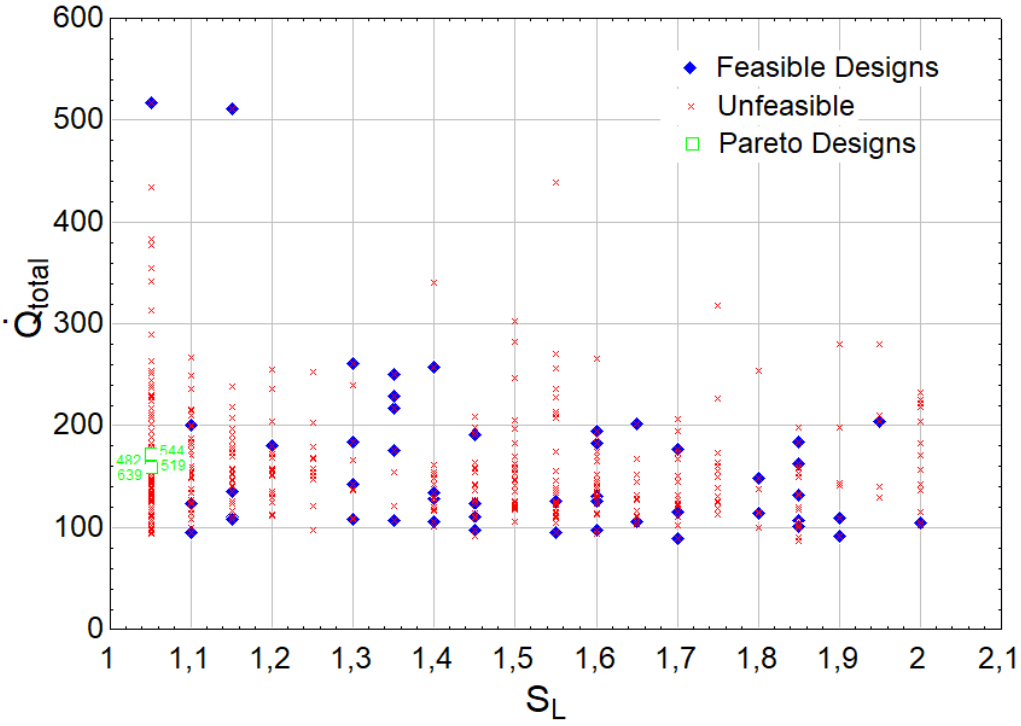
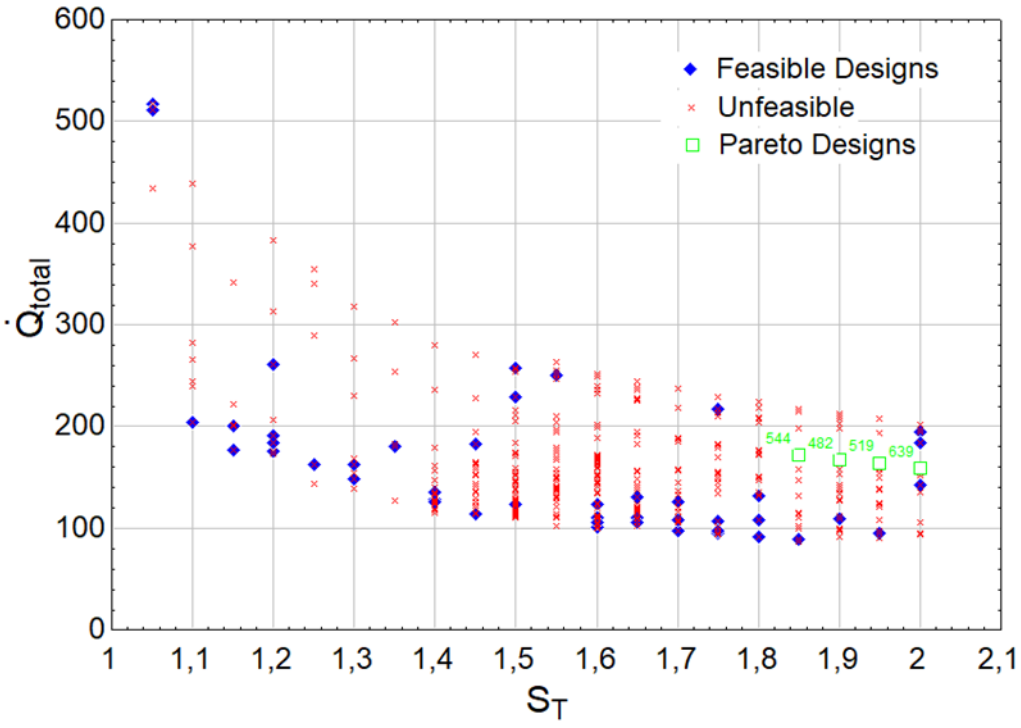


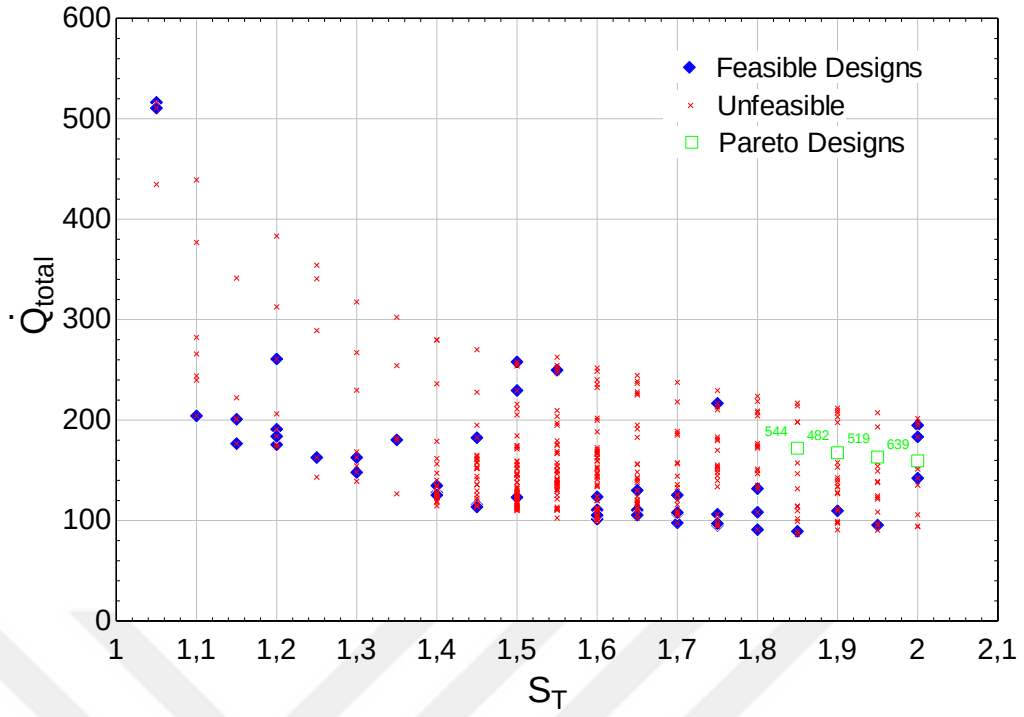
Figure A.18. Scatter of Nu_{ave} vs Re_{max}

Figure A.18 demonstrates the relationship between the Nu_{ave} vs Re_{max} for the diamond shaped geometry. It is observed that, most of the designs accumulate in the region of low Nu_{ave} and Re_{max}. Optimum design point with ID 544 has the Re_{max} value of 15542 and Nu_{ave} value of 78.65. Since optimum design values for circular tube arrangements are $Re_{max} = 10834$ and $Nu_{ave} = 71.428$, it can be said that optimum designs can have different Re_{max} and Nu_{ave} values due to geometrical flexibility and optimization constraints.

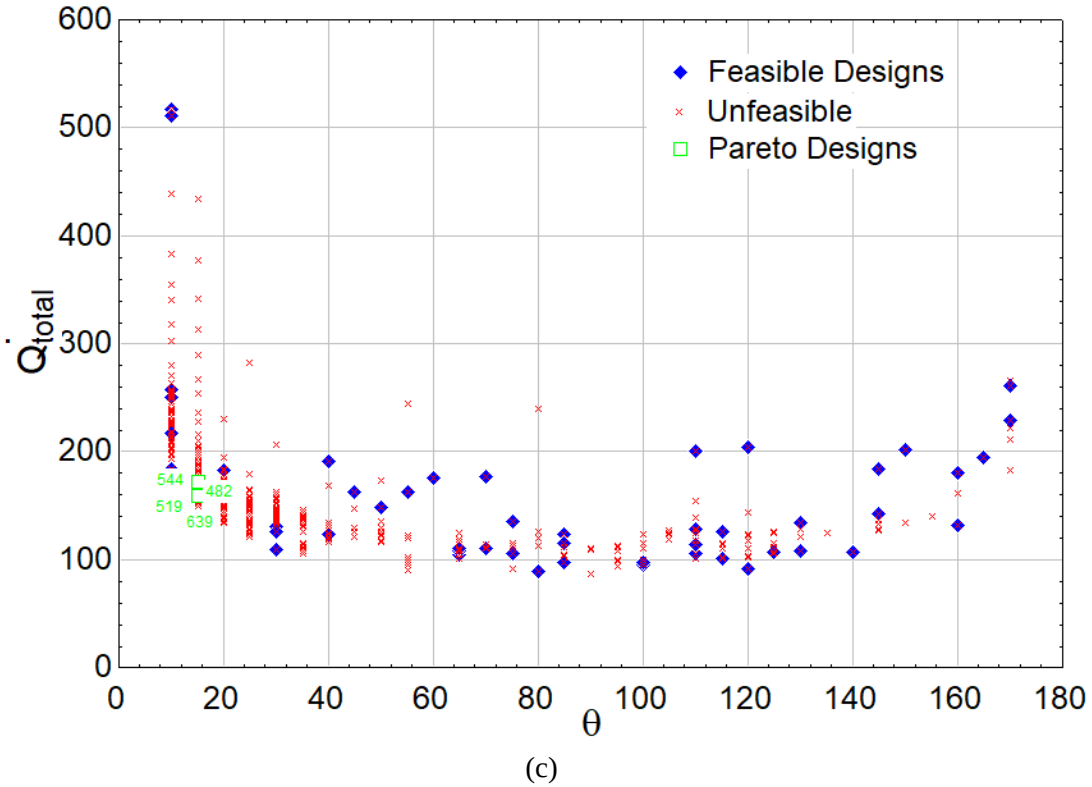

Feasible Designs
Unfeasible
Pareto Designs
$\dot{Q}_{total}$
S_L
600
500
400
300
200
100
0
1
1,1
1,2
1,3
1,4
1,5
1,6
1,7
1,8
1,9
2
2,1
482
544
639
519

(a)


Feasible Designs
Unfeasible
Pareto Designs
$\dot{Q}_{total}$
S_T
600
500
400
300
200
100
0
1
1,1
1,2
1,3
1,4
1,5
1,6
1,7
1,8
1,9
2
2,1
544
482
519
639



(b)



(c)

Figure A.19. (a) Scatter of s_L^* vs. $\dot{Q}_{total}$ (b) Scatter of s_T^* vs. $\dot{Q}_{total}$ (c) Scatter of θ vs. $\dot{Q}_{total}$

Figure A.19 (a), (b) and (c) present $\dot{Q}_{total}$ value as a function of s_L^*. s_T^* and θ, respectively. There is no feasible design obtained for s_L^* values higher than 1.65. Nevertheless, Pareto designs are achieved for s_L^*=1.05 which corresponds to the lower bound value of s_L^*. On the other hand, obtainable $\dot{Q}_{total}$ value range becomes narrower with increasing s_T^* values. Apparently, there are

feasible designs for all s_T^* values. Pareto designs are obtained when $s_T^* \geq 1.85$. Besides, $\dot{Q}_{total}$ values of Pareto designs decrease with the increment in s_T^* values. Optimization algorithm seek Pareto designs for the entire range of design variable theta, as shown in Figure A.19 (c). It can be easily seen that designs are denser for the lower values of θ. Optimization algorithm determined the feasible designs for the θ values below 30°. In contrast, all Pareto designs are obtained at 15°, which is 5° above the lower bound of design ranges.

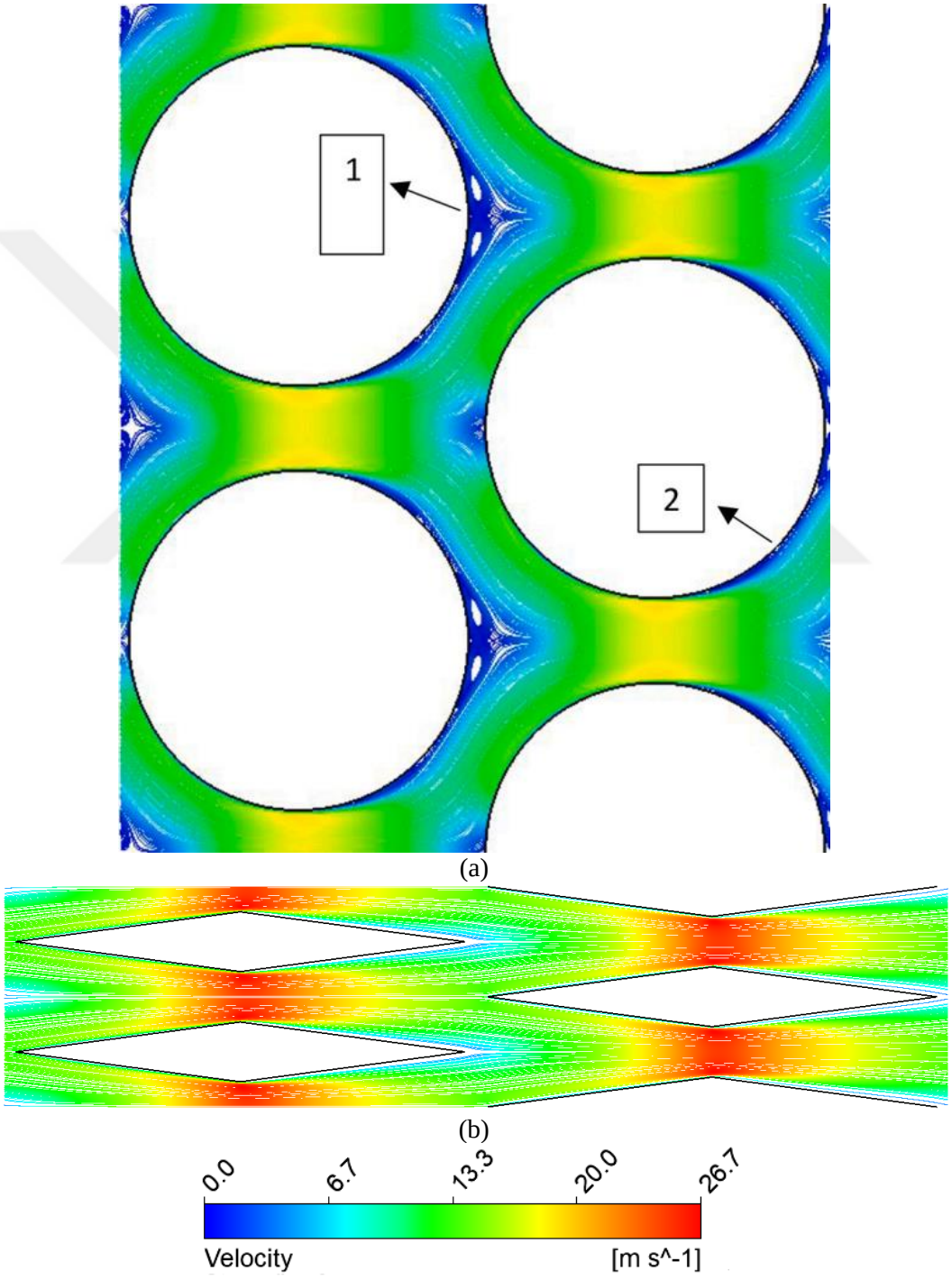
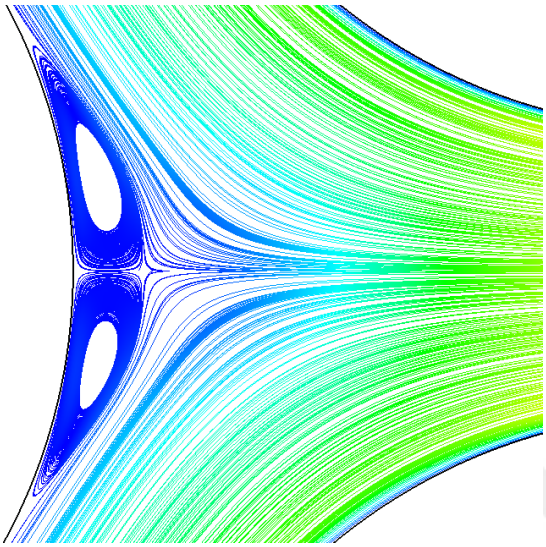
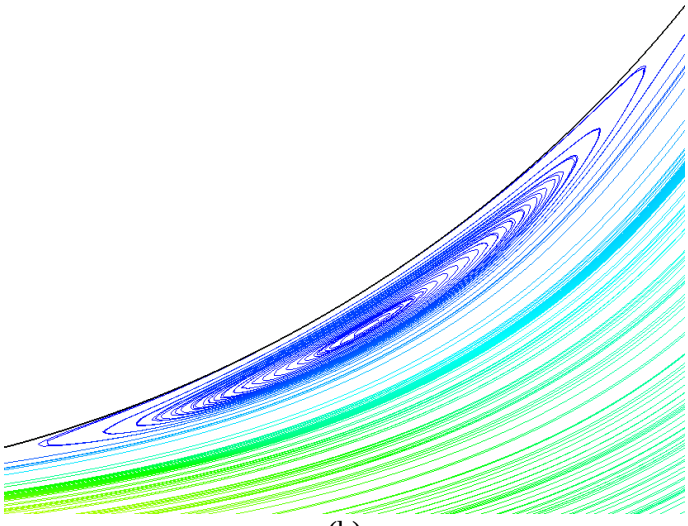


Figure A.20. Streamlines of optimum a) circular b) diamond shaped geometries

Figure A.20 indicates the streamlines of optimum both circular and diamond shaped geometries. It can be seen that maximum velocity is obtained in diamond shaped geometry due to having narrower minimum cross-sectional area. If the optimum design of circular design was found at the minimum s_T^*=1.05, it would be possible to achieve the same maximum velocity with diamond shaped geometry design. In the wake region, there is no vortex formation in optimum diamond shaped geometry whereas vortex formed in optimum circular geometry. Detailed view of two vortex region is demonstrated in Figure A.21. As can be seen from this figure, the flow separation occurred at the rear side of circles.



(a)



(b)

Figure A.21. Enlarge view of optimum circular shaped geometry streamlines

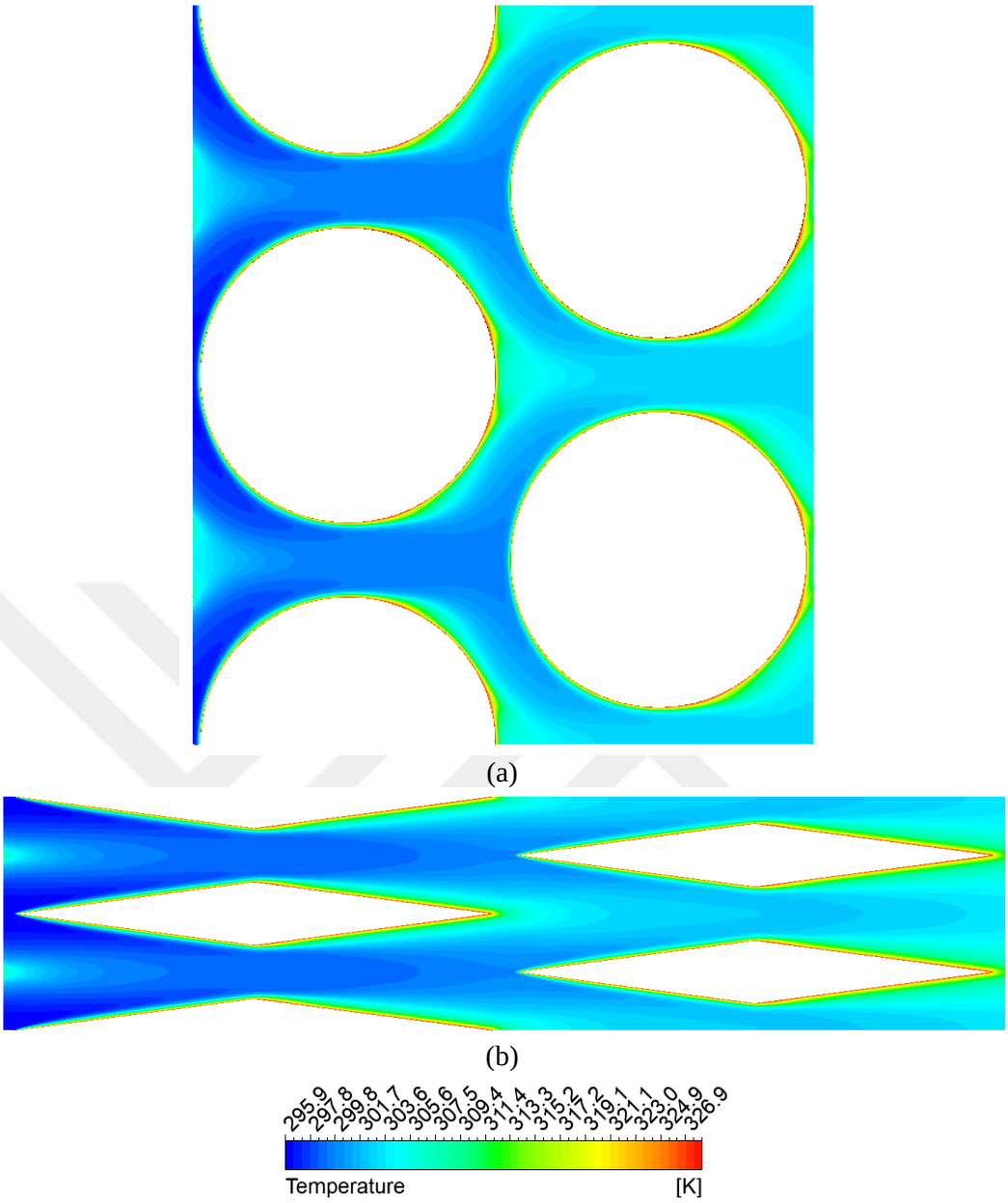


Figure A.22. Temperature contours of optimum a) circular b) diamond shaped geometries

Figure A.22 shows temperature contours of optimum both circular and diamond shaped geometries. For the optimum circular geometry, the thickness of the thermal boundary layer increases while the temperature gradient decreases after the separation point, resulting in less heat transfer in the wake region. Then, flow is re-attached to the circular geometry after the re-circulation zone. This phenomenon leads to an increase in the heat transfer as well as increase in temperature gradient increment before the second vortex region. For optimum diamond-shaped geometry, it is seen that no flow separation and vortex generation occurs due to the streamlined geometry of diamond-shape. Therefore, the temperature gradient gradually decreases along the geometry, resulting in higher heat transfer.

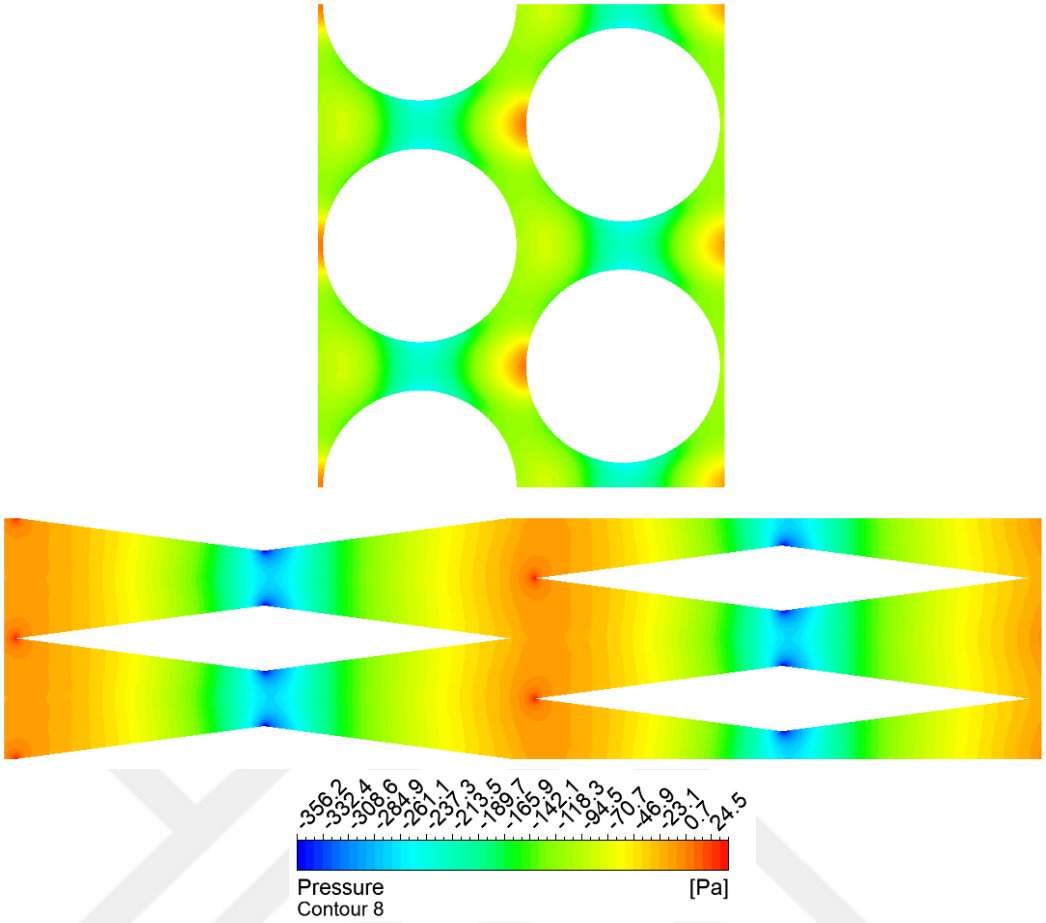


Figure A.23. Pressure contours of optimum a) circular b) diamond shaped geometries

Figure A.23 shows local static pressure contours of optimum both circular and diamond shaped geometries. As given before, pressure drop value is higher for optimum circular shaped geometry. However, maximum and minimum pressure values are obtained in diamond shaped geometry. In addition, maximum local pressure values are seen in the front stagnation points where velocity magnitude is zero and minimum values are obtained in the minimum flow cross-sectional area where velocity magnitude has a maximum value for both geometries. Moreover, local static pressure decreases along the geometry up to the minimum flow cross-section, and from this point, local pressure values start to increase.

It is important to note that streamlined geometries have larger heat transfer values compared to circular geometries. This result is also presented by Sayed Ahmet et al. (2014b; 2016b). Similar results were found for diamond shaped designs in this study. The optimization algorithm finds optimum design for streamlined geometries.

Due to our assumption of equivalent diameter with circular geometry, it is possible to change x and y values, lowering y value of diamond-shaped geometry result in increment in x value, thus this flexibility of diamond shaped geometry results in higher s_L^* and a much lower s_T^* value compared to circular geometry. Despite the fact that s_L^* increment results in higher volume, this increment is compensated by the much decrement in s_T^* value. Thus, for diamond-shaped geometries, we can achieve an almost 50% reduction in volume.